An optical functional analysis of amorphous semiconductors

by

Sanjida Begum Minar

B.Sc., Bangladesh University of Engineering and Technology, 2009

A THESIS SUBMITTED IN PARTIAL FULFILLMENT OF
THE REQUIREMENTS FOR THE DEGREE OF

MASTER OF APPLIED SCIENCE

in

The College of Graduate Studies

(Electrical Engineering)

THE UNIVERSITY OF BRITISH COLUMBIA

(Okanagan)

December 2012

Abstract

Models for the spectral dependence of the real and imaginary components of the dielectric function, appropriate for the case of amorphous semiconductors, are considered. In the first phase of this analysis, from an empirical expression for the imaginary part of the dielectric function, this expression corresponding to that of Jellison and Modine [G. E. Jellison, Jr. and F. A. Modine, "Parameterization of the optical functions of amorphous materials in the interband region," *Applied Physics Letters*, vol. 69, pp. 371-373, 1996], a closed-form expression for the real part of the dielectric function is determined using a Kramers-Kronig transformation. The resultant expression for the real component of the dielectric function corresponds with that of the model of Jellison and Modine. The subsequent comparison with experiment is found to be satisfactory. Then, in the latter stage of this analysis, through the application of a Kramers-Kronig transformation on an empirical model for the imaginary part of the dielectric function, this model stemming from

Abstract

a model for the distributions of electronic states, the spectral dependence of

the real part of the dielectric function is determined. Fits with the results

of experiment, taken over the near-infrared, visible, and near-ultraviolet, are

also found to be satisfactory.

Table of Contents

List of Tables

List of Figures

List of Symbols

ϵ_1	real part of the dielectric function
ϵ_2	imaginary part of the dielectric function
α	optical absorption coefficient
$I(z)$	intensity of light at position z
I_o	intensity of light at position $z = 0$
$n(E)$	spectral dependence of the refractive index
$k(E)$	spectral dependence of the extinction coefficient
q	electron charge
m	electron mass
V	illuminated volume
$\vec{\eta}$	polarization vector of the incident light
E	photon energy

E_v valence band band edge

E_{v_T} critical energy at which the exponential and square-root distribu-
tions interface in the valence band

E_c conduction band band edge

E_{c_T} critical energy at which the exponential and square-root distribu-
tions interface in the conduction band

E_g energy gap

γ_v breadth of the valence band tail

γ_c breadth of the conduction band tail

$|v\rangle$ single-spin electronic state associated with the valence band

$|c\rangle$ single-spin electronic state associated with the conduction band

$\vec{\boldsymbol{P}}$ momentum operator

$P^2(E)$ aggregate momentum matrix element squared average

$\mathcal{R}^2(E)$ aggregate dipole matrix element squared average

$\vec{\boldsymbol{\mathcal{R}}}$ the dipole operator

ρ_A density of silicon atoms

E_F Fermi energy level

$N_v(E)$ valence band density of states function

$N_c(E)$ conduction band density of states function

N_{vo} valence band density of states prefactor

N_{co} conduction band density of states prefactor

$J(E)$ joint density of states function

$E(t)$ time-dependent electric field

$J(t)$ time-dependent current density

$\Sigma(t)$ time-dependent conductivity

E_o resonance energy of a bound electron at which the transition of the electron occurs between two atomic states

C breadth of the region of anomalous dispersion

A Lorentz oscillator strength

E_d characteristic energy

List of Acronyms

a-Si   amorphous silicon

c-Si   crystalline silicon

μc-Si   microcrystalline silicon

DOS   density of states

JDOS   joint density of states

EGE   electron-gun evaporated

PECVD   plasma enhanced chemical vapor deposition

Acknowledgements

I am very thankful to my supervisor, Dr. Stephen Karrer O'Leary, for his guidance, full support, and constant encouragement throughout my thesis. I am grateful to him for keeping faith in me. His valuable advice always helped me to progress.

I owe particular thanks Dr. Mario Beaudoin, Research Associate, Manager of the AMPELs Advanced Nanofabrication Facility, UBC, for guiding me so wonderfully during the lab training period and helping me for enlarging my vision of science.

To my family

Chapter 1

Introduction

For the past half-century, electronics has played an important role in shaping the course of human development. In advanced industrial economies, such as Canada's, electronics has become a critical adjunct to modern life. Electronic devices are ubiquitous. They are found in houses, offices, recreational settings, vehicles, and appliances. They are used in communication systems, control systems, sensor systems, and in a plethora of other systems. With each passing year, new applications for electronic devices are conceived. Thus, the role that electronics plays in modern society continues to broaden.

The transistor is the fundamental building block upon which the electronics revolution has been built. While the first microprocessors, developed in the early 1970s, were comprised of about a thousand transistors, at the time of writing, 2012, the standard personal computer, available in most offices and homes, has in excess of a billion transistors. In the near term future, this

is only expected to exponentially increase, as it has for the past four decades; Moore [1] prophesized this exponential increase in the number of transistors on a processor in 1965, and, thus far, Moore's prophesy, or Moore's law, as this projection is now commonly referred to as, has held true.

The electronics revolution found its genesis with the development of the first transistor in 1947 [2, 3]. Transistors are comprised of conductors, insulators, and semiconductors. The fabrication of the first transistor was achieved as a result of a detailed and quantitative understanding of the material properties of these different materials. While the properties of conductors and insulators were relatively well understood by 1947, the understanding of the material properties of semiconductors was more rudimentary; at the time, semiconductors were considered more of a laboratory curiosity. Since that time, however, fundamental progress in electronics has been achieved through continued improvements in the understanding of the material properties of the materials used within electronic devices. The next generation of electronic device will undoubtedly rely upon an even greater understanding of these material properties. Accordingly, interest in the material properties of conductors, insulators, and particularly semiconductors, remains intense.

In conventional electronics, technological improvements have been achieved

as a consequence of making the constituent electronic devices, i.e., the transistors, smaller, faster, cheaper, and more reliable. There is, however, another class of electronic device that requires size in order to properly function. Flat panel displays [4, 5] and scanners [6], acting at the interface between the human and electronic worlds, are two such examples. Digital x-ray imagers [7] and photovoltaic solar cells [8, 9] are two other examples. These electronic devices are commonly referred to as examples of large area electronic devices. Starting out as a niche field in the late 1960s, large area electronics now constitutes a sizeable and growing fraction of the overall electronics enterprise; see Figure 1.1 [10].

In conventional electronics, the focus is on producing electronic devices with sub-micron feature sizes. In contrast, for large area electronics, the focus is on depositing materials as thin-films over large substrates, i.e., of the order of a square-meter [11]. For large area electronics, the uniformity of the resultant thin-films and the expense of the deposition process are of paramount concern. Crystalline silicon (c-Si), the workhorse of conventional electronics, can not be deposited as a thin-film. Accordingly, alternative electronic materials must be employed instead. Microcrystalline silicon (μc-Si) and amorphous silicon (a-Si) are two alternate silicon-based materials
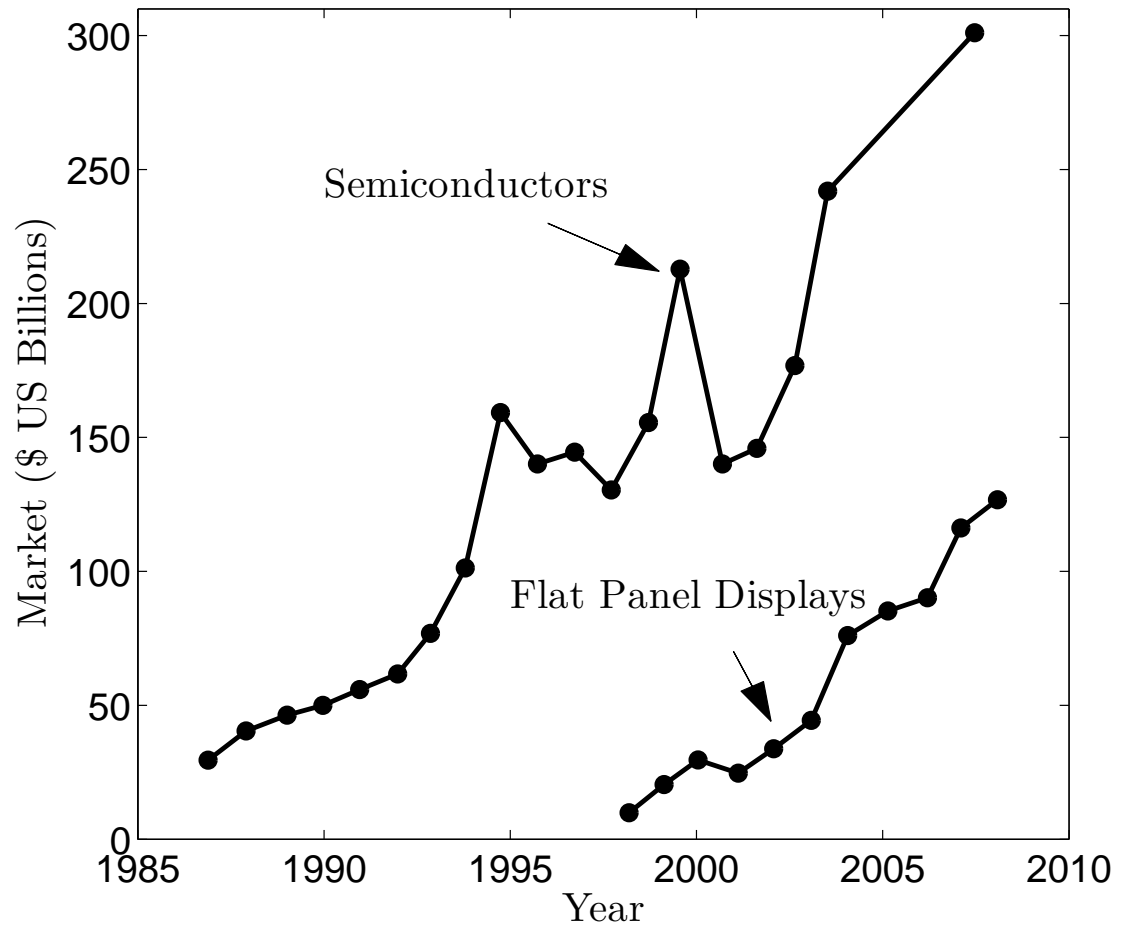
Figure 1.1: Semiconductor and flat panel display shipments plotted as a function of date. This data was obtained from the 2005 Information Society Technologies proposal for advancement [10].

commonly used in the large area electronics field.

The distinction between c-Si, μc-Si, and a-Si relates to the underlying distribution of atoms. In c-Si, the atoms are arranged in a periodic and ordered manner. In μc-Si, however, small crystallites, randomly oriented and separated by grain boundaries, are distributed throughout the volume. In a-Si, all residual crystalline order is absent, there being variations in the short-range bonding lengths and bonding angles. In Figure 1.2 [12], a schematic two-dimensional representation of the distribution of atoms within hypothetical crystalline, microcrystalline, and amorphous semiconductors is presented. The disorder that is present, in both μc-Si and a-Si, plays an important role in shaping the resultant properties of these materials.

While disorder is present within the atomic distributions of μc-Si and a-Si, there is still a considerable amount of order that is present in both of these materials. For both μc-Si and a-Si, most silicon atoms are bonded to four other silicon atoms, as in the case of c-Si. The bonding lengths and bonding angles, while exhibiting variations, are, on average, similar to those exhibited by c-Si. Accordingly, as the properties of a given material are primarily determined by its short-range order, many of the properties of these materials are similar to those of c-Si. The disorder that is present,
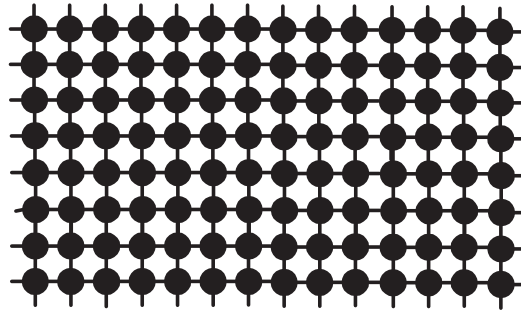
Crystalline semiconductor structure
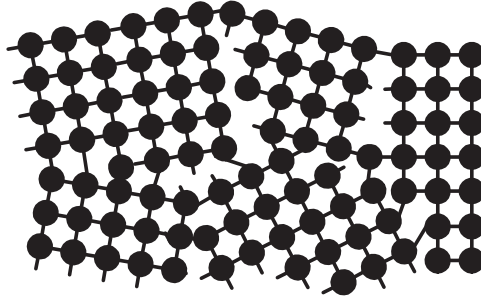
Polycrystalline semiconductor structure
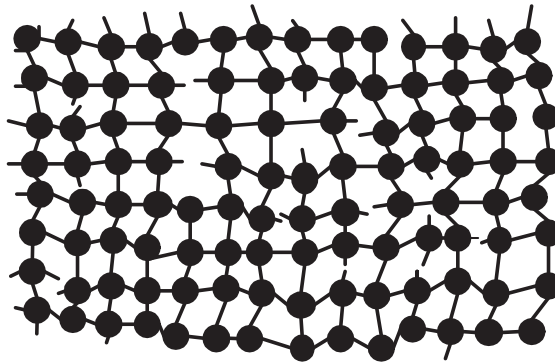
Amorphous semiconductor structure

Figure 1.2: A two-dimensional schematic representation of the atomic distributions associated with hypothetical crystalline, microcrystalline, and amorphous semiconductors. This figure is from Nguyen [12].

however, will lead to some important differences. These will be the focus of the subsequent analysis.

When a material is exposed to light, it will respond. Consider, for example, a beam of light incident upon a semi-infinite slab of material, as seen in Figure 1.3 [13]. Ignoring reflections from the slab, if the material comprising the slab is absorbing, assuming that the material within the slab is homogeneous, it is found that the intensity of the light exponentially attenuates as it propagates through the absorbing slab. In particular, it can be shown that the intensity of the light within the slab

$$I(z) \ = \ I_o \exp(-\alpha z), \tag{1.1}$$

where $I(z)$ denotes the intensity of the light at position z, I_o represents the incident light intensity, and α denotes the optical absorption coefficient; it is assumed that $z = 0$ corresponds to the interface between the vacuum and the absorbing slab. Representative attenuations of the light intensity, for a number of selections of the optical absorption coefficient, α, are depicted in Figure 1.4 [14].

The absorption that occurs within a semiconductor arises as a consequence of optical transitions from the occupied electronic states in the valence band to the unoccupied electronic states in the conduction band. In

light

Material

I(z)

I$_0$

z
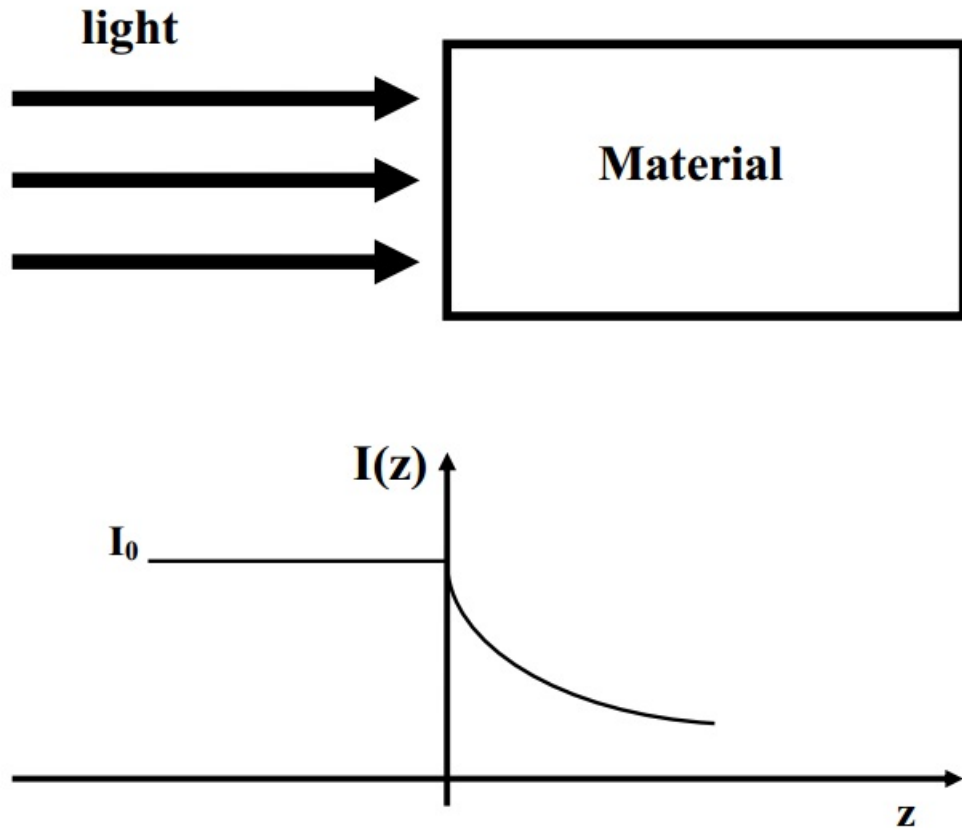
Figure 1.3: A schematic representation of the light intensity as a function of the penetration depth, z, with light normally incident upon the material propagating from the left. This figure is from Thevaril [13].
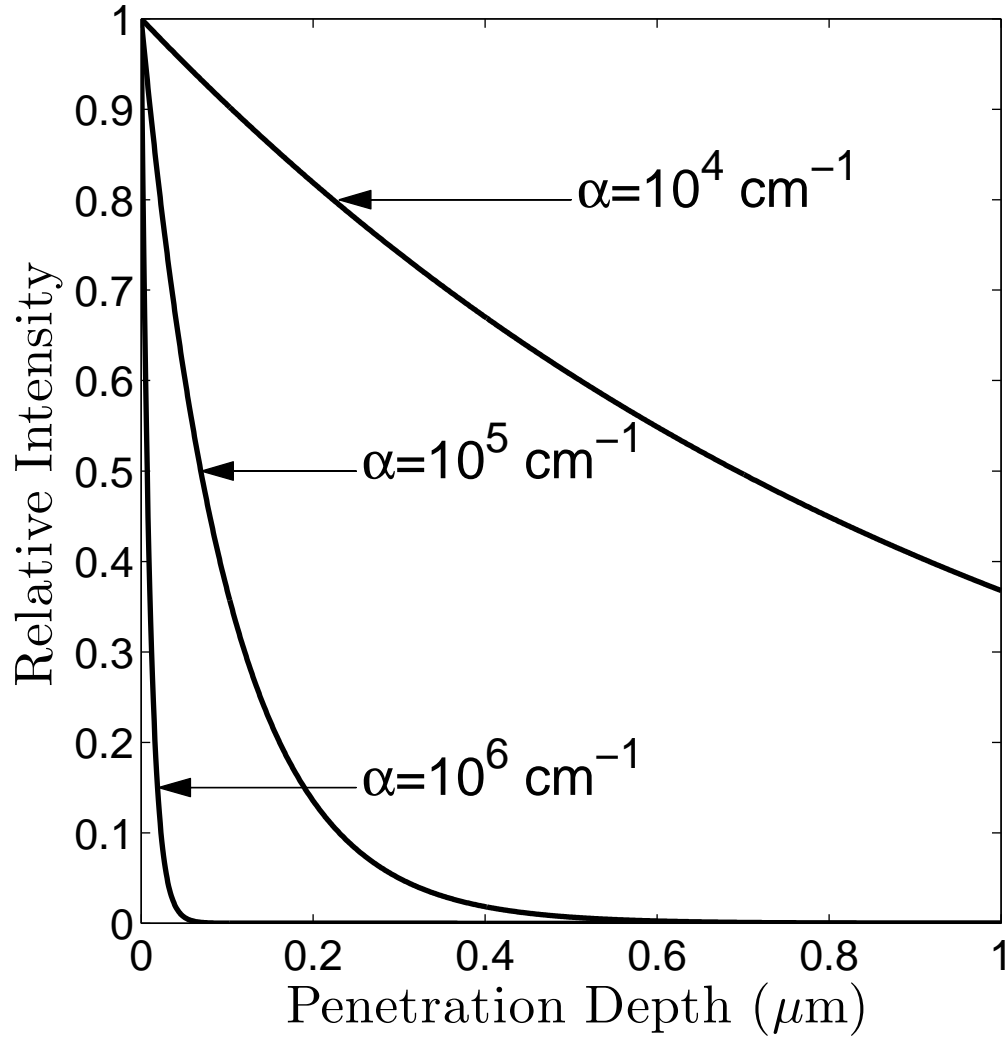
Figure 1.4: Variations in the relative intensity, $I(z)/I_o$, with the penetration depth, z, for different selections of the optical absorption coefficient, α. This figure is after Orapunt [14].

Figure 1.5, a representative optical transition is depicted. The optical response of a material depends critically upon the availability of electronic states and on the probability of the optical transitions between such electronic states. The distributions of valence band and conduction band electronic states determines the range of possible optical transitions. The optical transition matrix elements, that couple the electronic states between which optical transitions occur, determine the probability of such optical transitions occurring.

The optical response of a material may be characterized in terms of the spectral dependence of the optical absorption coefficient, $\alpha(E)$, where E denotes the photon energy of the photons within the beam of incident light. In a defect-free, disorderless semiconductor, this optical absorption coefficient terminates abruptly at the energy gap. Accordingly, measurements of the optical absorption spectrum allow one to determine the corresponding energy gap. In addition, the spectral dependence of the optical absorption coefficient beyond the energy gap provides information as to how the electronic states are distributed and on what the probability of the optical transitions between such states are. When disorder is introduced, however, the situation is more complicated, as there are now electronic states encroaching into the otherwise
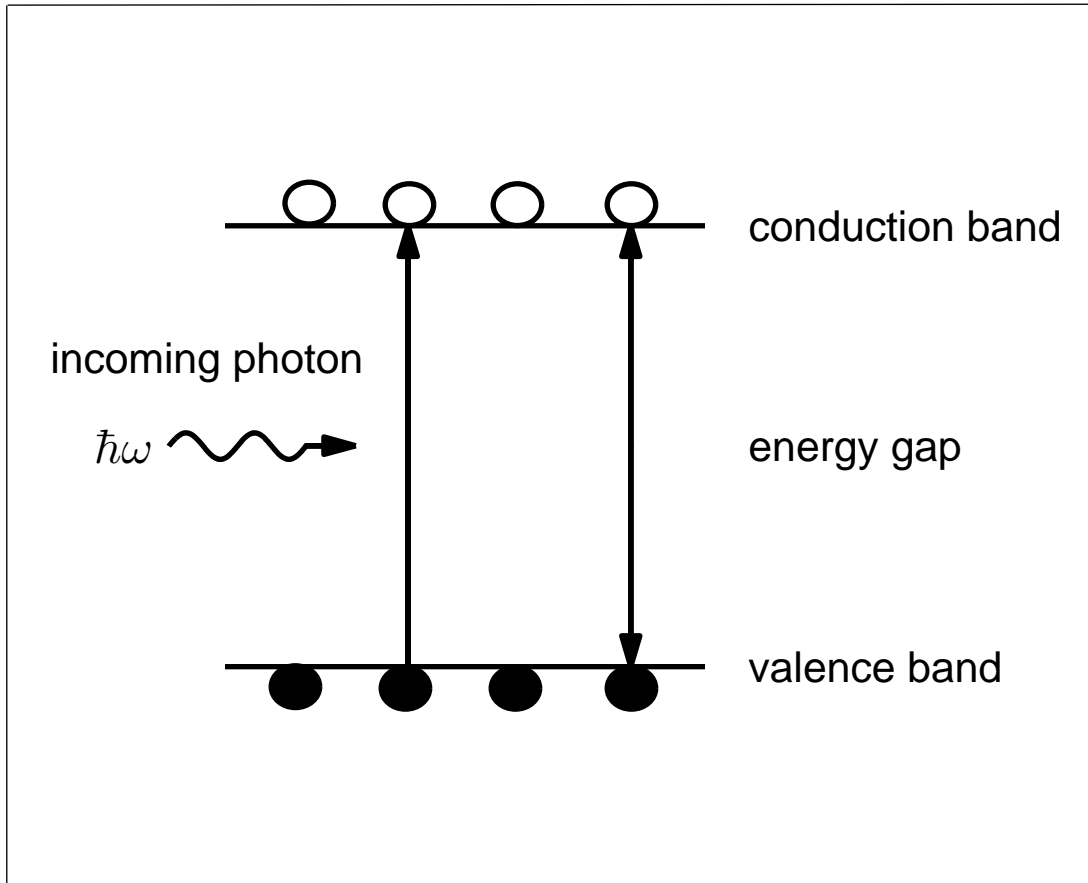
Figure 1.5: A representative optical transition, from an occupied electronic state in the valence band to an unoccupied electronic state in the conduction band.

empty energy gap region. Accordingly, the optical absorption spectrum no longer terminates abruptly at the energy gap. In fact, the definition of the energy gap itself becomes the subject of some controversy.

While $\alpha(E)$ is often experimentally measured, it is the real and imaginary parts of the dielectric function, $\epsilon_1(E)$ and $\epsilon_2(E)$, respectively, that are the more usual focus of theoretical attention. The complex dielectric function may be expressed as the sum over its real and imaginary components, i.e.,

$$\tilde{\epsilon}(E) \quad = \quad \epsilon_1(E) + i\epsilon_2(E), \tag{1.2}$$

where $\epsilon_1(E)$ and $\epsilon_2(E)$ denote the real and imaginary components of this dielectric function, respectively, and $i = \sqrt{-1}$. The optical absorption coefficient, $\alpha(E)$, may be related to the imaginary part of the dielectric function, $\epsilon_2(E)$, through the relationship

$$\alpha(E) \quad = \quad \frac{E}{\hbar c n(E)} \, \epsilon_2(E), \tag{1.3}$$

where $\hbar$ and c represent the reduced Planck's constant and the speed of light in a vacuum, respectively, and where $n(E)$ denotes the spectral dependence of the refractive index, where the complex refractive index,

$$\tilde{n}(E) \quad = \quad n(E) + ik(E), \tag{1.4}$$

$k(E)$ being the corresponding extinction coefficient. It is noted that the complex refractive index is related to the complex dielectric function through the relationship

$$\tilde{\epsilon}(E) \;=\; \tilde{n}^2(E). \tag{1.5}$$

From Eqs. (1.2), (1.4), and (1.5), one can thus conclude that

$$\epsilon_1(E) \;=\; n^2(E) - k^2(E), \tag{1.6}$$

and

$$\epsilon_2(E) \;=\; 2\,n(E)\,k(E). \tag{1.7}$$

These functions, $\alpha(E)$, $\epsilon_1(E)$, $\epsilon_2(E)$, $n(E)$, and $k(E)$, are collectively referred to as the optical functions, as they quantify the nature of the optical response of a given material. In this thesis, the optical response of amorphous semiconductors will be the focus of analysis. Following a presentation of the theoretical background required of this work, the analysis begins with a theoretical justification for the empirical model of Jellison and Modine [15], in which Kramers-Kronig consistent empirical expressions for $\epsilon_1(E)$ and $\epsilon_2(E)$ are formulated. Then, a model for the optical functions, i.e., $\epsilon_1(E)$ and $\epsilon_2(E)$, stemming from a model for the distributions of valence band and conduction

13

band electronic states, is developed. Finally, these models will be employed in order to fit some relevant experimental data. Conclusions, regarding the suitability of these models, will then be drawn from these fits. The main new results presented in this thesis pertain to the theoretical justification of the Kramers-Kronig consistent empirical expressions for $\epsilon_1(E)$ and $\epsilon_2(E)$ corresponding to the empirical model of Jellison and Modine [15] and the new model for these optical functions stemming from a model for the distributions of valence band and conduction band electronic states.

This thesis is organized in the following manner. In Chapter 2, the theoretical foundations for this analysis are provided. Then, in Chapter 3, a theoretical justification for the Kramers-Kronig consistent model of Jellison and Modine [15] is formulated. An alternate Kramers-Kronig model for the spectral dependence of $\epsilon_1(E)$ and $\epsilon_2(E)$, stemming from a model for the underlying distributions of valence band and conduction band electronic states, is then developed in Chapter 4. Finally, the conclusions of this analysis are presented in Chapter 5.

Chapter 2

Theoretical basis for analysis

2.1 The optical response of materials

The optical response of a material is primarily shaped by the distributions of valence band and conduction band electronic states and by the magnitude of the optical transition matrix elements which couple the electronic states between which optical transitions occur. The distributions of valence band and conduction band electronic states determines what optical transitions can occur in a given material. The magnitude of the optical transition matrix elements, however, determine the probability of such optical transitions occurring. The primary goal of this analysis is the development of Kramers-Kronig consistent models for the spectral dependence of the real and imaginary components of the dielectric function, $\epsilon_1(E)$ and $\epsilon_2(E)$, respectively, for the case of amorphous semiconductors. In order to achieve this goal, the role that each of these factors plays in shaping the optical

15

response of an amorphous semiconductor must be well understood.

In this chapter, the theoretical foundations for the work presented in this thesis are provided. Initially, an expression for the spectral dependence of the imaginary part of the dielectric function, $\epsilon_2(E)$, in terms of the valence band and conduction band energy levels and the magnitude of the corresponding optical transition matrix elements, is presented. Then, through the introduction of a number of suitable assumptions, a relationship between the valence band and conduction band distributions of electronic states and the spectral dependence of $\epsilon_2(E)$ is developed. Two particular formulations for this relationship are developed: (1) a momentum matrix element formulation, and (2) a dipole matrix element formulation, these formulations being related to each other. For each of these formulations, an aggregate matrix element is employed. The joint density of states (JDOS) function, $J(E)$, is introduced as a corollary to this analysis. The Kramers-Kronig relations are then presented, these relating the spectral dependence of $\epsilon_1(E)$ with $\epsilon_2(E)$ and the spectral dependence of $\epsilon_2(E)$ with $\epsilon_1(E)$. A number of models, for both $\epsilon_1(E)$ and $\epsilon_2(E)$, are then presented. Finally, three sets of experimental data, corresponding to different samples of a-Si, are presented, these experimental data sets being used in the subsequent analysis.

This chapter is organized in the following manner. In Section 2.2, an expression for the spectral dependence of the imaginary part of the dielectric function, $\epsilon_2(E)$, in terms of the valence band and conduction band energy levels and the magnitude of the corresponding optical transition matrix elements, is presented. Then, in Section 2.3, three critical assumptions are introduced, these allowing one to relate the spectral dependence of $\epsilon_2(E)$ with that of $J(E)$. In Section 2.4, a momentum matrix element formulation for the relationship between the imaginary part of the dielectric function, $\epsilon_2(E)$, and the distributions of the valence band and conduction band electronic states is developed, the JDOS function and the aggregate momentum matrix element being introduced as a byproduct of this particular formulation. A dipole matrix element formulation for the relationship between the imaginary part of the dielectric function, $\epsilon_2(E)$, and the distributions of the valence band and conduction band electronic states is then developed in Section 2.5, the aggregate dipole matrix element being proposed as a byproduct of this analysis. The free electron model, for the distributions of electronic states, is then presented in Section 2.6. The spectral dependence of this JDOS function, assuming free electron distributions of valence band and conduction band electronic states, is then presented in Section 2.7.

The Kramers-Kronig relationships between the real and imaginary parts of the dielectric function, $\epsilon_1(E)$ and $\epsilon_2(E)$, respectively, are discussed in Section 2.8, the time-symmetry requirements demanded of these relations being featured. A number of models for the spectral dependence of the optical functions, $\epsilon_1(E)$ and $\epsilon_2(E)$, are then presented in Section 2.9. Finally, experimental a-Si data sets, corresponding to $\epsilon_1(E)$ and $\epsilon_2(E)$, are presented in Section 2.10, these data sets being used in the subsequent analysis.

2.2 The spectral dependence of the imaginary part of the dielectric function

Optical transitions occur from occupied electronic states in the valence band (initial states) to unoccupied electronic states in the conduction band (final states). Within the framework of a one-electron picture, assuming linear optical response, Jackson *et al.* [16] assert that the imaginary part of the dielectric function,

$$\epsilon_2(E) = \left(\frac{2\pi q\hbar}{mE}\right)^2 \frac{2}{V} \sum_{v,c} |\vec{\boldsymbol{\eta}} \cdot \vec{\boldsymbol{P}}_{v,c}|^2 \delta(E_c - E_v - E), \qquad (2.1)$$

where q denotes the electron charge, m represents the electron mass, V is the illuminated volume, $\vec{\boldsymbol{\eta}}$ is the polarization vector of the incident light,

and E is the photon energy; the $\delta(\cdot)$ terms refer to the Dirac delta function. E_v and E_c denote the energy levels of representative valence band and conduction band electronic states, $|v\rangle$ and $|c\rangle$, respectively. $\vec{P}_{v,c}$ represents the momentum matrix element that couples these particular electronic states in an optical transition process; in quantum mechanics, this matrix element, $\vec{P}_{v,c} = \langle c|\vec{P}|v\rangle$, where $\vec{P}$ denotes the momentum operator. The $|\vec{\eta} \cdot \vec{P}_{v,c}|^2$ operation refers to taking the complex modulus squared of the complex number $\vec{\eta} \cdot \vec{P}_{v,c}$. The summation in Eq. (2.1) is performed over all of the occupied valence band and unoccupied conduction band single-spin electronic states.

2.3 Three critical assumptions

Eq. (2.1) expresses the spectral dependence of the imaginary part of the dielectric function, $\epsilon_2(E)$, in terms of the valence band and conduction band energy levels and the magnitude of the corresponding momentum matrix elements. This expression applies to both the crystalline and amorphous cases. In order to relate $\epsilon_2(E)$ with the underlying distributions of valence band and conduction band electronic states for the specific case of amorphous semiconductors, three critical assumptions are introduced into the analysis:

(1) it is assumed that the incident light is unpolarized, (2) it is assumed that the disorder that is present in an amorphous semiconductor completely relaxes the momentum conservation rules, and (3) it is assumed that zero-temperature statistics apply. The consequences of each approximation is outlined subsequently.

The absence of polarization simplifies Eq. (2.1). With random polarization, assuming that all of the significant momentum matrix elements are of the same order of magnitude, the average value of $|\vec{\eta} \cdot \vec{P}_{v,c}|^2$ reduces to $\frac{1}{3}|P_{v,c}|^2$, where $|P_{v,c}|$ denotes the amplitude of the momentum matrix element. As a result, Eq. (2.1) reduces to

$$\epsilon_2(E) \;=\; (2\pi q)^2 \, \frac{\hbar^2}{m^2 E^2} \frac{2}{3V} \sum_{v,c} |P_{v,c}|^2 \delta(E_c - E_v - E). \qquad (2.2)$$

In a crystalline semiconductor, momentum must be conserved in an optical transition. In an amorphous semiconductor, however, the momentum conservation rules are relaxed. That is, optical transitions can occur from every occupied state (of a particular spin) in the valence band to every unoccupied state (of the same spin) in the conduction band; spin-flips are not permitted during an optical transition. As a consequence, in a crystalline semiconductor, the $|P_{v,c}|$ values vary greatly, depending upon whether momentum is conserved or not, while in an amorphous semiconductor, $|P_{v,c}|$ is

essentially constant for all cases. This greatly simplifies the analysis.

The contrast between c-Si and a-Si is instructive. Consider the case of N silicon atoms. For the case of c-Si, from a given single-spin state in the valence band, four optical transitions are possible; there are $\frac{N}{2}$ possible values of crystal momentum for the case of c-Si. For the case of a-Si, however, $2N$ optical transitions are possible. These possible optical transitions are depicted in Figure 2.1. If the overall "optical strength" of c-Si and a-Si is similar, it seems likely that the $|P_{v,c}|$ matrix elements associated with the small number of possible c-Si optical transitions will be of a much greater magnitude than that of their more numerous a-Si counterparts. Later on in this analysis, a normalized matrix element is introduced in order to allow for a direct comparison between the c-Si and a-Si matrix elements, where the weighting factor is directly proportional to the ratio between the number of allowed optical transitions for the c-Si and a-Si cases.

The final assumption that is introduced into this analysis is that of zero-temperature statistics. In Figure 2.2, the occupancy function,

$$f(E) = \frac{1}{1 + \exp(\frac{E - E_F}{K_B T})},$$ (2.3)

is depicted as a function of an energy, E, for a variety of different temperature selections, E_F denoting the Fermi energy level. It is noted that as the
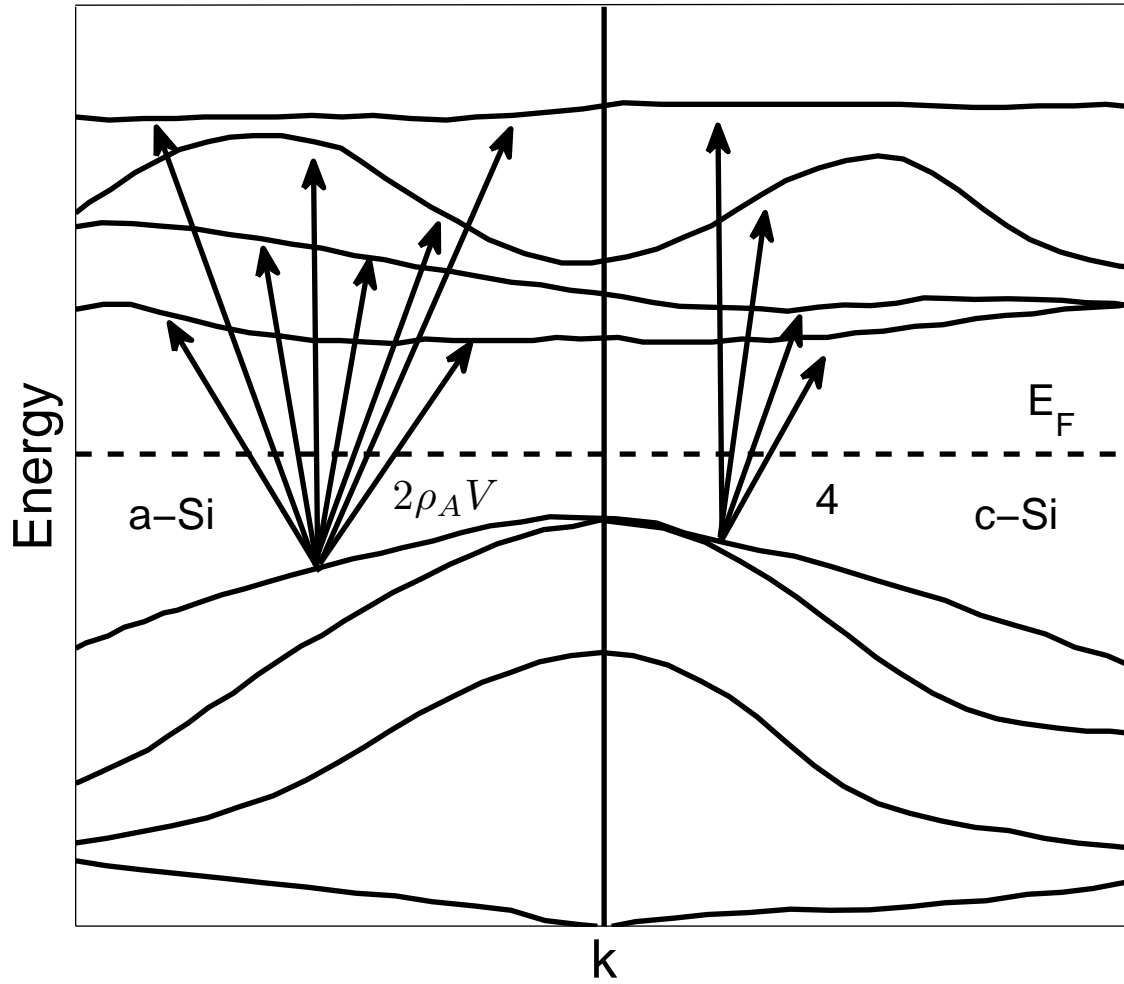
Figure 2.1: The possible optical transitions within c-Si and a-Si. This figure is after Jackson *et al.* [16].
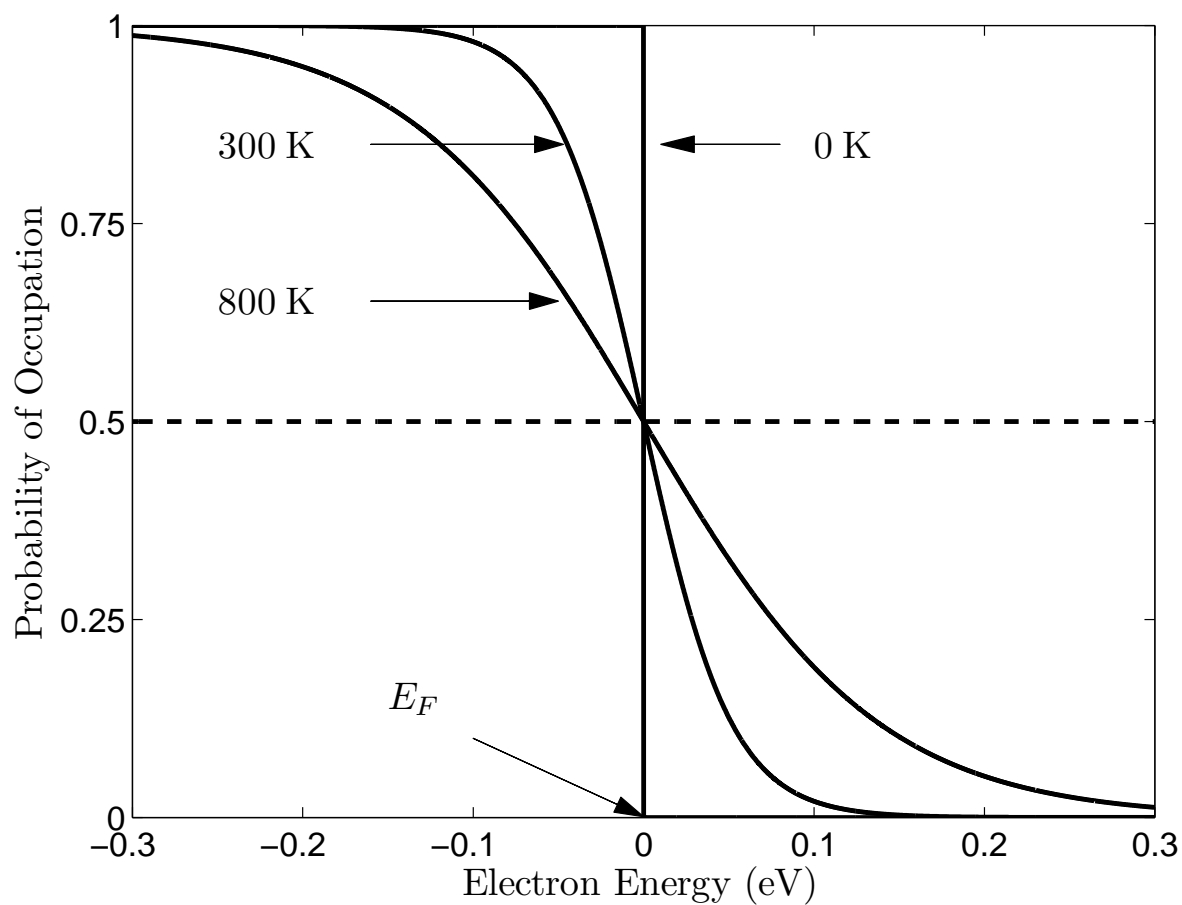
Figure 2.2: The occupancy function, $f(E)$, as a function of energy, E, for various selections of temperature. The Fermi energy level, E_F, is the reference energy level, i.e., $E_F = 0$ eV.

temperature goes to zero that this function, sometimes referred to as the Fermi-Dirac function, reduces to a step function, where the step occurs at the Fermi energy level, E_F. For the case of semiconductors, considering that the Fermi energy level, E_F, is typically in the middle of the energy gap, this implies that at zero temperature, all of the valence band electronic states are fully occupied and all of the conduction band electronic states are completely unoccupied. This assumption simplifies the subsequent analysis.

2.4 A momentum matrix element formulation

It will be assumed that the overall "optical strength" of c-Si is identical to that of a-Si. As was discussed earlier, if this is the case it would seem reasonable to expect that the small number of non-zero c-Si momentum matrix elements will be larger in magnitude than their much more numerous a-Si counterparts. In order to allow for a direct contrast between these matrix elements, one could conceive of normalizing the a-Si momentum matrix elements by a factor that is proportional to the ratio between the number of allowed optical transitions, i.e., $\frac{2N}{4}$. Letting ρ_A denote the density of silicon

atoms within a-Si, this normalization factor becomes $\frac{2\rho_A V}{4}$.

In order to allow for a direct relationship between $\epsilon_2(E)$ and the distributions of valence band and conduction band electronic states, one can introduce an aggregate momentum matrix element

$$P^2(E) \equiv \frac{\rho_A V}{2} \frac{\sum_{v,c} |P_{v,c}|^2 \delta(E_c - E_v - E)}{\sum_{v,c} \delta(E_c - E_v - E)}, \qquad (2.4)$$

where the $\frac{\rho_A V}{2}$ prefactor allows for a direct comparison between the momentum matrix elements associated with c-Si and a-Si. From Eqs. (2.2) and (2.4), it can now be shown that

$$\epsilon_2(E) = (2\pi q)^2 \frac{\hbar^2}{m^2 E^2} \frac{2}{3V} \left(\frac{2}{\rho_A V}\right) P^2(E) \sum_{v,c} \delta(E_c - E_v - E). \quad (2.5)$$

The term $\sum_{v,c} \delta(E_c - E_v - E)$ provides for the number of possible optical transitions between the occupied valence band and unoccupied conduction band electronic states separated by the energy E. Defining the JDOS function,

$$J(E) \equiv \frac{4}{V^2} \sum_{v,c} \delta(E_c - E_v - E), \qquad (2.6)$$

from Eq. (2.5), it can now be seen that

$$\epsilon_2(E) = (2\pi q)^2 \frac{\hbar^2}{m^2 E^2} \frac{2}{3V} \frac{V^2}{4} \left(\frac{2}{\rho_A V}\right) P^2(E) J(E). \qquad (2.7)$$

Thus, the spectral dependence of $\epsilon_2(E)$ reduces to a product of a prefactor, the reciprocal of E^2, the aggregate momentum matrix element, and the JDOS function, $J(E)$.

The valence band density of states (DOS) function, $N_v(E)$, where $N_v(E)\Delta E$ represents the number of valence band electronic states between $[E, E+\Delta E]$, per unit volume, may be expressed as the sum over all of the valence band single-spin electronic states divided by the volume, i.e.,

$$N_v(E) \;=\; \frac{2}{V}\sum_v \delta(E - E_v), \tag{2.8}$$

where the factor of 2 arises as a consequence of the fact that each electronic state is a single-spin state, i.e., there are two possible spins. Similarly, the conduction band DOS function, $N_c(E)$, where $N_c(E)\Delta E$ represents the number of conduction band electronic states between $[E, E + \Delta E]$, per unit volume, may be expressed as the sum over all of the conduction band single-spin electronic states divided by the volume, i.e.,

$$N_c(E) \;=\; \frac{2}{V}\sum_c \delta(E - E_c), \tag{2.9}$$

where the factor of 2 arises as a consequence of the fact that each electronic state is a single-spin state.

Assuming that all valence band states are fully occupied and that all

conduction band states are completely unoccupied, i.e., the zero-temperature assumption, it may be shown that the JDOS function may be expressed as an integral over the product of the valence band and conduction band DOS functions, i.e.,

$$J(E) \;\; = \;\; \int_{-\infty}^{\infty} N_v(\xi) N_c(E + \xi) d\xi. \tag{2.10}$$

From Eqs. (2.5) and (2.6), one can thus conclude that

$$\epsilon_2(E) \;\; = \;\; \frac{(2\pi q)^2}{3\rho_A} \frac{\hbar^2}{m^2 E^2} \, P^2(E) \, J(E). \tag{2.11}$$

For a wide variety of amorphous semiconductor experimental analyzes, it has been assumed that the aggregate momentum matrix element, $P^2(E)$, exhibits a constant spectral dependence with respect to energy, E. This is referred to as the constant momentum matrix element assumption. This assumption, which found its origins in the analysis at Tauc *et al.* [18], was widely accepted by researchers in the field until the early 1980s. Despite this acceptance, it lacks a theoretical justification. Moreover, Cody *et al.* [19] demonstrated that experimental results interpreted within the framework of this assumption are fundamentally inconsistent. Accordingly, other models for the spectral dependence of $\epsilon_2(E)$ are sought.

2.5 A dipole matrix element formulation

Cody *et al.* [19] provided experimental data which challenged the validity of the constant momentum matrix element assumption. For the purposes of their study, Cody *et al.* [19] prepared a large number of a-Si samples under identical conditions, but with different film thicknesses. They then measured the spectral dependence of the optical functions using transmission and reflectance measurements on these samples. Cody *et al.* [19] noted that while fits to this data, determined assuming a constant momentum matrix element, are satisfactory, they become greatly improved if one instead assumes a constant dipole matrix element. Moreover, such an assumption removes a film thickness dependence artifact that was noted by Cody *et al.* [19] within the framework of the constant momentum matrix element assumption. Accordingly, it is instructive to recast our formulation in terms of the spectral dependence of the dipole matrix element.

Taking into account the experimental evidence provided by Cody *et al.* [19], Jackson *et al.* [16] recast Eq. (2.1) into a form in which the matrix elements are instead expressed in terms of the dipole matrix elements as opposed to the momentum matrix elements, i.e., $\vec{\mathcal{R}}_{v,c} = \langle c|\vec{\mathcal{R}}|v\rangle$, where $\vec{\mathcal{R}}$ denotes the

dipole operator. From the commutator relations, Jackson *et al.* [16] find that

$$\sum_{v,c} |\eta \cdot \boldsymbol{P}_{v,c}|^2 \delta(E_c - E_v - E) = \left(\frac{mE}{\hbar}\right)^2 \sum_{v,c} |\eta \cdot \boldsymbol{\mathcal{R}}_{v,c}|^2 \delta(E_c - E_v - E).$$

(2.12)

As before, if the incident light is unpolarized, the average value of $|\vec{\eta} \cdot \vec{\mathcal{R}}_{v,c}|^2$ reduces to $\frac{1}{3}|\mathcal{R}_{v,c}|^2$, where $|\mathcal{R}_{v,c}|$ denotes the amplitude of the dipole matrix element. Accordingly, Jackson *et al.* [16] conclude that

$$\epsilon_2(E) = (2\pi q)^2 \frac{2}{3V} \sum_{v,c} |\mathcal{R}_{v,c}|^2 \delta(E_c - E_v - E).$$

(2.13)

Introducing an aggregate dipole matrix element, defined and normalized in a manner similar to that introduced earlier for the case of the momentum matrix formalism, Jackson *et al.* [16] proposed that,

$$\mathcal{R}^2(E) \equiv \frac{\rho_A V}{2} \frac{\sum_{v,c} |\mathcal{R}_{v,c}|^2 \delta(E_c - E_v - E)}{\sum_{v,c} \delta(E_c - E_v - E)},$$

(2.14)

where, as before, ρ_A denotes the atomic density. For this definition, it is noted that Eq. (2.13) may be represented as

$$\epsilon_2(E) = (2\pi q)^2 \frac{2}{3V} \left(\frac{2}{\rho_A V}\right) \mathcal{R}^2(E) \sum_{v,c} \delta(E_c - E_v - E).$$

(2.15)

From Eqs. (2.6) and (2.15), one can thus conclude that

$$\epsilon_2(E) = \frac{(2\pi q)^2}{3\rho_A} \mathcal{R}^2(E) J(E).$$

(2.16)

29

That is, the spectral dependence of the imaginary part of the dielectric function, $\epsilon_2(E)$, is proportional to the product of a prefactor, $\mathcal{R}^2(E)$, and $J(E)$. Given that the density of the silicon atoms within a-Si is typically around 4.4×10^{22} cm^{-3} [17], it can thus be seen that, for the specific case of a-Si, Eq. (2.16) may be re-expressed as

$$\epsilon_2(E) \;\; = \;\; 4.3 \times 10^{-45} \, \mathcal{R}^2(E) \, J(E), \qquad (2.17)$$

where $\mathcal{R}^2(E)$ is in units of Å^2 and $J(E)$ is in the units of cm^{-6}eV^{-1} [16, 17]. In light of the experimental results of Cody *et al.* [19], the spectral dependence of $\mathcal{R}^2(E)$ is often assumed to be constant. This is referred to as the constant dipole matrix element assumption.

It is noted, from Eqs. (2.11) and (2.16), that the relationship between the aggregate momentum matrix element squared average and the aggregate dipole matrix element squared average is found to be

$$P^2(E) \;\; = \;\; \frac{m^2 E^2}{\hbar^2} \, \mathcal{R}^2(E). \qquad (2.18)$$

Eq. (2.18) allows one to relate the one formulation for the spectral dependence of the imaginary part of the dielectric function, $\epsilon_2(E)$, with the other.

2.6 Free electron model of the DOS functions

The spectral dependence of the JDOS function depends upon a convolution over the valence band and conduction band DOS functions; recall Eq. (2.10). Accordingly, the determination of these functions is of paramount concern. While the exact form of these DOS functions depends critically upon the exact potential distribution, the free electron DOS function provides a useful limiting result that is often employed for theoretical benchmarking purposes.

Consider the electronic states within a cubic box, of dimensions $L \times L \times L$, surrounded by an infinitely high potential barrier, as seen in Figure 2.3. It will be assumed that the potential within the box itself is nil. From quantum mechanics, for steady-state conditions, the wavefunctions associated with the corresponding bound electron states may be determined from Schrödinger's equation, i.e.,

$$\frac{\hbar^2}{2m} \, \bigtriangledown^2 \Psi(\vec{r}) + V(\vec{r})\Psi(\vec{r}) \;\; = \;\; E\Psi(\vec{r}), \tag{2.19}$$

where $\hbar$, m, $V(\vec{r})$, and E represent the reduced Planck's constant, the mass of the electron, the potential energy, and the electron energy, respectively.

$V(x,y,z) = 0$ - inside box

$V(x,y,z) = \infty$ - outside box
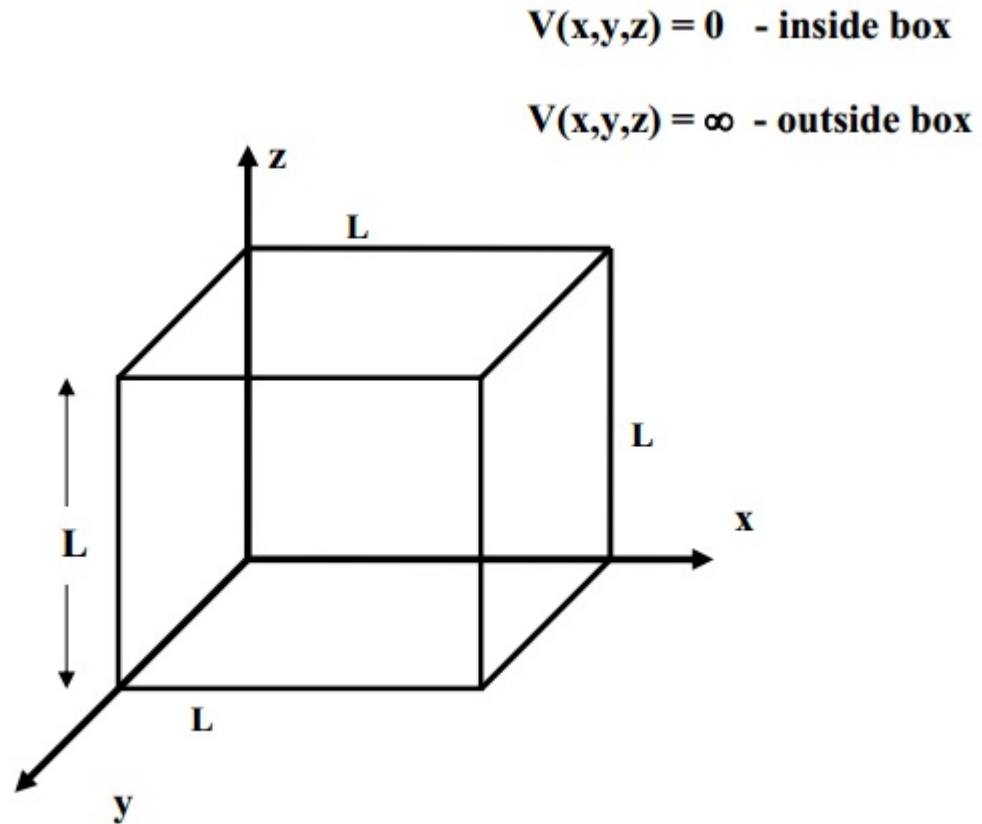
Figure 2.3: A schematic representation of a three-dimensional potential energy well. This figure is from Thevaril [13].

$\bigtriangledown^2$ denotes the mathematical operator $\frac{\partial}{\partial x^2} + \frac{\partial}{\partial y^2} + \frac{\partial}{\partial z^2}$ in three-dimensions. It may be shown that

$$\Psi(\vec{r}) \;=\; \Psi_{n_x,n_y,n_z}(x,y,z) = \left(\frac{2}{L}\right)^{3/2} \sin\left(\frac{\pi n_x}{L}x\right) \sin\left(\frac{\pi n_y}{L}y\right) \sin\left(\frac{\pi n_z}{L}z\right),$$

$$(2.20)$$

where n_x, n_y, and n_z are positive integers, associated with the electron motion in the different directions; these are the quantum numbers. The energy of the corresponding electronic states may be found by substituting the obtained wavefunction, i.e., Eq. (2.20), back into the Schrödinger's equation, i.e.,

$$E_{n_x,n_y,n_z} \;=\; \frac{\hbar^2}{2m}\left[\left(\frac{\pi n_x}{L}\right)^2 + \left(\frac{\pi n_y}{L}\right)^2 + \left(\frac{\pi n_z}{L}\right)^2\right], \qquad (2.21)$$

where E_{n_x,n_y,n_z} represents the energy associated with the n_x, n_y, and n_z wavefunction, $\Psi_{n_x,n_y,n_z}(x,y,z)$, the labeling integers, n_x, n_y, and n_z, exactly corresponding to the aforementioned quantum numbers.

In the continuum limit, i.e., for E sufficiently large, the corresponding DOS function may be shown to be

$$N(E) \;=\; \begin{cases} \sqrt{2}\,\dfrac{m^{3/2}}{\pi^2 \hbar^3}\sqrt{E}, & E \geq 0 \\[4ex] 0, & E < 0 \end{cases}. \qquad (2.22)$$

33

Eq. (2.22) is often referred to the free electron DOS model; within the well, the potential is nil, i.e., the electrons are "free". This form for the DOS function is often assumed in analyzes of amorphous semiconductors.

2.7 The spectral dependence of the JDOS function

It is often useful to employ the free-electron model for the valence band and conduction band DOS functions in the evaluation of the JDOS function. This model suggests that the distribution of electronic states exhibits a square-root functional dependence on the energy above the conduction band minimum and below the valence band maximum. Following O'Leary [17], one can set the valence band DOS function

$$N_v(E) = \begin{cases} 0, & E > E_v \\ \\ N_{vo}\sqrt{E_v - E}, & E \leq E_v \end{cases}, \qquad (2.23)$$

and the conduction band DOS function

$$
N_c(E) \;=\;
\begin{cases}
N_{co}\sqrt{E - E_c}, & E \geq E_c \\[2em]
0, & E < E_c
\end{cases}
\;,
\tag{2.24}
$$

where N_{vo} and N_{co} represent the valence band and conduction band DOS prefactors, respectively, and E_v and E_c represent the valence band and conduction band band edges; these DOS functions are also known as the Tauc DOS functions. The resultant distributions of electronic states, for this specific case, are depicted in Figure 2.4, nominal values of N_{vo}, N_{co}, E_v, and E_c being employed for the purposes of this analysis; in particular, N_{vo} and N_{co} are both set to 2×10^{22} cm^{-3} eV$^{-3/2}$, E_v is set to 0 eV, and E_c is set to 2 eV, these values being representative of the case of a-Si. Through the use of Eq. (2.10), it may be shown that

$$
J(E) \;=\; N_{vo}N_{co}
\begin{cases}
\dfrac{\pi}{8}(E - E_g)^2, & E \geq E_g \\[2em]
0, & E < E_g
\end{cases}
\;,
\tag{2.25}
$$

where $E_g \equiv E_c - E_v$ represents the energy gap of the material. The spectral dependence of the corresponding JDOS function is depicted in Figures 2.5 and 2.6. This is known as the Tauc JDOS function after the pioneering work
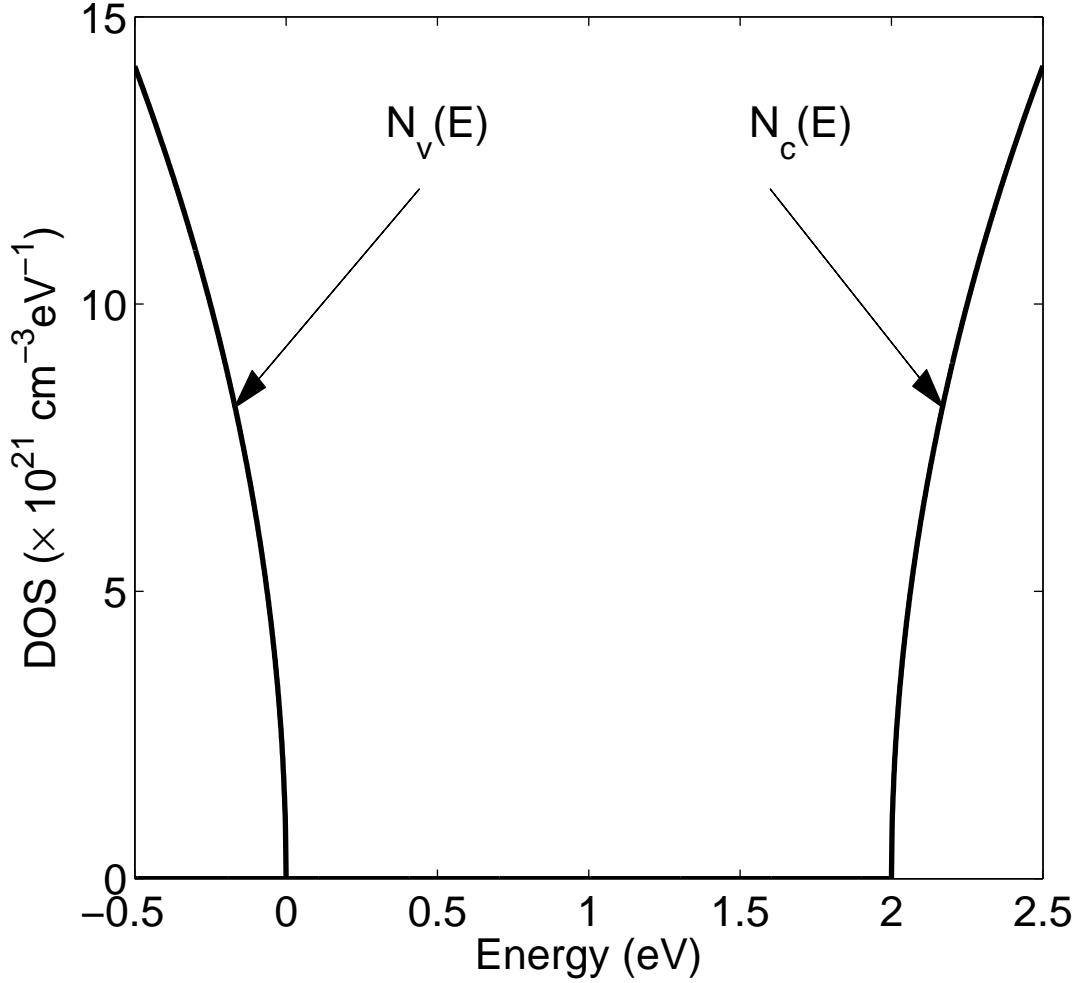
Figure 2.4: The valence band DOS function, $N_v(E)$, and the conduction band DOS function, $N_c(E)$, plotted as a function of energy, E, determined through Eqs. (2.23) and (2.24), respectively, assuming the nominal DOS modeling parameter selections, $N_{vo} = N_{co} = 2 \times 10^{22}$ cm^{-3} eV$^{-3/2}$, $E_v = 0$ eV, and $E_c = 2$ eV. These values are representative of the case of a-Si.
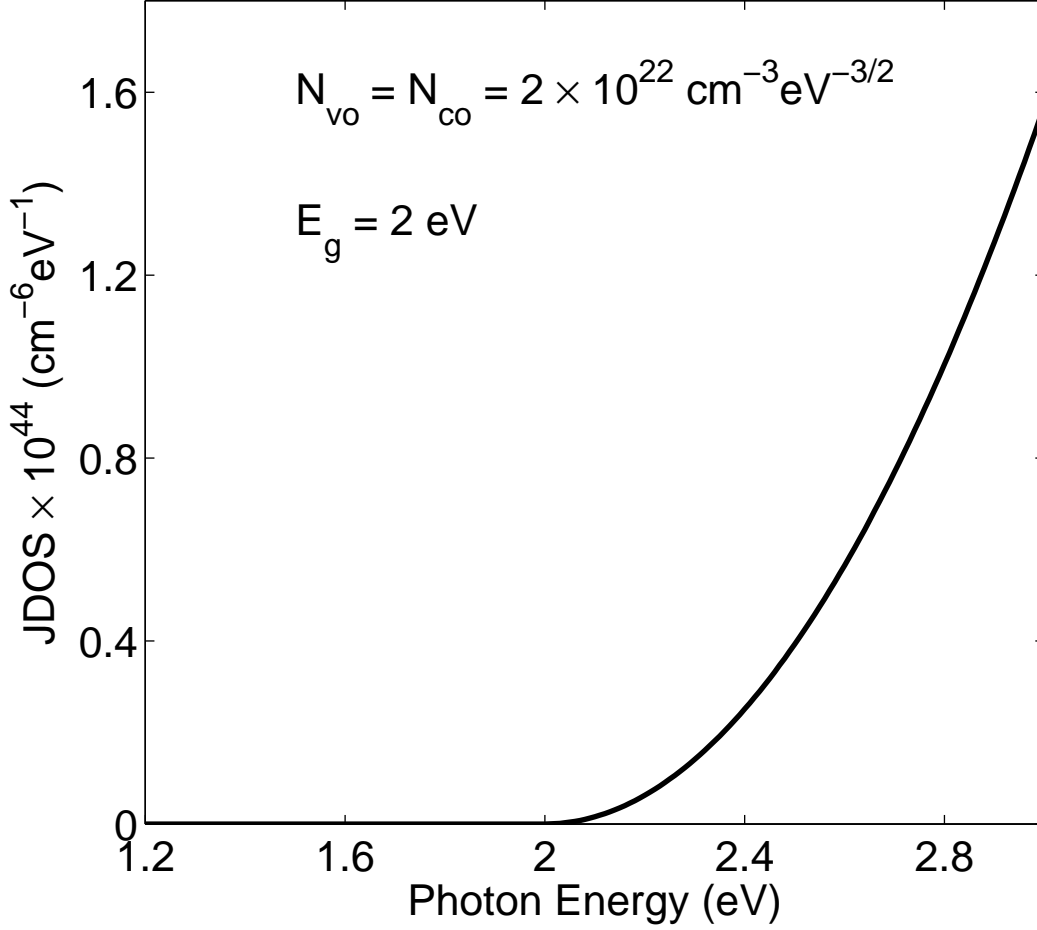
Figure 2.5: The JDOS function, $J(E)$, plotted as a function of the photon energy, E, determined through Eq. (2.25), assuming the nominal DOS modeling parameter selections, $N_{vo} = N_{co} = 2 \times 10^{22}$ cm^{-3} eV$^{-3/2}$, $E_v = 0$ eV, and $E_c = 2$ eV. These values are representative of the case of a-Si. This plot is depicted on a linear scale.
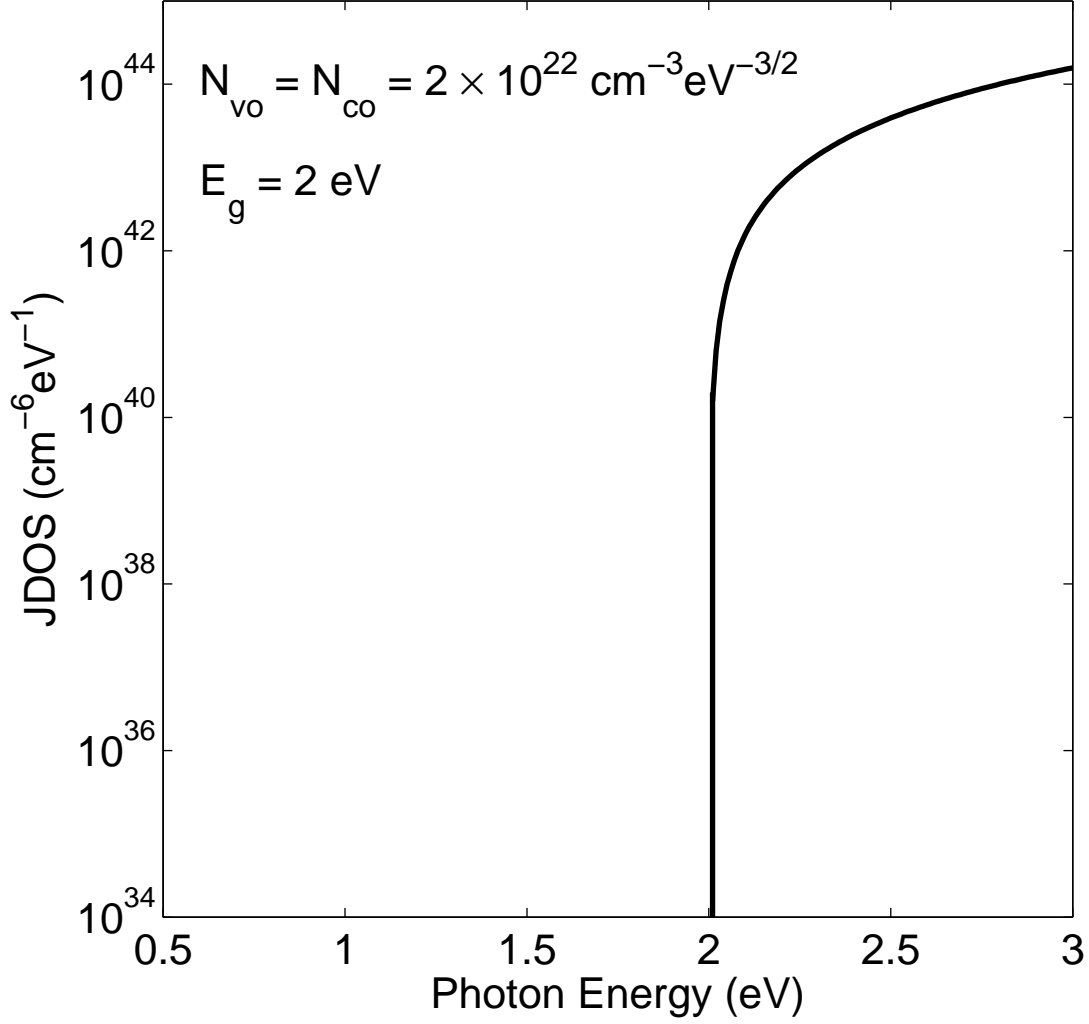
Figure 2.6: The JDOS function, $J(E)$, plotted as a function of the photon energy, E, determined through Eq. (2.25), assuming the nominal DOS modeling parameter selections, $N_{vo} = N_{co} = 2 \times 10^{22}$ cm^{-3} eV$^{-3/2}$, $E_v = 0$ eV, and $E_c = 2$ eV. These values are representative of the case of a-Si. This plot is depicted on a logarithmic scale.

of Tauc *et al.* [18].

2.8   Kramers-Kronig relations

As a consequence of causality, there is a relationship between the spectral dependence of the real and imaginary parts of the dielectric function, $\epsilon_1(E)$ and $\epsilon_2(E)$, respectively. Consider a time-dependent electric field, $E(t)$, applied to a solid that produces a current density, $J(t)$, in response. The variations with respect to position of these quantities are neglected. If only weak fields are considered, then a general linear relationship between E and J exists, where

$$J(t) \;=\; \int_{-\infty}^{\infty} \Sigma(t - t')\, E(t')dt', \tag{2.26}$$

$\Sigma(t)$ denoting the time-dependent conductivity. Through a Fourier transform on Eq. (2.26), one obtains

$$\mathcal{J}(\omega) \;=\; \sigma(\omega)\xi(\omega), \tag{2.27}$$

where $\mathcal{J}(\omega)$, $\xi(\omega)$, and $\sigma(\omega)$ are the Fourier transforms of J, E, and Σ, respectively, i.e.,

$$\mathcal{J}(\omega) = \int_{-\infty}^{\infty} J(t)e^{i\omega t}dt, \tag{2.28a}$$

$$\xi(\omega) = \int_{-\infty}^{\infty} E(t)e^{i\omega t}dt, \tag{2.28b}$$

and

$$\sigma(\omega) = \int_{-\infty}^{\infty} \Sigma(t)e^{i\omega t}dt. \tag{2.28c}$$

It is also noted that the inverse Fourier transforms become

$$J(t) = \frac{1}{2\pi} \int_{-\infty}^{\infty} \mathcal{J}(\omega)e^{-i\omega t}d\omega, \tag{2.29a}$$

$$E(t) = \frac{1}{2\pi} \int_{-\infty}^{\infty} \xi(\omega)e^{-i\omega t}d\omega, \tag{2.29b}$$

and

$$\Sigma(t) = \frac{1}{2\pi} \int_{-\infty}^{\infty} \sigma(\omega)e^{-i\omega t}d\omega. \tag{2.29c}$$

In order to further the analysis, two critical assumptions have to be made: (1) $\Sigma(t)$ is zero for negative values of its argument, and (2) $J(t) = 0$ for $t < t_0$, where t_0 is the earliest value of t' for which $E(t') \neq 0$. The first assumption leads to the fact that $\sigma(\omega)$ is an analytic function in the upper half of the complex ω plane. According to Cauchy's theorem, the integral in Eq. (2.29c) should vanish for $\sigma(\omega)$ being analytic in the upper half plane. It may thus

be shown that

$$\sigma(\omega_0) \;=\; \frac{1}{2\pi i} \oint_{C_1} \frac{\sigma(\omega)}{\omega - \omega_0} d\omega. \tag{2.30}$$

At first, the contour of integration of Eq. (2.30) may be chosen to be a small

circle, C_1, about ω_0, as shown in Figure 2.7. It is known that the distortion

of C_1 into a larger contour of integration, C_2, does not change the result; see

Figure 2.7, i.e.,

$$\sigma(\omega_0) \;=\; \frac{1}{2\pi i} \oint_{C_1} \frac{\sigma(\omega)}{\omega - \omega_0} d\omega = \frac{1}{2\pi i} \oint_{C_2} \frac{\sigma(\omega)}{\omega - \omega_0} d\omega. \tag{2.31}$$

Assuming that $\sigma(\omega) \to 0$ for $|\omega| \to \infty$, then only contributions from the

real axis play a role in determining the integral in Eq. (2.30). Considering

that ω_r is the frequency along the real axis, then it may be shown that

$$\sigma(\omega_0) \;=\; \frac{1}{2\pi i} \int_{-\infty}^{\infty} \frac{\sigma(\omega_r)}{\omega_r - \omega_0} d\omega_r. \tag{2.32}$$

It is noted that ω_0 may be expressed as

$$\omega_0 \;=\; \omega + i\omega'. \tag{2.33}$$

Since

$$\lim_{\omega' \to 0} \frac{1}{\omega_r - \omega - i\omega'} \;=\; P\frac{1}{\omega_r - \omega} + i\pi\delta(\omega_r - \omega), \tag{2.34}$$

41
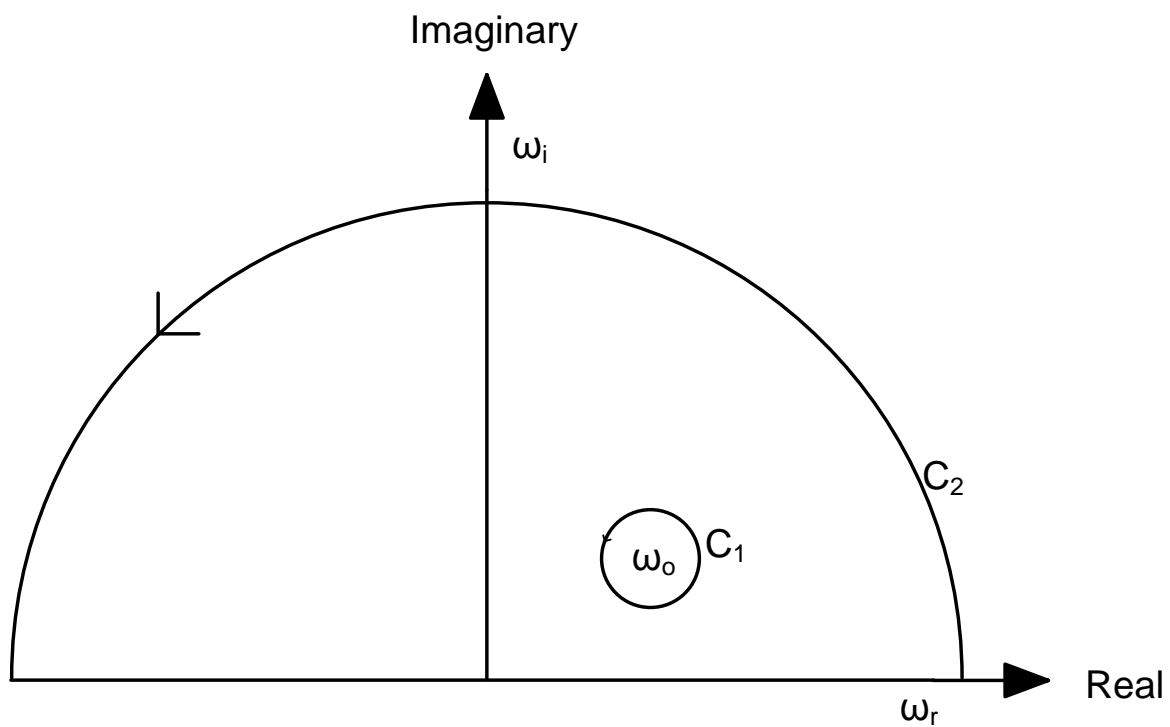
Figure 2.7: Contours of integration for Eq. (2.30).

where P denotes the principal value, from Eqs. (2.32) and (2.34), it is seen that

$$\sigma(\omega) \;=\; \frac{1}{\pi i} P \int_{-\infty}^{\infty} \frac{\sigma(\omega_r)}{\omega_r - \omega}\, d\omega_r. \tag{2.35}$$

From Eq. (2.35), it is seen that $\sigma(\omega)$ is a complex quantity, i.e.,

$$\sigma(\omega) \;=\; \sigma_1(\omega) + i\sigma_2(\omega). \tag{2.36}$$

Thus, it can be seen that

$$\sigma_1(\omega) = \frac{1}{\pi} P \int_{-\infty}^{\infty} \frac{\sigma_2(\omega_r)}{\omega_r - \omega}\, d\omega_r, \tag{2.37a}$$

and

$$\sigma_2(\omega) = -\frac{1}{\pi} P \int_{-\infty}^{\infty} \frac{\sigma_1(\omega_r)}{\omega_r - \omega}\, d\omega_r. \tag{2.37b}$$

That is, $\sigma_1(\omega)$ and $\sigma_2(\omega)$ are Hilbert transforms of each other. As a real $E(t)$ produces a real $J(t)$, then the time-dependent conductivity, $\sigma(t)$, must also be real. This requires that

$$[\sigma_1(\omega_r) + i\sigma_2(\omega_r)]^* \;=\; \sigma(-\omega_r). \tag{2.38}$$

As a result,

$$\sigma_1(\omega_r) = \sigma_1(-\omega_r), \tag{2.39a}$$

and

$$\sigma_2(\omega_r) = -\sigma_2(-\omega_r). \tag{2.39b}$$

So, from Eq. (2.37a), it is seen that

$$
\begin{aligned}
\sigma_1(\omega) &= \frac{1}{\pi} P \left[\int_{-\infty}^{0} \frac{\sigma_2(\omega_r)}{\omega_r - \omega} \, d\omega_r + \int_{0}^{\infty} \frac{\sigma_2(\omega_r)}{\omega_r - \omega} \, d\omega_r \right], \\
&= \frac{1}{\pi} P \int_{0}^{\infty} \sigma_2(\omega_r) \left[\frac{1}{\omega_r - \omega} + \frac{1}{\omega_r + \omega} \right] d\omega_r, \\
&= \frac{2}{\pi} P \int_{0}^{\infty} \frac{\omega_r \sigma_2(\omega_r)}{\omega_r^2 - \omega^2} \, d\omega_r.
\end{aligned} \tag{2.40}
$$

Similarly,

$$
\sigma_2(\omega) = -\frac{2\omega}{\pi} P \int_{0}^{\infty} \frac{\sigma_1(\omega_r)}{\omega_r^2 - \omega^2} \, d\omega_r. \tag{2.41}
$$

Eqs. (2.40) and (2.41) constitute the Kramers-Kronig relations, applied to conductivity.

It is also possible to develop Kramers-Kronig relations for the real and imaginary parts of the dielectric function. Since

$$
\epsilon(\omega) = \epsilon_0 + i \frac{\sigma(\omega)}{\omega}, \tag{2.42}
$$

it may be shown that

$$
\epsilon_1(\omega) = 1 - \left[\frac{\sigma_2(\omega)}{\epsilon_0 \omega} \right], \tag{2.43a}
$$

and

$$
\epsilon_2(\omega) = \frac{\sigma_1(\omega)}{\epsilon_0 \omega}. \tag{2.43b}
$$

Thus,

$$\epsilon_1(\omega) = 1 + \frac{2}{\pi} P \int_0^\infty \frac{\omega_r \epsilon_2(\omega_r)}{\omega_r^2 - \omega^2} \, d\omega_r, \tag{2.44a}$$

and

$$\epsilon_2(\omega) = \frac{2}{\pi\omega} P \int_0^\infty \frac{\omega_r^2[1 - \epsilon_1(\omega_r)]}{\omega_r^2 - \omega^2} \, d\omega_r. \tag{2.44b}$$

So, the real part of the dielectric function, $\epsilon_1(E)$, is related to the imaginary part of the dielectric function, $\epsilon_2(E)$, through the Kramers-Kronig transformation,

$$\epsilon_1(E) = \epsilon_{1\infty} + \frac{2}{\pi} P \int_{E_g}^\infty \frac{u\epsilon_2(u)}{u^2 - E^2} \, du, \tag{2.45}$$

where $\epsilon_{1\infty}$ should ideally be set to unity. Similarly, the imaginary part of the dielectric function, $\epsilon_2(E)$, is related to the real part of the dielectric function, $\epsilon_1(E)$, through the Kramers-Kronig transformation

$$\epsilon_2(E) = \frac{2}{\pi E} P \int_0^\infty \frac{u^2[1 - \epsilon_1(u)]}{u^2 - E^2} \, du. \tag{2.46}$$

The conditions developed in Eqs. (2.39a) and (2.39b) mandate that

$$\epsilon_1(E) = \epsilon_1(-E), \tag{2.47a}$$

and

$$\epsilon_2(E) = -\epsilon_2(-E). \tag{2.47b}$$

These are referred to as the time-symmetry requirements mandated of the Kramers-Kronig relations.

2.9   Review of models

Within the framework of the momentum matrix element and the dipole matrix element formulations, the imaginary part of the dielectric function, $\epsilon_2(E)$, may be expressed as the product of the corresponding aggregate optical transition matrix element, the JDOS function, and some other function of the photon energy. The optical transition matrix elements play an important role in shaping the spectral dependence of the imaginary part of the dielectric function, $\epsilon_2(E)$. Models for the spectral dependence of the imaginary part of the dielectric function, $\epsilon_2(E)$, have been developed assuming a constant momentum matrix element, i.e., a momentum matrix element that is independent of the photon energy, E. Examples include the model of Forouhi and Bloomer [20], the model of McGahan *et al.* [21], and the model of Jellison and Modine [15].

This assumption of a constant momentum matrix element was first suggested by Tauc *et al.* [18]. In fact, Tauc *et al.* [18] suggested that the zero-

intercept of the plot of $\sqrt{\alpha E}$ as a function of E, where α represents the corresponding optical absorption coefficient, allows one to define the "optical bandgap" of these materials if the aggregate momentum matrix element is constant and the valence band and conduction band DOS functions are square-root in form, i.e., of the form presented in Eqs. (2.23) and (2.24). Based upon a linear response formalism for $\epsilon_2(E)$, Tauc *et al.* [18] derived an expression for $\epsilon_2(E)$ that characterizes the absorption edge of amorphous semiconductors. They concluded that

$$\epsilon_2(E) \propto \frac{(E - E_g)^2}{E^2},\tag{2.48}$$

for $E > E_g$, where E_g denotes the corresponding "optical bandgap". Eq. (2.48) may be used to describe the interband optical transition mechanism for the optical response of such a material, and thus, $\epsilon_2(E) = 0$ for $E < E_g$.

Recalling Eq. (1.7), i.e., $\epsilon_2(E) = 2n(E)k(E)$, where $n(E)$ represents the spectral dependence of the refractive index and $k(E)$ denotes the spectral dependence of the extinction coefficient, Forouhi and Bloomer [20] suggest an expression for the extinction coefficient

$$k_{FB}(E) \ = \ \frac{A(E - E_g)^2}{E^2 - BE + C},\tag{2.49}$$

where A, B, and C are treated as empirical fitting parameters. The term

$(E - E_g)^2$ in Eq. (2.49) represents the assumed form for the JDOS function of the material itself, and arises from the assumed square-root valence band and conduction band DOS functions; recall Eq. (2.25). This formulation was then used in order to fit experimental optical functions corresponding to amorphous diamond-like carbon films [15, 21, 22, 24]. Unfortunately, as was pointed out by McGahan and Woollam [21, 22], the Forouhi and Bloomer [20] model is unable to describe the spectral dependence of these optical functions correctly. In particular, the Forouhi and Bloomer [20] formulation provides for negative band gaps, a clearly unphysical result [15, 22]. McGahan *et al.* [21] made some modifications to the Forouhi and Bloomer [20] model, and this was shown to successfully fit several n and k experimental data sets.

Unfortunately, the Forouhi and Bloomer [20] and McGahan *et al.* [21] formulations have several fundamental problems, these being nicely summarized by Jellison and Modine [15]. They are as listed below:

- While experiment indicates that $\epsilon_2(E) \to 0$ as $E \to \infty$, both the models of Forouhi and Bloomer [20] and McGahan *et al.* [21] instead approach non-zero values for $\epsilon_2(E)$ as $E \to \infty$.

- Both the models of Forouhi and Bloomer [20] and McGahan *et al.* [21] fail to satisfy the Kramers-Kronig time-symmetry requirements,

48

i.e., Eqs. (2.47a) and (2.47b), which mandate that

$$k(-E) = -k(E). \qquad (2.50)$$

Jellison and Modine [15] developed a new parameterized model for the optical functions associated with an amorphous semiconductor that does not have the problems listed above. In particular, they developed a Tauc-Lorentz expression for the imaginary part of the dielectric function, $\epsilon_2(E)$, based on the Tauc JDOS function [18, 25], i.e., Eq. (2.25), and the Lorentz oscillator [26]. They then determined the corresponding spectral dependence of the real part of the dielectric function, $\epsilon_1(E)$, using a Kramers-Kronig transformation, i.e., Eq. (2.45). As with the models of Forouhi and Bloomer [20] and McGahan *et al.* [21], the model of Jellison and Modine [15] is cast within the framework of the constant momentum matrix element assumption.

2.10   Experimental results

In the subsequent analysis, models for the spectral dependence of the real and imaginary components of the dielectric function, $\epsilon_1(E)$ and $\epsilon_2(E)$, respectively, are fit to a-Si optical function experimental data, and from these fits, the "best" model parameters are determined, i.e., the modeling parameters

that produce the "best" fits with the corresponding experimental data. The experimental a-Si optical function data considered is from Piller [30], Synowicki [31], and Ferluato *et al.* [32], these experimental results corresponding to samples of electron-gun evaporated (EGE) a-Si, and plasma enhanced chemical vapor deposition (PECVD) prepared a-Si; the experimental data from Piller [30] was obtained from a sample of EGE a-Si, the experimental data from Synowicki [31] was obtained from a sample of PECVD a-Si, and the experimental data from Ferluato *et al.* [32] was obtained from a sample of PECVD a-Si, these samples being referred to as EGE a-Si, PECVD a-Si I, and PECVD a-Si II, respectively. These three sets of experimental data are shown in Figures 2.8 and 2.9, the spectral dependence of the real part of the dielectric function being depicted in Figure 2.8 and the spectral dependence of the imaginary part of the dielectric function being depicted in Figure 2.9. The EGE a-Si [30] experimental data set was collected from an electron-gun evaporated a-Si sample, with silicon as the substrate [30]. For the case of the PECVD a-Si I [31] experimental data sets, fused silica was used as the substrate [31]. For the case of the PECVD a-Si II [32] experimental data sets, glass was used as the substrate [32].
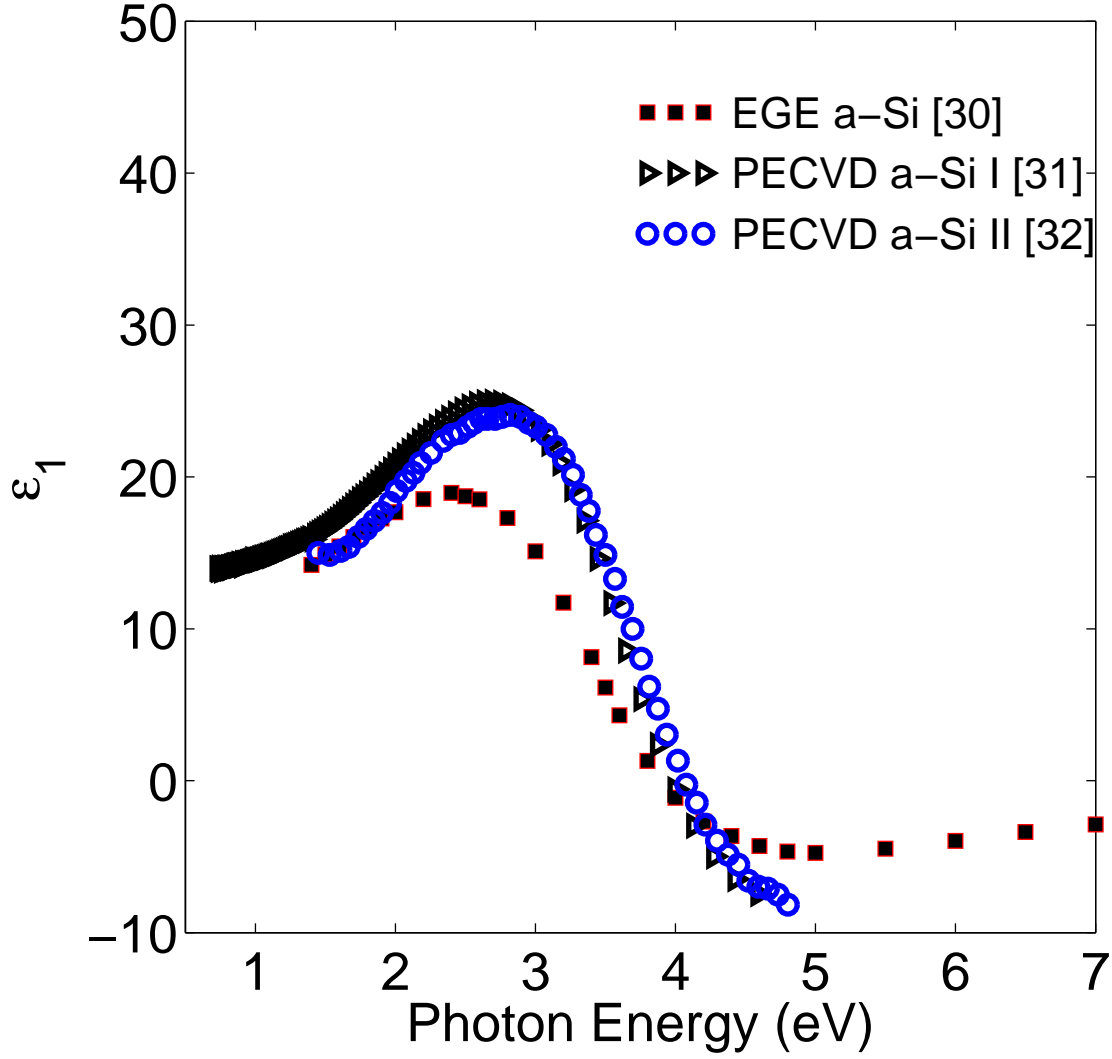
Figure 2.8: The three experimental data sets, i.e., EGE a-Si [30], PECVD a-Si I [31], and PECVD a-Si II [32], for the real part of the dielectric function, $\epsilon_1(E)$, as a function of the photon energy, E.
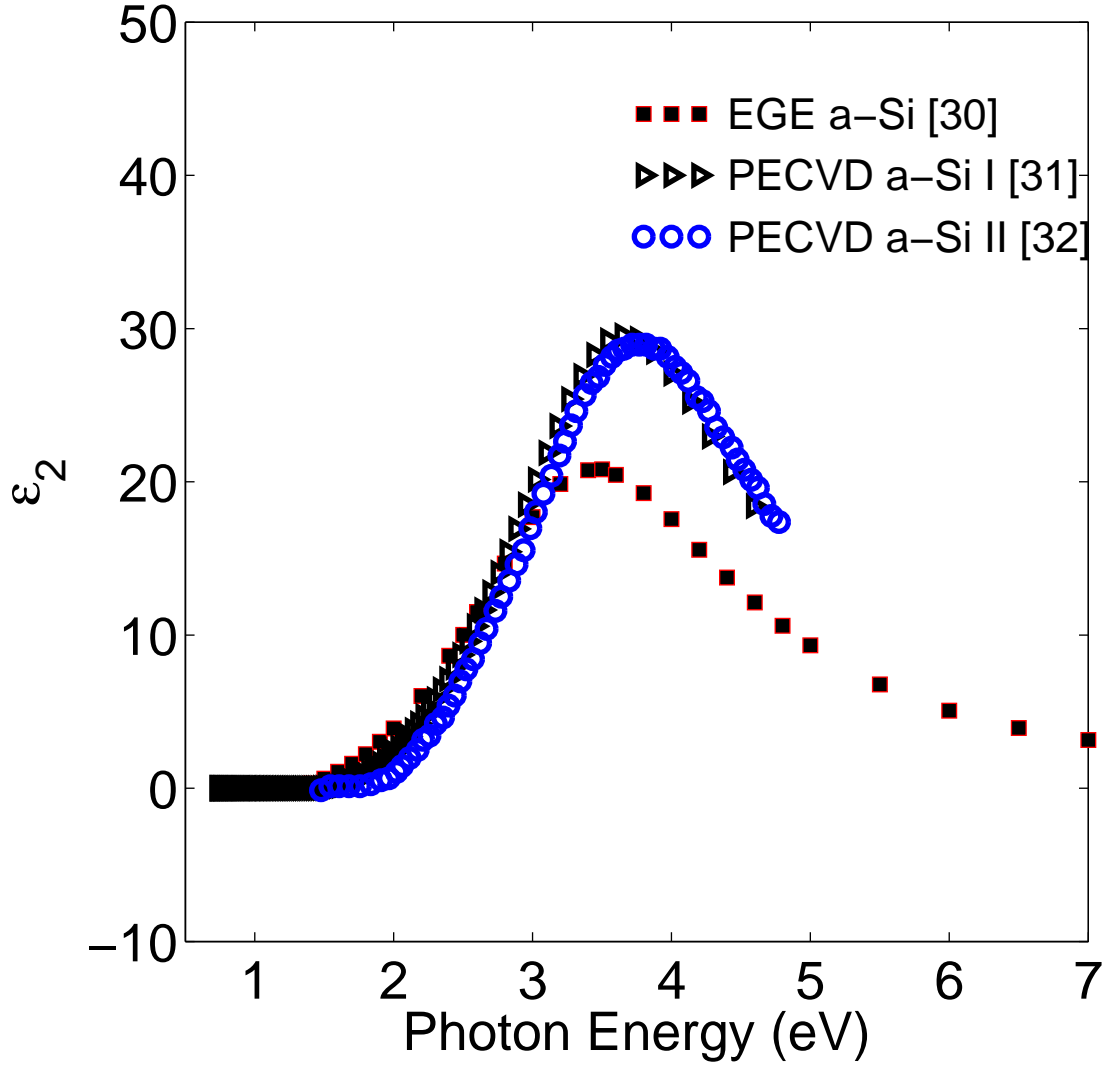
Figure 2.9: The three experimental data sets, i.e., EGE a-Si [30], PECVD a-Si I [31], and PECVD a-Si II [32], for the imaginary part of the dielectric function, $\epsilon_2(E)$, as a function of the photon energy, E.

Chapter 3

The model of Jellison and

Modine

3.1 Empirical models for the optical

functions associated with an amorphous

semiconductor

For the purposes of materials characterization and device design, empirical models for the optical functions of an amorphous semiconductor have been sought. Forouhi and Bloomer [20] and McGahan *et al.* [21] have proposed empirical models for such functions. Unfortunately, these models have a number of shortcomings. While experiment indicates that as $E \to \infty$, $\epsilon_2(E) \to 0$, both the models of Forouhi and Bloomer [20] and McGahan *et*

al. [21] yield non-zero values for $\epsilon_2(E)$ as $E \to \infty$. The models of Forouhi and Bloomer [20] and McGahan *et al.* [21] have the additional problem of being obtained using unphysical expressions for $\epsilon_2(E)$. In particular, the proposed models for $\epsilon_2(E)$ do not terminate exact at the energy gap. Finally, both the models of Forouhi and Bloomer [20] and McGahan *et al.* [21] fail to satisfy the time-symmetry requirements mandated of the Kramers-Kronig relations; recall Eqs. (2.47a) and (2.47b).

In 1996, Jellison and Modine [15] developed a new parameterized model for the optical functions associated with an amorphous semiconductor that remedies some of the problems found with these previous models. In this approach, a physically-based model for the imaginary part of the dielectric function, $\epsilon_2(E)$, is proposed. This model includes a Tauc JDOS function. i.e., Eq. (2.25), and a Lorentzian momentum matrix element. Then, through the use of a Kramers-Kronig transformation on $\epsilon_2(E)$, i.e., Eq. (2.45), the spectral dependence of the real part of the dielectric function, $\epsilon_1(E)$, is determined.

This chapter is organized in the following manner. In Section 3.2, the Lorentz model is described. In Section 3.3, Jellison and Modine's model for the spectral dependence of the real and imaginary components of the

dielectric function, $\epsilon_1(E)$ and $\epsilon_2(E)$, respectively, is presented [15]. Then, in Section 3.4, an explicit determination of the spectral dependence of $\epsilon_1(E)$ from the use of a Kramers-Kronig transformation on $\epsilon_2(E)$, i.e., Eq. (2.45), is provided. Finally, a fit with the results of experiment is presented in Section 3.5.

3.2   The Lorentz model

According to the Lorentz model, an atom with electrons bounded by the nucleus may be considered in the same way as a small mass bounded to a large mass by a spring. The motion of an electron bound to the nucleus may be described by

$$m\,\frac{d^2\boldsymbol{r}}{dt^2} + mC\,\frac{d\boldsymbol{r}}{dt} + m\omega_0^2\boldsymbol{r} \;=\; -q\boldsymbol{E}_{\text{loc}}, \tag{3.1}$$

where m denotes the electron mass, q represents the electron charge, and $\boldsymbol{E}_{\text{loc}}$ is the driving local electric field acting on the electron. It may be shown that

$$\tilde{\boldsymbol{r}} \;=\; -\frac{e\boldsymbol{E}_{\text{loc}}}{m}\,\frac{1}{(\omega_0^2 - \omega^2) - iC\omega}, \tag{3.2}$$

and the induced dipole moment is

$$\tilde{\boldsymbol{p}} = \frac{e^2 \boldsymbol{E}_{\text{loc}}}{m} \frac{1}{(\omega_0^2 - \omega^2) - iC\omega}. \tag{3.3}$$

There is a linear relationship between $\tilde{\boldsymbol{p}}$ and $\boldsymbol{E}_{\text{loc}}$ if the displacement r is assumed to be sufficiently small. That is,

$$\tilde{\boldsymbol{p}} = \tilde{\alpha}(\omega) \boldsymbol{E}_{\text{loc}}, \tag{3.4}$$

where $\tilde{\alpha}(\omega)$ is the frequency-dependent atomic polarizability. From Eqs. (3.3) and (3.4), it may be shown that

$$\tilde{\alpha}(\omega) = \frac{e^2}{m} \frac{1}{(\omega_0^2 - \omega^2) - iC\omega}. \tag{3.5}$$

The complex dielectric function, $\tilde{\epsilon}$, may be expressed in terms of the complex polarizability, $\tilde{\alpha}$, by

$$\tilde{\epsilon} = 1 + 4\pi N \tilde{\alpha}, \tag{3.6}$$

where N denotes the number of atoms per unit volume. From Eqs. (3.5) and (3.6), it may be shown that

$$\tilde{\epsilon} = 1 + \frac{4\pi N e^2}{m} \frac{1}{(\omega_0^2 - \omega^2) - iC\omega}. \tag{3.7}$$

Since the complex dielectric function, $\tilde{\epsilon}$, may be expressed as the sum over its real and imaginary components, i.e.,

$$\tilde{\epsilon} = \epsilon_1 + i\epsilon_2, \tag{3.8}$$

56

where ϵ_1 and ϵ_2 denote the real and imaginary components of the dielectric function, respectively, it can be seen that

$$\epsilon_1 = 1 + \frac{4\pi N e^2}{m} \frac{\omega_0^2 - \omega^2}{(\omega_0^2 - \omega^2)^2 + C^2 \omega^2}, \tag{3.9a}$$

and

$$\epsilon_2 = \frac{4\pi N e^2}{m} \frac{C\omega}{(\omega_0^2 - \omega^2)^2 + C^2 \omega^2}, \tag{3.9b}$$

Jellison and Modine [15] used this simple Lorentz model in their proposed parameterized model for the spectral dependence of the imaginary part of the dielectric function, ϵ_2, shown in the subsequent analysis.

3.3 Model for the optical functions

Within the framework of the momentum matrix element formulation, i.e., Eq. (2.1), Jellison and Modine [15] propose a Tauc-Lorentz expression for the imaginary part of the dielectric function, $\epsilon_2(E)$, i.e., $\epsilon_2(E)$ is essentially proportional to the product of a Tauc JDOS function and a Lorentz oscillator. Specifically, Jellison and Modine [15] suggest that

$$\epsilon_{2TL}(E) = \begin{cases} 0, & E \leq E_g \\ \\ \dfrac{AE_oCE}{(E^2 - E_o^2)^2 + C^2 E^2} \dfrac{(E - E_g)^2}{E^2}, & E > E_g \end{cases}, \tag{3.10}$$

57

where the four modeling parameters, E_o, C, E_g, and A, are in units of energy.

Here, E_o denotes the resonance energy of a bound electron at which the transition of the electron occurs between two atomic states, A represents the oscillator strength, C is the breadth of the region of anomalous dispersion, and E_g is the energy gap.

Jellison and Modine [15] determine the real part of the dielectric function, $\epsilon_1(E)$, using a Kramers-Kronig transformation on $\epsilon_2(E)$. That is,

$$\epsilon_1(E) = \epsilon_{1\infty} + \frac{2}{\pi} P \int_{E_g}^{\infty} \frac{u\epsilon_2(u)}{u^2 - E^2} \, du, \tag{3.11}$$

where P represents the Cauchy principal part of the integral. An additional fitting parameter, $\epsilon_{1\infty}$, is included in order to obtain the desired fits; in the actual Kramers-Kronig relations, $\epsilon_{1\infty}$ is unity. This integral may be solved, in closed-form, to yield

$$
\begin{aligned}
\epsilon_1(E) = \ & \epsilon_{1\infty} + \frac{1}{2} \frac{A}{\pi} \frac{C}{\zeta^4} \frac{a_{\ln}}{\alpha E_o} \ln \left[\frac{E_g^2 + E_o^2 + \alpha E_g}{E_g^2 + E_o^2 - \alpha E_g} \right] \\
& - \frac{A}{\pi\zeta^4} \frac{a_{a\tan}}{E_o} \left[\pi - \tan^{-1}\left(\frac{2E_g + \alpha}{C}\right) + \tan^{-1}\left(\frac{-2E_g + \alpha}{C}\right) \right] \\
& + 2\frac{AE_o}{\pi\alpha\zeta^4} E_g \left[E^2 - \gamma^2 \right] \left[\pi + 2 \tan^{-1}\left(\frac{2(\gamma^2 - E_g^2)}{\alpha C}\right) \right] \\
& - \frac{AE_o C}{\pi\zeta^4} \frac{E^2 + E_g^2}{E} \ln \frac{|E_g - E|}{(E_g + E)} \\
& + \frac{2AE_o C}{\pi\zeta^4} E_g \ln \left[\frac{[(E_g + E)|E_g - E|]}{\sqrt{(E_o^2 - E_g^2)^2 + E_g^2 C^2)}} \right],
\end{aligned}
\tag{3.12}
$$

where

$$a_{\ln} = (E_g^2 - E_o^2)E^2 + E_g^2 C^2 - E_o^2(E_o^2 + 3E_g^2), \tag{3.13a}$$

$$a_{a\tan} = (E^2 - E_o^2)(E_o^2 + E_g^2) + E_g^2 C^2, \tag{3.13b}$$

$$\zeta^4 = [(E^2 - E_o^2)^2 + C^2 E^2], \tag{3.13c}$$

$$\chi = \sqrt{4E_o^2 - C^2}, \tag{3.13d}$$

and

$$\gamma = \sqrt{E_o^2 - \frac{C^2}{2}}, \tag{3.13e}$$

E_o, C, E_g, and A being as defined earlier.

The two closed-form expressions for the optical functions, $\epsilon_1(E)$ and $\epsilon_2(E)$, respectively, i.e., Eqs. (3.10) and (3.12), provide a Kramers-Kronig consistent model for the optical functions of an amorphous semiconductor. This model avoids many of the problems associated with the models of Foroughi and Bloomer [20] and McGahan *et al.* [21]. That is, $\epsilon_2(E)$ approaches zero as $E \to \infty$, the model for $\epsilon_2(E)$ is physically based, and finally, these optical function expressions obey the time-symmetry requirements mandated of the Kramers-Kronig relations, i.e., Eqs. (2.47a) and (2.47b). Jellison and Modine [15] then employed this model in order to fit a variety of experimental optical function data for the spectral dependence of $\epsilon_1(E)$ and $\epsilon_2(E)$, and

drew a number of conclusions into the character of the materials considered.

3.4 Derivation

3.4.1 Definitions

From Eqs. (3.10) and (3.11), it is seen that

$$\epsilon_1(E) \;=\; \epsilon_{1\infty} + \frac{2AE_oC}{\pi} P \int_{E_g}^{\infty} \frac{(u - E_g)^2}{(u^2 - E^2)[(u^2 - E_o^2)^2 + C^2u^2]} \, du \quad (3.14)$$

Letting

$$f(u) \;=\; \frac{(u - E_g)^2}{(u^2 - E^2)[(u^2 - E_o^2)^2 + C^2u^2]}, \quad (3.15)$$

the analysis starts with a partial fraction expansion of this polynomial expression in terms of the roots of its denominator. As the denominator is a 6th-order polynomial, it has six roots, two of which may be seen immediately, from inspection, to be E and $-E$, respectively. Accordingly, the corresponding partial fraction expansion may be expressed as

$$f(u) \;=\; \frac{A_1}{u + E} + \frac{A_2}{u - E} + \frac{A_3}{u - r_1} + \frac{A_4}{u - r_2} + \frac{A_5}{u - r_3} + \frac{A_6}{u - r_4}, \quad (3.16)$$

where A_1, A_2, A_3, A_4, A_5, and A_6 are the co-efficients of the partial fraction expansions, r_1, r_2, r_3, and r_4 being the other four, as yet unknown, roots of the denominator of $f(u)$.

3.4.2 Root calculation through expansion of the denominator

The roots of $f(u)$ may be determined by setting

$$(u^2 - E_o^2)^2 + C^2 u^2 \;=\; 0. \tag{3.17}$$

Expanding Eq. (3.17) fully, one can see that

$$u^4 - u^2(2E_o^2 - C^2) + E_o^4 \;=\; 0.$$

Factoring the u^2 term, this equation reduces to

$$u^2 \;=\; \frac{2E_o^2 - C^2 \pm \sqrt{(2E_o^2 - C^2)^2 - 4E_o^4}}{2},$$

which leads to

$$u^2 \;=\; E_o^2 - \frac{C^2}{2} \pm i\frac{C}{2}\sqrt{4E_o^2 - C^2}.$$

Noting that

$$u^2 \;=\; \left(\frac{\sqrt{4E_o^2 - C^2}}{2} \pm i\frac{C}{2}\right)^2,$$

it is seen that

$$u \;=\; \pm\left(\frac{\sqrt{4E_o^2 - C^2}}{2} \pm i\frac{C}{2}\right).$$

Letting

$$a = \frac{\sqrt{4E_o^2 - C^2}}{2},$$

and

$$b = \frac{C}{2},$$

it is seen that the four roots of $f(u)$ are

$$r_1 = a + ib, \tag{3.18a}$$

$$r_2 = a - ib, \tag{3.18b}$$

$$r_3 = -a + ib, \tag{3.18c}$$

and

$$r_4 = -a - ib. \tag{3.18d}$$

Through inspection, the following relationships are seen amongst these roots, i.e.,

$$r_2 = r_1^*,$$

$$r_3 = -r_1^*,$$

$$r_4 = -r_1,$$

$$r_1 = -r_3^*,$$

$$r_2 = -r_3,$$

and

$$r_4 = r_3^*.$$

3.4.3 Calculation of the coefficients

The coefficients, A_1, A_2, A_3, A_4, A_5, and A_6, may be determined using the usual approach for a partial fraction expansion. That is, for the partial fraction expansion,

$$f(z) = \sum_i \frac{A_i}{z - z_i}, \tag{3.19}$$

if all the roots, z_i, are distinct, then it may be seen that

$$A_i = (z - z_i)f(z)|_{z=z_i}. \tag{3.20}$$

Noting that all of the roots associated with the denominator of $f(u)$ are distinct, employing the approach suggested in Eq. (3.20), the coefficients A_1, A_2, A_3, A_4, A_5, and A_6 will be determined. For the case of these coefficients, a polar notation is employed, i.e., the imaginary number

$$p + iq = \sqrt{p^2 + q^2} \exp\left(i \tan^{-1}\left[\frac{q}{p}\right]\right), \tag{3.21}$$

may instead be expressed as

$$p + iq = \sqrt{p^2 + q^2} \angle \tan^{-1}\left[\frac{q}{p}\right], \tag{3.22}$$

where this last expression corresponds to polar notation. That is, every complex number is expressed in this particular polar form. An alternate form for this polar notation

$$\text{abs}\,(p + iq) \;=\; \sqrt{p^2 + q^2}, \tag{3.23}$$

and

$$\arg\,(p + iq) \;=\; \tan^{-1}\left[\frac{q}{p}\right], \tag{3.24}$$

may be employed.

Determination of A_1

$$
\begin{aligned}
A_1 \;&=\; f(u)(u + E)|_{u=-E}, \\
&=\; \frac{(-E - E_g)^2}{(-E - E)[(E^2 - E_o^2)^2 + C^2 E^2]}, \\
&=\; -\frac{(E + E_g)^2}{2E[(E^2 - E_o^2)^2 + C^2 E^2]}.
\end{aligned}
\tag{3.25}
$$

Determination of A_2

$$
\begin{aligned}
A_2 \;&=\; f(u)(u - E)|_{u=E}, \\
&=\; \frac{(E - E_g)^2}{(E + E)[(E^2 - E_o^2)^2 + C^2 E^2]}, \\
&=\; \frac{(E - E_g)^2}{2E[(E^2 - E_o^2)^2 + C^2 E^2]}.
\end{aligned}
\tag{3.26}
$$

Determination of A_3

$$A_3 = f(u)(u - r_1)|_{u=r_1},$$

$$= \frac{(r_1 - E_g)^2}{(r_1^2 - E^2)(r_1 - r_2)(r_1 - r_3)(r_1 - r_4)},$$

$$= \frac{(r_1 - E_g)^2}{(r_1^2 - E^2)(r_1 - r_1^*)(r_1 + r_1^*)(r_1 + r_1)},$$

$$= \frac{(r_1 - E_g)^2}{(r_1^2 - E^2)(r_1 - r_1^*)(r_1 + r_1^*)2r_1}. \tag{3.27}$$

Now, by substituting $r_1 = a + ib$, the factors in the numerator and the denominator of Eq. (3.27) may be determined and expressed in polar form. For the numerator, this yields

$$(r_1 - E_g)^2 = (a + ib - E_g)^2,$$

$$= (a - E_g)^2 - b^2 + i2b(a - E_g),$$

$$= \sqrt{((a - E_g)^2 - b^2)^2 + 4b^2(a - E_g)^2} \angle \tan^{-1}\left[\frac{2b(a - E_g)}{(a - E_g)^2 - b^2}\right],$$

$$= \left[(a - E_g)^2 + b^2\right] \angle \tan^{-1}\left[\frac{2b(a - E_g)}{(a - E_g)^2 - b^2}\right].$$

The polar form for the other factors in the denominator of Eq. (3.27) may now be expressed as

$$r_1^2 - E^2 = \sqrt{(a^2 - b^2 - E^2)^2 + 4a^2b^2} \angle \tan^{-1}\left[\frac{2ab}{a^2 - b^2 - E^2}\right],$$

$$2(r_1 - r_1^*)(r_1 + r_1^*) = 8ab\angle\left[\frac{\pi}{2}\right],$$

and

$$r_1 = \sqrt{a^2 + b^2} \angle \tan^{-1} \left[\frac{b}{a} \right].$$

So, the coefficient, A_3, may be expressed in polar form as

$$
\begin{aligned}
A_3 &= \frac{[(a - E_g)^2 + b^2] \angle \left[\tan^{-1} \frac{2b(a - E_g)}{(a - E_g)^2 - b^2} \right]}{\sqrt{(a^2 - b^2 - E^2)^2 + 4a^2 b^2} \angle \left[\tan^{-1} \frac{2ab}{a^2 - b^2 - E^2} \right]} \times \\
&\quad \frac{1}{\sqrt{a^2 + b^2} \angle \left[\tan^{-1} \frac{b}{a} \right] \left[8ab \angle \frac{\pi}{2} \right]}, \\
&= \frac{[(a - E_g)^2 + b^2]}{8ab [\sqrt{(a^2 - b^2 - E^2)^2 + 4a^2 b^2}] [\sqrt{a^2 + b^2}]} \\
&\quad \times \angle \left[\tan^{-1} \frac{2b(a - E_g)}{(a - E_g)^2 - b^2} - \tan^{-1} \frac{2ab}{a^2 - b^2 - E^2} - \tan^{-1} \frac{b}{a} - \frac{\pi}{2} \right].
\end{aligned}
$$

Thus, it is seen that

$$\mathrm{abs}(A_3) = \frac{[(a - E_g)^2 + b^2]}{8ab [\sqrt{(a^2 - b^2 - E^2)^2 + 4a^2 b^2}] [\sqrt{a^2 + b^2}]}, \tag{3.28a}$$

and that

$$\arg(A_3) = -\frac{\pi}{2} + \tan^{-1} \left[\frac{2b(a - E_g)}{(a - E_g)^2 - b^2} \right] - \tan^{-1} \left[\frac{2ab}{a^2 - b^2 - E^2} \right]$$

$$- \tan^{-1} \left[\frac{b}{a} \right]. \tag{3.28b}$$

Determination of A_4

$$
\begin{aligned}
A_4 &= f(u)(u - r_2)|_{u=r_2}, \\[2mm]
&= \frac{(r_2 - E_g)^2}{(r_2^2 - E^2)(r_2 - r_1)(r_2 - r_3)(r_2 - r_4)}, \\[2mm]
&= \frac{(r_1^* - E_g)^2}{(r_1^{*2} - E^2)(r_1^* - r_1)(r_1 + r_1^*)(r_1^* + r_1^*)}, \\[2mm]
&= \frac{(r_1^* - E_g)^2}{2r_1^*(r_1^{*2} - E^2)(r_1^* - r_1)(r_1 + r_1^*)}.
\end{aligned}
\tag{3.29}
$$

Now, by substituting $r_1^* = a - ib$, the factors in the numerator and the denominator of Eq. (3.29) may be determined and expressed in polar form. For the numerator, this yields

$$
\begin{aligned}
(r_1^* - E_g)^2 &= (a - ib - E_g)^2, \\[2mm]
&= \sqrt{((a - E_g)^2 - b^2)^2 + 4b^2(a - E_g)^2}\angle - \tan^{-1}\left[\frac{2b(a - E_g)}{(a - E_g)^2 - b^2}\right], \\[2mm]
&= [(a - E_g)^2 + b^2]\angle - \tan^{-1}\left[\frac{2b(a - E_g)}{(a - E_g)^2 - b^2}\right].
\end{aligned}
$$

The polar form for the other factors in the denominator of Eq. (3.29) may be expressed as

$$
r_1^{*2} - E^2 = \sqrt{(a^2 - b^2 - E^2)^2 + 4a^2b^2}\angle - \tan^{-1}\left[\frac{2ab}{a^2 - b^2 - E^2}\right],
$$

$$
2(r_1^* - r_1)(r_1 + r_1^*) = 8ab\angle\left[\frac{-\pi}{2}\right],
$$

and

$$
r_1^* = \sqrt{a^2 + b^2}\angle - \tan^{-1}\left[\frac{b}{a}\right].
$$

Thus,

$$\text{abs}(A_4) = \frac{[(a - E_g)^2 + b^2]}{8ab[\sqrt{(a^2 - b^2 - E^2)^2 + 4a^2b^2}][\sqrt{a^2 + b^2}]}, \tag{3.30a}$$

and

$$\arg(A_4) = \frac{\pi}{2} - \tan^{-1}\left[\frac{2b(a - E_g)}{(a - E_g)^2 - b^2}\right] + \tan^{-1}\left[\frac{2ab}{a^2 - b^2 - E^2}\right]$$

$$+ \tan^{-1}\left[\frac{b}{a}\right]. \tag{3.30b}$$

Through inspection, it is seen that $\text{abs}(A_4) = \text{abs}(A_3)$ and that $\arg(A_4) = -\arg(A_3)$,

i.e., $A_3 = A_4^*$.

Determination of A_5

$$A_5 = f(u)(u - r_3)|_{u=r_3},$$

$$= \frac{(r_3 - E_g)^2}{(r_3^2 - E^2)(r_3 - r_1)(r_3 - r_2)(r_3 - r_4)},$$

$$= \frac{(r_3 - E_g)^2}{(r_3^2 - E^2)(r_3 - r_3^*)(r_3 + r_3^*)(r_3 + r_3)},$$

$$= \frac{(r_3 - E_g)^2}{(r_3^2 - E^2)(r_3 - r_3^*)(r_3 + r_3^*)2r_3}. \tag{3.31}$$

For this equation, for the numerator,

$$(r_3 - E_g)^2 = (-a + ib - E_g)^2,$$

$$= \sqrt{((a + E_g)^2 - b^2)^2 + 4b^2(a + E_g)^2}\angle - \tan^{-1}\left[\frac{2b(a + E_g)}{(a + E_g)^2 - b^2}\right],$$

$$= [(a + E_g)^2 + b^2]\angle - \tan^{-1}\left[\frac{2b(a + E_g)}{(a + E_g)^2 - b^2}\right].$$

68

Similarly, for the denominator,

$$r_3^2 - E^2 = \sqrt{(a^2 - b^2 - E^2)^2 + 4a^2b^2} \angle - \tan^{-1}\left[\frac{2ab}{a^2 - b^2 - E^2}\right],$$

$$2(r_3 - r_3^*)(r_3 + r_3^*) = 8ab\angle\left[\frac{-\pi}{2}\right],$$

and

$$r_3 = \sqrt{a^2 + b^2}\angle\tan^{-1}\left[\frac{b}{-a}\right].$$

Thus,

$$\text{abs}(A_5) = \frac{[(a + E_g)^2 + b^2]}{8ab[\sqrt{(a^2 - b^2 - E^2)^2 + 4a^2b^2}][\sqrt{a^2 + b^2}]}, \tag{3.32a}$$

and

$$\arg(A_5) = \frac{\pi}{2} - \tan^{-1}\left[\frac{2b(a + E_g)}{(a + E_g)^2 - b^2}\right] + \tan^{-1}\left[\frac{2ab}{a^2 - b^2 - E^2}\right]$$

$$- \tan^{-1}\left[\frac{b}{-a}\right]. \tag{3.32b}$$

Determination of A_6

$$
\begin{aligned}
A_6 &= f(u)(u - r_4)|_{u=r_4}, \\
&= \frac{(r_4 - E_g)^2}{(r_4^2 - E^2)(r_4 - r_1)(r_4 - r_2)(r_4 - r_3)}, \\
&= \frac{(r_3^* - E_g)^2}{(r_3^{*2} - E^2)(r_3^* - r_3)(r_3^* + r_3^*)(r_3^* + r_3)}, \\
&= \frac{(r_3^* - E_g)^2}{(r_3^{*2} - E^2)(r_3^* - r_3)(r_3 + r_3^*)2r_3^*}. \tag{3.33}
\end{aligned}
$$

Here, the numerator of Eq. (3.33) yields

$$
\begin{aligned}
(r_3^* - E_g)^2 &= (-a - ib - E_g)^2, \\
&= [(a + E_g)^2 + b^2] \angle \tan^{-1} \left[\frac{2b(a + E_g)}{(a + E_g)^2 - b^2} \right].
\end{aligned}
$$

Similarly, the terms in the denominator of Eq. (3.33) yield

$$
r_3^{*2} - E^2 = \sqrt{(a^2 - b^2 - E^2)^2 + 4a^2 b^2} \angle \tan^{-1} \left[\frac{2ab}{a^2 - b^2 - E^2} \right],
$$

$$
2(r_3^* - r_3)(r_3 + r_3^*) = 8ab \angle \left[\frac{\pi}{2} \right],
$$

and

$$
r_3^* = \sqrt{a^2 + b^2} \angle - \tan^{-1} \left[\frac{b}{-a} \right].
$$

Thus,

$$
\text{abs}(A_6) = \frac{[(a + E_g)^2 + b^2]}{8ab[\sqrt{(a^2 - b^2 - E^2)^2 + 4a^2 b^2}][\sqrt{a^2 + b^2}]}, \tag{3.34a}
$$

and

$$
\arg(A_6) = -\frac{\pi}{2} + \tan^{-1} \left[\frac{2b(a + E_g)}{(a + E_g)^2 - b^2} \right] - \tan^{-1} \left[\frac{2ab}{a^2 - b^2 - E^2} \right]
$$

$$
+ \tan^{-1} \left[\frac{b}{-a} \right]. \tag{3.34b}
$$

Through inspection, it is also seen that $\text{abs}(A_5) = \text{abs}(A_6)$ and that $\arg(A_5) = -\arg(A_6)$, i.e., $A_5 = A_6^*$.

3.4.4 Grouping the terms in the partial fraction

expression

In Section 3.4.3, it was seen that $A_3 = A_4^*$ and that $A_5 = A_6^*$. These relations may be used in order to group the terms associated with the coefficients in the partial fraction expansion.

Grouping the terms associated with A_3 and A_4

The terms associated with A_3 and A_4 in the partial fraction expansion may be combined as follows:

$$
\begin{aligned}
\frac{A_3}{u - r_1} + \frac{A_4}{u - r_2} &= \frac{\text{abs}(A_3)\angle(\arg(A_3))}{u - a - ib} + \frac{\text{abs}(A_4)\angle\arg(A_4))}{u - a + ib}, \\
&= \frac{\text{abs}(A_3)\angle(\arg(A_3))}{\sqrt{(u-a)^2 + b^2}\angle\left[-\tan^{-1}\left(\frac{b}{u-a}\right)\right]} \\
&\quad + \frac{\text{abs}(A_3)\angle - [\arg(A_3)]}{\sqrt{(u-a)^2 + b^2}\angle\left[\tan^{-1}\left(\frac{b}{u-a}\right)\right]}, \\
&= \frac{\text{abs}(A_3)}{\sqrt{(u-a)^2 + b^2}}\angle\left[\arg(A_3) + \tan^{-1}\left(\frac{b}{u-a}\right)\right] \\
&\quad + \frac{\text{abs}(A_3)}{\sqrt{(u-a)^2 + b^2}}\angle - \left[\arg(A_3) + \tan^{-1}\left(\frac{b}{u-a}\right)\right].
\end{aligned}
$$

Letting,

$$x = \arg(A_3) + \tan^{-1}\left(\frac{b}{u-a}\right),$$

and

$$k = \frac{\mathrm{abs}(A_3)}{\sqrt{(u-a)^2 + b^2}},$$

it may be seen that

$$
\begin{aligned}
\frac{A_3}{u - r_1} + \frac{A_4}{u - r_2} &= k\angle x + k\angle - x, \\
&= k(e^{ix} + e^{-ix}), \\
&= 2k\cos x,
\end{aligned}
$$

$$
\begin{aligned}
&= 2\frac{\mathrm{abs}(A_3)}{\sqrt{(u-a)^2 + b^2}}\cos\left[\arg(A_3) + \tan^{-1}\left(\frac{b}{u-a}\right)\right], \\
&= 2\frac{\mathrm{abs}(A_3)}{\sqrt{(u-a)^2 + b^2}}\cos\left[\arg(A_3)\right]\frac{u-a}{\sqrt{(u-a)^2 + b^2}} \\
&\quad -2\frac{\mathrm{abs}(A_3)}{\sqrt{(u-a)^2 + b^2}}\sin\left[\arg(A_3)\right]\frac{b}{\sqrt{(u-a)^2 + b^2}}, \\
&= 2\,\mathrm{abs}(A_3)\cos\left[\arg(A_3)\right]\frac{u-a}{(u-a)^2 + b^2} \\
&\quad -2\,\mathrm{abs}(A_3)\sin\left[\arg(A_3)\right]\frac{b}{(u-a)^2 + b^2}.
\end{aligned}
$$

Letting

$$c_3 = 2\operatorname{abs}(A_3)\cos[\arg(A_3)],$$

and

$$c_4 = -2\operatorname{abs}(A_3)\sin[\arg(A_3)],$$

it is also seen that,

$$\frac{A_3}{u - r_1} + \frac{A_4}{u - r_2} \quad = \quad c_3\frac{u - a}{(u - a)^2 + b^2} + c_4\frac{b}{(u - a)^2 + b^2}. \qquad (3.35)$$

Grouping the terms associated with A_5 and A_6

The terms associated with A_5 and A_6 in the partial fraction expansion may be combined as follows:

$$
\begin{aligned}
\frac{A_5}{u - r_3} + \frac{A_6}{u - r_4} &= \frac{\mathrm{abs}(A_5)\angle\left[\arg(A_5)\right]}{u + a - ib} + \frac{\mathrm{abs}(A_5)\angle -\left[\arg(A_5)\right]}{u + a + ib}, \\
&= \frac{\mathrm{abs}(A_5)\angle\left[\arg(A_5)\right]}{\sqrt{(u+a)^2 + b^2}\angle\left[-\tan^{-1}\left(\frac{b}{u+a}\right)\right]} \\
&\quad + \frac{\mathrm{abs}(A_5)\angle -\left[\arg(A_5)\right]}{\sqrt{(u-a)^2 + b^2}\angle\left[\tan^{-1}\left(\frac{b}{u+a}\right)\right]}, \\
&= \frac{\mathrm{abs}(A_5)}{\sqrt{(u+a)^2 + b^2}}\angle\left[\arg(A_5) + \tan^{-1}\left(\frac{b}{u+a}\right)\right] + \\
&\quad \frac{\mathrm{abs}(A_5)}{\sqrt{(u+a)^2 + b^2}}\angle -\left[\arg(A_5) + \tan^{-1}\left(\frac{b}{u+a}\right)\right], \\
&= 2\frac{\mathrm{abs}(A_5)}{\sqrt{(u+a)^2 + b^2}}\cos\left[\arg(A_5) + \tan^{-1}\left(\frac{b}{u+a}\right)\right], \\
&= 2\frac{\mathrm{abs}(A_5)}{\sqrt{(u+a)^2 + b^2}}\cos\left[\arg(A_5)\right]\frac{u + a}{\sqrt{(u+a)^2 + b^2}} \\
&\quad -2\frac{\mathrm{abs}(A_5)}{\sqrt{(u+a)^2 + b^2}}\sin\left[\arg(A_5)\right]\frac{b}{\sqrt{(u+a)^2 + b^2}}, \\
&= 2\mathrm{abs}(A_5)\cos\left[\arg(A_5)\right]\frac{u + a}{(u+a)^2 + b^2} \\
&\quad -2\mathrm{abs}(A_5)\sin[\arg(A_5)]\frac{b}{(u+a)^2 + b^2}.
\end{aligned}
$$

Letting

$$
c_5 = 2\,\mathrm{abs}(A_5)\cos[\arg(A_5)],
$$

and

$$c_6 = -2 \operatorname{abs}(A_5) \sin[\arg(A_5)].$$

it is seen that,

$$\frac{A_5}{u - r_3} + \frac{A_6}{u - r_4} = c_5 \frac{u + a}{(u + a)^2 + b^2} + c_6 \frac{b}{(u + a)^2 + b^2}. \qquad (3.36)$$

3.4.5 Summary of the partial fraction expansion

From Eqs. (3.16), (3.35), and (3.36), it is thus seen that

$$
\begin{aligned}
f(u) &= \frac{A_1}{u + E} + \frac{A_2}{u - E} + \frac{A_3}{u - r_1} + \frac{A_4}{u - r_2} + \frac{A_5}{u - r_3} + \frac{A_6}{u - r_4}, \\
&= \frac{A_1}{u + E} + \frac{A_2}{u - E} + c_3 \frac{u - a}{(u - a)^2 + b^2} + c_4 \frac{b}{(u - a)^2 + b^2} \\
&\quad + c_5 \frac{u + a}{(u + a)^2 + b^2} + c_6 \frac{b}{(u + a)^2 + b^2},
\end{aligned}
\qquad (3.37)
$$

where

$$A_1 = \frac{-(E + E_g)^2}{2E[(E^2 - E_o^2)^2 + C^2 E^2]}, \qquad (3.38\text{a})$$

$$A_2 = \frac{(E - E_g)^2}{2E[(E^2 - E_o^2)^2 + C^2 E^2]}, \qquad (3.38\text{b})$$

$$c_3 = 2 \operatorname{abs}(A_3) \cos[\arg(A_3)], \qquad (3.38\text{c})$$

$$c_4 = -2 \operatorname{abs}(A_3) \sin[\arg(A_3)], \qquad (3.38\text{d})$$

$$c_5 = 2 \operatorname{abs}(A_5) \cos[\arg(A_5)], \qquad (3.38\text{e})$$

and

$$c_6 = -2 \operatorname{abs}(A_5) \sin[\arg(A_5)]. \tag{3.38f}$$

3.4.6 Evaluation of the constants c_3, c_4, c_5, and c_6

Calculation of c_3

From Eq. (3.38c), it is seen that

$$c_3 = 2\operatorname{abs}(A_3) \cos[\arg(A_3)], \tag{3.39}$$

where, from Eq. (3.28b),

$$\arg(A_3) = -\frac{\pi}{2} + \tan^{-1}\left[\frac{2b(a - E_g)}{(a - E_g)^2 - b^2}\right] - \tan^{-1}\left[\frac{2ab}{a^2 - b^2 - E^2}\right]$$
$$- \tan^{-1}\left[\frac{b}{a}\right].$$

Letting

$$x = \tan^{-1}\left[\frac{2b(a - E_g)}{(a - E_g)^2 - b^2}\right],$$

$$y = \tan^{-1}\left[\frac{-2ab}{a^2 - b^2 - E^2}\right],$$

and

$$z = \tan^{-1}\left[\frac{-b}{a}\right],$$

it is seen that

$$\arg(A_3) = -\frac{\pi}{2} + x + y + z.$$

Noting that

$$\cos[\arg(A_3)] = \cos(-\frac{\pi}{2} + x + y + z) = \sin(x + y + z),$$

it may be seen that

$$\cos[\arg(A_3)] = \cos x \, \cos y \, \sin z - \sin x \, \sin y \, \sin z$$

$$+ \sin x \, \cos y \, \cos z + \cos x \, \sin y \, \cos z.$$

Letting

$$x = \tan^{-1}\left[\frac{2b(a - E_g)}{(a - E_g)^2 - b^2}\right],$$

one observes that

$$\cos x = \frac{(a - E_g)^2 - b^2}{(a - E_g)^2 + b^2},$$

and

$$\sin x = \frac{2b(a - E_g)}{(a - E_g)^2 + b^2}.$$

Similarly, letting

$$y = \tan^{-1}\left[\frac{-2ab}{a^2 - b^2 - E^2}\right],$$

one observes that

$$\cos y = \frac{a^2 - b^2 - E^2}{\sqrt{(a^2 - b^2 - E^2)^2 + (2ab)^2}},$$

and

$$\sin y = \frac{-2ab}{\sqrt{(a^2 - b^2 - E^2)^2 + (2ab)^2}}.$$

Letting

$$z = \tan^{-1}\left[\frac{-b}{a}\right],$$

it is seen that

$$\cos z = \frac{a}{\sqrt{(a^2 + b^2)}},$$

and

$$\sin z = \frac{-b}{\sqrt{(a^2 + b^2)}}.$$

Substituting the results for $\text{abs}(A_3)$, as well as the cosine and sine of x, y, and z, respectively, into Eq. (3.39) yields

$$c_3 = 2\,\text{abs}(A_3)\cos[\arg(A_3)],$$

$$c_3 = \frac{2}{8ab(a^2 + b^2)[(a^2 - b^2 - E^2)^2 + 4a^2b^2]} \times$$

$$\begin{bmatrix} -b \times [((a - E_g)^2 - b^2)(a^2 - b^2 - E^2) - 2b(a - E_g)(-2ab)] \\ \\ + \\ \\ a \times [2b(a - E_g)(a^2 - b^2 - E^2) + ((a - E_g)^2 - b^2)(-2ab)] \end{bmatrix},$$

$$= \frac{2}{8ab(a^2 + b^2)[(a^2 - b^2 - E^2)^2 + 4a^2b^2]} \times$$

$$\begin{bmatrix} 2b(a - E_g)[a(a^2 - b^2 - E^2) - 2ab^2] \\ \\ - \\ \\ ((a - E_g)^2 - b^2)[b(a^2 - b^2 - E^2) + 2a^2b] \end{bmatrix}.$$

Calculation of c₄

From Eq. (3.38d), it is seen that

$$c_4 = -2 \operatorname{abs}(A_3) \sin[\arg(A_3)], \tag{3.40}$$

where, from Eq. (3.28b),

$$\arg(A_3) = -\frac{\pi}{2} + \tan^{-1}\left[\frac{2b(a - E_g)}{(a - E_g)^2 - b^2}\right] - \tan^{-1}\left[\frac{2ab}{a^2 - b^2 - E^2}\right]$$

$$- \tan^{-1}\left[\frac{b}{a}\right].$$

Similarly, it is seen that

$$
\sin[\arg(A_3)] = \sin(-\frac{\pi}{2} + x + y + z) = -\cos(x + y + z)
$$

$$
= -[\cos x \, \cos y \, \cos z - \sin x \, \sin y \, \cos z
$$

$$
- \sin x \, \cos y \, \sin z - \cos x \, \sin y \, \sin z].
$$

Thus,

$$
c_4 = -2 \, \mathrm{abs}(A_3) \, \sin[\arg(A_3)],
$$

$$
= \frac{2}{8ab(a^2 + b^2)[(a^2 - b^2 - E^2)^2 + 4a^2b^2]} \times
$$

$$
\begin{bmatrix}
a \times [((a - E_g)^2 - b^2)(a^2 - b^2 - E^2) - 2b(a - E_g)(-2ab)] \\
\\
- \\
\\
b \times [-2b(a - E_g)(a^2 - b^2 - E^2) - ((a - E_g)^2 - b^2)(-2ab)]
\end{bmatrix},
$$

$$
= \frac{1}{4ab(a^2 + b^2)[(a^2 - b^2 - E^2)^2 + 4a^2b^2]} \times
$$

$$
\begin{bmatrix}
2b(a - E_g)[b(a^2 - b^2 - E^2) + 2a^2b] \\
\\
+ \\
\\
+((a - E_g)^2 - b^2)[a(a^2 - b^2 - E^2) - 2ab^2]
\end{bmatrix}.
$$

Calculation of c₅

From Eq. (3.38e),

$$c_5 = 2\,\mathrm{abs}(A_5)\cos[\arg(A_5)], \qquad (3.41)$$

where, from Eq. (3.32b),

$$\arg(A_5) = \frac{\pi}{2} - \tan^{-1}\left[\frac{2b(a+E_g)}{(a+E_g)^2 - b^2}\right] + \tan^{-1}\left[\frac{2ab}{a^2 - b^2 - E^2}\right] - \tan^{-1}\left[\frac{b}{-a}\right].$$

Letting

$$x = \tan^{-1}\left[\frac{-2b(a+E_g)}{(a+E_g)^2 - b^2}\right],$$

$$y = \tan^{-1}\left[\frac{2ab}{a^2 - b^2 - E^2}\right],$$

and

$$z = \tan^{-1}\left[\frac{-b}{-a}\right],$$

it is seen that

$$\arg(A_5) = \frac{\pi}{2} + x + y + z.$$

Noting that

$$\cos[\arg(A_5)] = \cos(\frac{\pi}{2} + x + y + z) = -\sin(x + y + z),$$

it may also be seen that

$$\cos\left[\arg(A_5)\right] = -\left[\cos x \ \cos y \ \sin z - \sin x \ \sin y \ \sin z\right.$$

$$+ \sin x \ \cos y \ \cos z + \cos x \ \sin y \ \cos z\right].$$

Letting

$$x = \tan^{-1}\left[\frac{-2b(a + E_g)}{(a + E_g)^2 - b^2}\right],$$

one observes that

$$\cos x = \frac{(a + E_g)^2 - b^2}{(a + E_g)^2 + b^2},$$

and

$$\sin x = \frac{-2b(a + E_g)}{(a + E_g)^2 + b^2}.$$

Similarly, letting

$$y = \tan^{-1}\left[\frac{2ab}{a^2 - b^2 - E^2}\right],$$

one observes that

$$\cos y = \frac{a^2 - b^2 - E^2}{\sqrt{(a^2 - b^2 - E^2)^2 + (2ab)^2}},$$

and

$$\sin y = \frac{2ab}{\sqrt{(a^2 - b^2 - E^2)^2 + (2ab)^2}}.$$

Letting

$$z = \tan^{-1}\left[\frac{-b}{-a}\right],$$

it is seen that

$$\cos z = \frac{-a}{\sqrt{(a^2 + b^2)}},$$

and

$$\sin z = \frac{-b}{\sqrt{(a^2 + b^2)}}.$$

Substituting the results of $\text{abs}(A_5)$, as well as the cosine and sine of x, y, and z into Eq. (3.41), yields

$$c_5 = 2\,\text{abs}(A_5)\,\cos[\arg(A_5)],$$

$$= \frac{-2}{8ab(a^2 + b^2)[(a^2 - b^2 - E^2)^2 + 4a^2b^2]} \times$$

$$\begin{bmatrix} -b \times [((a + E_g)^2 - b^2)(a^2 - b^2 - E^2) - (-2b(a + E_g))\,2ab] \\ \\ - \\ \\ a \times [-2b(a + E_g)(a^2 - b^2 - E^2) + ((a + E_g)^2 - b^2)\,2ab] \end{bmatrix},$$

$$= \frac{2}{8ab(a^2 + b^2)[(a^2 - b^2 - E^2)^2 + 4a^2b^2]} \times$$

$$\begin{bmatrix} -2b(a + E_g)[a(a^2 - b^2 - E^2) - 2ab^2] \\ \\ + \\ \\ ((a + E_g)^2 - b^2)[b(a^2 - b^2 - E^2) + 2a^2b] \end{bmatrix}.$$

Calculation of c$_6$

From Eq. (3.38f),

$$c_6 = -2 \operatorname{abs}(A_5) \sin[\arg(A_5)], \qquad (3.42)$$

where, from Eq. (3.32b),

$$\arg(A_5) = \frac{\pi}{2} - \tan^{-1}\left[\frac{2b(a + E_g)}{(a + E_g)^2 - b^2}\right] + \tan^{-1}\left[\frac{2ab}{a^2 - b^2 - E^2}\right]$$
$$- \tan^{-1}\left[\frac{b}{-a}\right].$$

Similarly,

$$\sin[\arg(A_5)] = \sin(\frac{\pi}{2} + x + y + z) = \cos(x + y + z),$$

$$= \cos x \, \cos y \, \cos z - \sin x \, \sin y \, \cos z$$

$$- \sin x \, \cos y \, \sin z - \cos x \, \sin y \, \sin z.$$

Thus, it may be seen that

$$c_6 = -2 \operatorname{abs}(A_5) \sin[\arg(A_5)],$$

$$= \frac{-2}{8ab(a^2 + b^2)[(a^2 - b^2 - E^2)^2 + 4a^2b^2]} \times$$

$$\left[\begin{array}{c} -a \times [((a + E_g)^2 - b^2)(a^2 - b^2 - E^2) - (-2b(a + E_g))\, 2ab] \\[2mm] - \\[2mm] b \times [-2b(a + E_g)(a^2 - b^2 - E^2) - ((a + E_g)^2 - b^2)\, 2ab] \end{array}\right],$$

$$= \frac{1}{4ab(a^2+b^2)[(a^2-b^2-E^2)^2+4a^2b^2]} \times$$

$$\left[\begin{array}{c} 2b(a+E_g)[b(a^2-b^2-E^2)+2a^2b] \\ \\ + \\ \\ ((a+E_g)^2-b^2)[a(a^2-b^2-E^2)-2ab^2] \end{array}\right].$$

3.4.7 Main integration

So, from Eq.(3.14), it is seen that

$$\begin{aligned} \epsilon_1(E) &= \epsilon_{1\infty} + \frac{2AE_oC}{\pi}P\int_{E_g}^{\infty}\frac{(u-E_g)^2}{(u^2-E^2)[(u^2-E_o^2)^2+C^2u^2]}\,du, \\ &= \epsilon_{1\infty} + \frac{2AE_oC}{\pi}P\int_{E_g}^{\infty}f(u)\,du. \end{aligned} \tag{3.43}$$

From the partial fraction expansion of Eq. (3.37), this yields

$$\begin{aligned} \int_{E_g}^{\infty}f(u)\,du &= \int_{E_g}^{\infty}\frac{A_1}{u+E}\,du + \int_{E_g}^{\infty}\frac{A_2}{u-E}\,du \\ &+ \int_{E_g}^{\infty}c_3\frac{u-a}{(u-a)^2+b^2}\,du \\ &+ \int_{E_g}^{\infty}c_4\frac{b}{(u-a)^2+b^2}\,du \\ &+ \int_{E_g}^{\infty}c_5\frac{u+a}{(u+a)^2+b^2}\,du \\ &+ \int_{E_g}^{\infty}c_6\frac{b}{(u+a)^2+b^2}\,du, \end{aligned}$$

In order to avoid improper integrals, the integrals will all be taken to t, and then t will go to infinity, i.e., $t \to \infty$. Thus, it can be seen that

$$\implies \int_{E_g}^t f(u)\, du = \int_{E_g}^t \frac{A_1}{u + E}\, du + \int_{E_g}^t \frac{A_2}{u - E}\, du$$

$$+ \int_{E_g}^t c_3 \frac{u - a}{(u - a)^2 + b^2}\, du$$

$$+ \int_{E_g}^t c_4 \frac{b}{(u - a)^2 + b^2}\, du$$

$$+ \int_{E_g}^t c_5 \frac{u + a}{(u + a)^2 + b^2}\, du$$

$$+ \int_{E_g}^t c_6 \frac{b}{(u + a)^2 + b^2}\, du. \tag{3.44}$$

Sequentially integrating the terms in Eq. (3.44), it is thus seen that

$$\int_{E_g}^t \frac{A_1}{u + E}\, du = A_1 \int_{E_g}^t \frac{1}{u + E}\, du,$$

$$= A_1 \left[\ln(u + E)\right]_{E_g}^t,$$

$$= A_1 \left[\ln(t + E)\right] - A_1 \ln(E_g + E), \tag{3.45}$$

and

$$\int_{E_g}^t \frac{A_2}{u - E}\, du = A_2 \left[\lim_{\epsilon \to 0} \int_{E_g}^{E - \epsilon} \frac{1}{u - E}\, du + \lim_{\epsilon \to 0} \int_{E + \epsilon}^t \frac{1}{u - E}\, du\right],$$

$$= A_2 \left[\lim_{\epsilon \to 0} \ln |u - E|_{E_g}^{E - \epsilon} + \lim_{\epsilon \to 0} \ln |u - E|_{E + \epsilon}^t\right],$$

$$= A_2 \left[\lim_{\epsilon \to 0} \ln | - \epsilon|\right] - A_2 \left[\ln |E_g - E| + \ln |t - E|\right]$$

$$- A_2 \left[\lim_{\epsilon \to 0} \ln |\epsilon|\right],$$

$$= A_2 \left[\ln |t - E|\right] - A_2 \ln |E_g - E|. \tag{3.46}$$

Now, for

$$\int_{E_g}^{t} c_3 \frac{u-a}{(u-a)^2+b^2}\, du,$$

letting

$$w = (u-a)^2 + b^2,$$

$$\implies dw = 2(u-a)\, du,$$

it may be seen that

$$\int_{E_g}^{t} c_3 \frac{u-a}{(u-a)^2+b^2}\, du = \frac{c_3}{2} \int_{(E_g-a)^2+b^2}^{(t-a)^2+b^2} \frac{1}{w}\, dw, \qquad (3.47)$$

$$= \frac{c_3}{2}\left[\ln[(t-a)^2+b^2]\right]$$

$$-\frac{c_3}{2}\ln[(E_g-a)^2+b^2]. \qquad (3.48)$$

Again, for

$$\int_{E_g}^{t} c_4 \frac{b}{(u-a)^2+b^2}\, du,$$

letting

$$(u-a) = b\tan\theta,$$

$$\implies du = b\sec^2\theta\, d\theta,$$

it is seen that

$$
\begin{aligned}
c_4 \int_{E_g}^{t} \frac{b}{(u-a)^2 + b^2} \, du \; &= \; c_4 \int_{E_g}^{t} \frac{b \sec^2 \theta}{b^2 \tan^2 \theta + b^2} \, d\theta, \\[2mm]
&= \; c_4 \left[\theta \right]_{E_g}^{t}, \\[2mm]
&= \; c_4 \left[\tan^{-1} \left(\frac{u-a}{b} \right) \right]_{E_g}^{t}, \\[2mm]
&= \; c_4 \left[\frac{\pi}{2} - \tan^{-1} \left(\frac{E_g - a}{b} \right) \right]. \quad [\text{as } t \to \infty]
\end{aligned}
$$

$$(3.49)$$

Similarly,

$$
\begin{aligned}
\int_{E_g}^{t} c_5 \frac{u+a}{(u+a)^2 + b^2} \, du \; &= \; \frac{c_5}{2} \left[\ln[(t+a)^2 + b^2]] \right. \\[2mm]
& \qquad - \frac{c_5}{2} \ln[(E_g + a)^2 + b^2], \qquad (3.50) \\[2mm]
\int_{E_g}^{t} c_6 \frac{b}{(u+a)^2 + b^2} \, du \; &= \; c_6 \left[\frac{\pi}{2} - \tan^{-1} \left(\frac{E_g + a}{b} \right) \right]. \qquad (3.51)
\end{aligned}
$$

From Eq. (3.44), it is seen that

$$
\begin{aligned}
\int_{E_g}^{t} f(u) du \; &= \; A_1 \left[\ln(t+E) \right] - A_1 \ln(E_g + E) \\[2mm]
& \quad + A_2 \left[\ln|t - E| \right] - A_2 \ln |E_g - E|
\end{aligned}
$$

$$+\frac{c_3}{2}\left[\ln[(t-a)^2+b^2]\right]-\frac{c_3}{2}\ln[(E_g-a)^2+b^2]$$

$$+c_4\left[\frac{\pi}{2}-\tan^{-1}\left(\frac{E_g-a}{b}\right)\right]$$

$$+\frac{c_5}{2}\left[\ln[(t+a)^2+b^2]\right]-\frac{c_5}{2}\ln[(E_g+a)^2+b^2]$$

$$+c_6\left[\frac{\pi}{2}-\tan^{-1}\left(\frac{E_g+a}{b}\right)\right]. \tag{3.52}$$

Letting

$$\phi_1=\ln(t+E)]-\ln(E_g+E),$$

$$\phi_2=\ln|t-E|-\ln|E_g-E|,$$

$$\phi_3=\ln[(t-a)^2+b^2]-\ln[(E_g-a)^2+b^2],$$

$$\phi_4=\frac{\pi}{2}-\tan^{-1}\left(\frac{E_g-a}{b}\right),$$

$$\phi_5=\ln[(t+a)^2+b^2]-\ln[(E_g+a)^2+b^2],$$

and

$$\phi_6=\frac{\pi}{2}-\tan^{-1}\left(\frac{E_g+a}{b}\right),$$

Eq. (3.52) leads to

$$\int_{E_g}^{\infty}f(u)du\ =\ A_1\phi_1+A_2\phi_2+\frac{c_3}{2}\phi_3+\frac{c_5}{2}\phi_5+c_4\phi_4+c_6\phi_6. \tag{3.53}$$

3.4.8 Summation by parts

For simplicity, the summation, depicted in Eq. (3.53), is performed in parts such that

$$
\begin{aligned}
\text{term 1} &= A_1\phi_1 + A_2\phi_2, \\
\text{term 2} &= \frac{c_3}{2}\phi_3 + \frac{c_5}{2}\phi_5, \\
\text{term 3} &= c_4\phi_4 + c_6\phi_6.
\end{aligned}
$$

From Eq. (3.53), it is thus seen that

$$
\int_{E_g}^{\infty} f(u)du = \underbrace{A_1\phi_1 + A_2\phi_2}_{\text{term 1}} + \underbrace{\frac{c_3}{2}\phi_3 + \frac{c_5}{2}\phi_5}_{\text{term 2}} + \underbrace{c_4\phi_4 + c_6\phi_6}_{\text{term 3}}.
$$

Calculation of term 1

term 1

$$
\begin{aligned}
&= A_1\phi_1 + A_2\phi_2, \\
&= \frac{-(E+E_g)^2}{2E[(E^2-E_o^2)^2+C^2E^2]}\phi_1 + \frac{(E-E_g)^2}{2E[(E^2-E_o^2)^2+C^2E^2]}\phi_2, \\
&= \frac{E^2+E_g^2}{2E[(E^2-E_o^2)^2+C^2E^2]}[\phi_2-\phi_1] - \frac{2EE_g}{2E[(E^2-E_o^2)^2+C^2E^2]}[\phi_2+\phi_1], \\
&= \frac{E^2+E_g^2}{2E[(E^2-E_o^2)^2+C^2E^2]}[\phi_2-\phi_1] - \frac{E_g}{[(E^2-E_o^2)^2+C^2E^2]}[\phi_2+\phi_1], \\
&= \frac{E^2+E_g^2}{2E\zeta^4}[\phi_2-\phi_1] - \frac{E_g}{\zeta^4}[\phi_2+\phi_1],
\end{aligned}
$$

where

$$\phi_2 - \phi_1 = \ln|t - E| - \ln|E_g - E| - \ln(t + E)] + \ln(E_g + E),$$

$$= \ln\frac{|t - E|}{t + E} + \ln\frac{(E_g + E)}{|E_g - E|},$$

$$= \ln\frac{(E_g + E)}{|E_g - E|}, \quad [\text{as } t \to \infty]$$

$$\phi_2 + \phi_1 = \ln|t - E| - \ln|E_g - E| + \ln(t + E)] - \ln(E_g + E),$$

$$= \ln[(t + E)|t - E|] - \ln[(E_g + E)|E_g - E|].$$

Calculation of term 2:

term 2

$$= \frac{c_3}{2}\phi_3 + \frac{c_5}{2}\phi_5,$$

$$= \frac{1}{8ab(a^2 + b^2)[(a^2 - b^2 - E^2)^2 + 4a^2b^2]} \times$$

$$\begin{bmatrix} 2b(a - E_g)[a(a^2 - b^2 - E^2) - 2ab^2]\phi_3 \\ - \\ ((a - E_g)^2 - b^2)[b(a^2 - b^2 - E^2) + 2a^2b]\phi_3 \\ + \\ -2b(a + E_g)[a(a^2 - b^2 - E^2) - 2ab^2]\phi_5 \\ + \\ ((a + E_g)^2 - b^2)[b(a^2 - b^2 - E^2) + 2a^2b]\phi_5 \end{bmatrix},$$

$$= \frac{1}{8ab(a^2 + b^2)[(a^2 - b^2 - E^2)^2 + 4a^2b^2]} \times$$

$$\begin{bmatrix} 2ba[a(a^2 - b^2 - E^2) - 2ab^2][\phi_3 - \phi_5] \\ - \\ (a^2 + E_g^2 - b^2)[b(a^2 - b^2 - E^2) + 2a^2b][\phi_3 - \phi_5] \\ + \\ -2bE_g[a(a^2 - b^2 - E^2) - 2ab^2][\phi_3 + \phi_5] \\ + \\ 2aE_g[b(a^2 - b^2 - E^2) + 2a^2b][\phi_3 + \phi_5] \end{bmatrix},$$

92

$$= \frac{1}{8a(E_o^2 - \frac{C^2}{4} + \frac{C^2}{4})[(E_o^2 - \frac{C^2}{4} - \frac{C^2}{4} - E^2)^2 + 4(E_o^2 - \frac{C^2}{4})\frac{C^2}{4}]} \times$$

$$\begin{bmatrix} 2a^2(a^2 - 3b^2 - E^2)[\phi_3 - \phi_5] \\ - \\ (a^2 - b^2 + E_g^2)(3a^2 - b^2 - E^2)[\phi_3 - \phi_5] \\ + \\ [-2abE_g(a^2 - b^2 - E^2) + 2abE_g 2b^2][\phi_3 + \phi_5] \\ + \\ [2abE_g(a^2 - b^2 - E^2) + 2abE_g 2a^2][\phi_3 + \phi_5] \end{bmatrix},$$

$$= \frac{1}{8a\, E_o^2[(E^2 - E_o^2)^2 + C^2 E^2]} \times$$

$$\begin{bmatrix} [2(E_o^2 - \frac{C^2}{4})(E_o^2 - C^2 - E^2)][\phi_3 - \phi_5] \\ - \\ [(E_o^2 - \frac{C^2}{2} + E_g^2)(3E_o^2 - C^2 - E^2)][\phi_3 - \phi_5] \end{bmatrix}$$

$$+ \frac{E_g}{2[(E^2 - E_o^2)^2 + C^2 E^2]}[\phi_3 + \phi_5],$$

$$= \frac{-E_o^4 + E_g^2 C^2 + E_g^2 E^2 - E_o^2 E^2 - 3E_o^2 E_g^2}{8a\, E_o^2[(E^2 - E_o^2)^2 + C^2 E^2]}[\phi_3 - \phi_5]$$

$$+ \frac{E_g}{2[(E^2 - E_o^2)^2 + C^2 E^2]}[\phi_3 + \phi_5],$$

$$= \frac{(E_g^2 - E_o^2)E^2 + E_g^2 C^2 - E_o^2(E_o^2 + 3E_g^2)}{8a\, E_o^2[(E^2 - E_o^2)^2 + C^2 E^2]}[\phi_3 - \phi_5]$$

$$+ \frac{E_g}{2[(E^2 - E_o^2)^2 + C^2 E^2]}[\phi_3 + \phi_5],$$

$$= \frac{a_{\ln}}{4\chi\, E_o^2\, \zeta^4}[\phi_3 - \phi_5] + \frac{E_g}{2\, \zeta^4}[\phi_3 + \phi_5],$$

where

$$\begin{aligned}
\phi_3 - \phi_5 &= \ln[(t-a)^2 + b^2] - \ln[(E_g - a)^2 + b^2] \\
&\quad - \ln[(t+a)^2 + b^2] + \ln[(E_g + a)^2 + b^2], \\
&= \ln\frac{(t-a)^2 + b^2}{(t+a)^2 + b^2} + \ln\frac{[(E_g + a)^2 + b^2]}{[(E_g - a)^2 + b^2]}, \\
&= \ln\frac{[E_g^2 + a^2 + b^2 + 2aE_g]}{[E_g^2 + a^2 + b^2 - 2aE_g]}, \quad [\text{as } t \to \infty] \\
&= \ln\frac{[E_g^2 + E_o^2 + 2aE_g]}{[E_g^2 + E_o^2 - 2aE_g]}, \\
&= \ln\frac{[E_g^2 + Eo^2 + \chi E_g]}{[E_g^2 + Eo^2 - \chi E_g]}, \quad [\text{recall that}, \chi = \sqrt{4E_o^2 - C^2} = 2a]
\end{aligned}$$

$$\begin{aligned}
\phi_3 + \phi_5 &= \ln[(t-a)^2 + b^2] - \ln[(E_g - a)^2 + b^2] \\
&\quad + \ln[(t+a)^2 + b^2] - \ln[(E_g + a)^2 + b^2], \\
&= \ln[[(t-a)^2 + b^2][(t+a)^2 + b^2]] \\
&\quad - \ln[[(E_g - a)^2 + b^2][(E_g + a)^2 + b^2]], \\
&= \ln[[(t-a)^2 + b^2][(t+a)^2 + b^2]] \\
&\quad - \ln[(E_g^2 + E_o^2 + \chi E_g)(E_g^2 + E_o^2 - \chi E_g)], \\
&= \ln[[(t-a)^2 + b^2][(t+a)^2 + b^2]] - \ln[(E_o^2 - E_g^2)^2 + E_g^2 C^2)].
\end{aligned}$$

3.4.9 Calculation of term 3:

term 3

$$= c_4\phi_4 + c_6\phi_6,$$

$$= \frac{1}{4ab(a^2+b^2)[(a^2-b^2-E^2)^2+4a^2b^2]} \times$$

$$\begin{bmatrix} 2b(a-E_g)[b(a^2-b^2-E^2)+2a^2b]\phi_4 \\ + \\ ((a-E_g)^2-b^2)[a(a^2-b^2-E^2)-2ab^2]\phi_4 \\ + \\ 2b(a+E_g)[b(a^2-b^2-E^2)+2a^2b]\phi_6 \\ + \\ ((a+E_g)^2-b^2)[a(a^2-b^2-E^2)-2ab^2]\phi_6 \end{bmatrix},$$

$$= \frac{2b^2a(3a^2-b^2-E^2)+a(a^2+E_g^2-b^2)(a^2-3b^2-E^2)}{4ab(a^2+b^2)[(a^2-b^2-E^2)^2+4a^2b^2]}[\phi_4+\phi_6]$$
$$+\frac{2b^2E_g(3a^2-b^2-E^2)+2a^2E_g(a^2-3b^2-E^2)}{4ab(a^2+b^2)[(a^2-b^2-E^2)^2+4a^2b^2]}[\phi_6-\phi_4],$$

$$= \frac{2b^2(3a^2-b^2-E^2)+(a^2+E_g^2-b^2)(a^2-3b^2-E^2)}{2C\,E_o^2[(E^2-E_o^2)^2+C^2E^2]}[\phi_4+\phi_6]$$
$$+\frac{2E_g[b^2(3a^2-b^2-E^2)+a^2(a^2-3b^2-E^2)]}{\chi\,C\,E_o^2[(E^2-E_o^2)^2+C^2E^2]}[\phi_6-\phi_4],$$

$$= \frac{\frac{C^2}{2}(3E_o^2-C^2-E^2)+(E_o^2-\frac{C^2}{2}+E_g^2)(E_o^2-C^2-E^2)}{2C\,E_o^2[(E^2-E_o^2)^2+C^2E^2]}[\phi_4+\phi_6]$$
$$+\frac{2E_g[\frac{C^2}{4}(3E_o^2-C^2-E^2)+(E_o^2-\frac{C^2}{4})(E_o^2-C^2-E^2)]}{\chi\,C\,E_o^2[(E^2-E_o^2)^2+C^2E^2]}[\phi_6-\phi_4],$$

$$= \frac{E_o^4 - E^2 E_o^2 + E_o^2 E_g^2 - E_g^2 E^2 - E_g^2 C^2}{2C \, E_o^2[(E^2 - E_o^2)^2 + C^2 E^2]}[\phi_4 + \phi_6]$$

$$+ \frac{2E_g[-\frac{E_o^2 C^2}{2} + E_o^4 - E_o^2 E^2]}{\chi \, C \, E_o^2[(E^2 - E_o^2)^2 + C^2 E^2]}[\phi_6 - \phi_4],$$

$$= \frac{-[(E^2 - E_o^2)(E_o^2 + E_g^2) + E_g^2 C^2]}{2C \, E_o^2[(E^2 - E_o^2)^2 + C^2 E^2]}[\phi_4 + \phi_6]$$

$$+ \frac{2E_g[E^2 - E_o^2 + \frac{C^2}{2}]}{\chi \, C \, [(E^2 - E_o^2)^2 + C^2 E^2]}[\phi_4 - \phi_6],$$

$$= \frac{-a_{a \tan}}{2C \, E_o^2 \, \zeta^4}[\phi_4 + \phi_6] + \frac{2E_g[E^2 - \gamma^2]}{\chi C \zeta^4}[\phi_4 - \phi_6].$$

where

$$\phi_4 + \phi_6 = \frac{\pi}{2} - \tan^{-1}\left(\frac{E_g - a}{b}\right) + \frac{\pi}{2} - \tan^{-1}\left(\frac{E_g + a}{b}\right),$$

$$= \pi - \tan^{-1}\left(\frac{E_g + a}{b}\right) + \tan^{-1}\left(\frac{-E_g + a}{b}\right),$$

$$= \pi - \tan^{-1}\left(\frac{2E_g + 2a}{C}\right) + \tan^{-1}\left(\frac{-2E_g + 2a}{C}\right),$$

$$= \pi - \tan^{-1}\left(\frac{2E_g + \chi}{C}\right) + \tan^{-1}\left(\frac{-2E_g + \chi}{C}\right),$$

$$\phi_4 - \phi_6, = \frac{\pi}{2} - \tan^{-1}\left(\frac{E_g - a}{b}\right) - \frac{\pi}{2} + \tan^{-1}\left(\frac{E_g + a}{b}\right),$$

$$= \tan^{-1}\left(\frac{2ab}{b^2 - a^2 + E_g^2}\right),$$

$$= \tan^{-1}\left(\frac{\chi C}{-2(a^2 - b^2 - E_g^2)}\right),$$

$$= \frac{\pi}{2} + \tan^{-1}\left(\frac{2(a^2 - b^2 - E_g^2)}{\chi C}\right),$$

$$\left[\text{recall that, } \tan^{-1}\left(\frac{y}{x}\right) = \frac{\pi}{2} + \tan^{-1}\left(\frac{-x}{y}\right)\right]$$

$$= \frac{\pi}{2} + \tan^{-1} \left(\frac{2(E_o^2 - \frac{C^2}{2} - E_g^2)}{\chi C} \right),$$

$$= \frac{\pi}{2} + \tan^{-1} \left(\frac{2(\gamma^2 - E_g^2)}{\chi C} \right).$$

3.4.10 Summation of term 1, term 2 and term 3

term 1+term 2+term 3

$$= \frac{E^2 + E_g^2}{2E\zeta^4}[\phi_2 - \phi_1] - \frac{E_g}{\zeta^4}[\phi_2 + \phi_1]$$

$$+ \frac{a_{\ln}}{4\chi E_o^2 \zeta^4}[\phi_3 - \phi_5] + \frac{E_g}{2.\zeta^4}[\phi_3 + \phi_5]$$

$$+ \frac{-a_{a\tan}}{2CE_o^2\zeta^4}[\phi_4 + \phi_6] + \frac{2E_g[E^2 - \gamma^2]}{\chi C\zeta^4}[\phi_4 - \phi_6],$$

$$= \frac{E^2 + E_g^2}{2E\zeta^4} \ln \left[\frac{(E_g + E)}{|E_g - E|} \right] - \frac{E_g}{\zeta^4} \ln \left[(t + E)|t - E| \right]$$

$$+ \frac{E_g}{\zeta^4} \ln[(E_g + E)|E_g - E|]$$

$$+ \frac{a_{\ln}}{8aE_o^2\zeta^4} \ln \left[\frac{[E_g^2 + E_o^2 + \chi E_g]}{[E_g^2 + E_o^2 - \chi E_g]} \right]$$

$$+ \frac{E_g}{2\zeta^4} \ln[[(t - a)^2 + b^2][(t + a)^2 + b^2]]$$

$$- \frac{E_g}{2\zeta^4} \ln[(E_o^2 - E_g^2)^2 + E_g^2 C^2)]$$

$$- \frac{a_{a\tan}}{2CE_o^2\zeta^4} \left[\pi - \tan^{-1} \left(\frac{2E_g + \chi}{C} \right) + \tan^{-1} \left(\frac{-2E_g + \chi}{C} \right) \right]$$

$$+ \frac{2E_g[E^2 - \gamma^2]}{\chi C\zeta^4} \left[\frac{\pi}{2} + \tan^{-1} \left(\frac{2(\gamma^2 - E_g^2)}{\chi C} \right) \right], [\text{here } t \to \infty]$$

$$
= \frac{a_{\ln}}{4\chi E_o^2 \zeta^4} \ln \left[\frac{E_g^2 + E_o^2 + \chi E_g}{E_g^2 + E_o^2 - \chi E_g} \right]
$$

$$
- \frac{a_{a\tan}}{2CE_o^2 \zeta^4} \left[\pi - \tan^{-1}\left(\frac{2E_g + \chi}{C} \right) + \tan^{-1}\left(\frac{-2E_g + \chi}{C} \right) \right]
$$

$$
+ \frac{E_g[E^2 - \gamma^2]}{\chi C \zeta^4} \left[\pi + 2\tan^{-1}\left(\frac{2(\gamma^2 - E_g^2)}{\chi C} \right) \right]
$$

$$
- \frac{E^2 + E_g^2}{2E\zeta^4} \ln \left[\frac{|E_g - E|}{(E_g + E)} \right] + \frac{E_g}{\zeta^4} \ln \left[\frac{[(E_g + E)|E_g - E|]}{\sqrt{(E_o^2 - E_g^2)^2 + E_g^2 C^2)}} \right].
$$

3.4.11 Final Tauc-Lorentz expression for the model of

Jellison and Modine

Now, from Eq. (3.43),

$$
\epsilon_1(E) = \epsilon_{1\infty} + \frac{2AE_oC}{\pi} P \int_{E_g}^{\infty} f(u)du,
$$

$$
= \epsilon_{1\infty} + \frac{2AE_oC}{\pi}[\text{term } 1 + \text{term } 2 + \text{term } 3],
$$

$$
= \epsilon_{1\infty} + \frac{2AE_oC}{\pi} \frac{a_{\ln}}{4\chi E_o^2 \zeta^4} \ln \left[\frac{E_g^2 + E_o^2 + \chi E_g}{E_g^2 + E_o^2 - \chi E_g} \right]
$$

$$
- \frac{2AE_oC}{\pi} \frac{a_{a\tan}}{2CE_o^2 \zeta^4} \left[\pi - \tan^{-1}\left(\frac{2E_g + \chi}{C} \right) + \tan^{-1}\left(\frac{-2E_g + \chi}{C} \right) \right]
$$

$$
+ \frac{2AE_oC}{\pi} \frac{E_g[E^2 - \gamma^2]}{\chi C \zeta^4} \left[\pi + 2\tan^{-1}\left(\frac{2(\gamma^2 - E_g^2)}{\chi C} \right) \right]
$$

$$
- \frac{2AE_oC}{\pi} \frac{E^2 + E_g^2}{2E\zeta^4} \ln \left[\frac{|E_g - E|}{(E_g + E)} \right]
$$

$$
+ \frac{2AE_oC}{\pi} \frac{E_g}{\zeta^4} \ln \left[\frac{[(E_g + E)|E_g - E|]}{\sqrt{(E_o^2 - E_g^2)^2 + E_g^2 C^2)}} \right].
$$

$$
\begin{aligned}
\implies \epsilon_1(E) \; = \; & \epsilon_{1\infty} + \frac{1}{2}\frac{A}{\pi}\frac{C}{\zeta^4}\frac{a_{\ln}}{\chi E_o}\ln\left[\frac{E_g^2 + E_o^2 + \chi E_g}{E_g^2 + E_o^2 - \chi E_g}\right] \\
& - \frac{A}{\pi\zeta^4}\frac{a_{a\,\tan}}{E_o}\left[\pi - \tan^{-1}\left(\frac{2E_g + \chi}{C}\right) + \tan^{-1}\left(\frac{-2E_g + \chi}{C}\right)\right] \\
& + 2\frac{AE_o}{\pi\chi\zeta^4}E_g[E^2 - \gamma^2]\left[\pi + 2\tan^{-1}\left(\frac{2(\gamma^2 - E_g^2)}{\chi C}\right)\right] \\
& - \frac{AE_oC}{\pi\zeta^4}\frac{E^2 + E_g^2}{E}\ln\left[\frac{|E_g - E|}{(E_g + E)}\right] \\
& + \frac{2AE_oC}{\pi\zeta^4}E_g\ln\left[\frac{[(E_g + E)|E_g - E|]}{\sqrt{(E_o^2 - E_g^2)^2 + E_g^2C^2)}}\right],
\end{aligned}
$$

this being the same result as that in Eq. (3.12), all terms being defined in the same manner.

3.5 Comparing the results of the Jellison and Modine model with experimental data

The parameterized model for the optical functions, $\epsilon_1(E)$ and $\epsilon_2(E)$, of Jellison and Modine [15] is now fit with the results of experiment. The experimental results that are considered include that of Piller [30], Synowicki [31], and Ferluato *et al.* [32], these experimental results corresponding to the EGE a-Si, PECVD a-Si I, and PECVD a-Si II experimental data sets mentioned

in Section 2.10, respectively; these experimental data sets are further described in Section 2.10. The approach that is adopted for each experimental fit involves the selection of the modeling parameters that "best-fits" the corresponding experimental data set. This is achieved through a selection of modeling parameters, a determination of the corresponding spectral dependencies of the optical functions, $\epsilon_1(E)$ and $\epsilon_2(E)$, and a comparison with the results of experiments. The "best-fit" is obtained through visual inspection. Through a sweep over a range of parameter values, the parameter selections that "best-fit" the corresponding experimental optical functions is determined. It is noted that, in all cases, the results of the model of Jellison and Modine [15] agree with that of experiment over most of the spectrum considered. The "best-fit" parameter values, corresponding to the different experimental fits, are tabulated in Table 3.1. The resultant fits, and the corresponding experimental data sets, are depicted in Figures 3.1, 3.2, and 3.3, these corresponding to the experimental results of EGE a-Si, PECVD a-Si I, and PECVD a-Si II, respectively.

Table 3.1: The "best-fit" a-Si modeling parameter selections employed for the Tauc-Lorentz model of Jellison and Modine [15] for fits to experimental data corresponding to EGE a-Si, PECVD a-Si I, and PECVD a-Si II.

parameter (units)	EGE a-Si [30]	PECVD a-Si I [31]	PECVD a-Si II [32]
A (eV)	125	196	203
E_o (eV)	3.43	3.64	3.72
C (eV)	2.54	2.3	2.1
E_g (eV)	1.21	1.51	1.68
$\epsilon_{1\infty}$	1.0	1.0	0.65
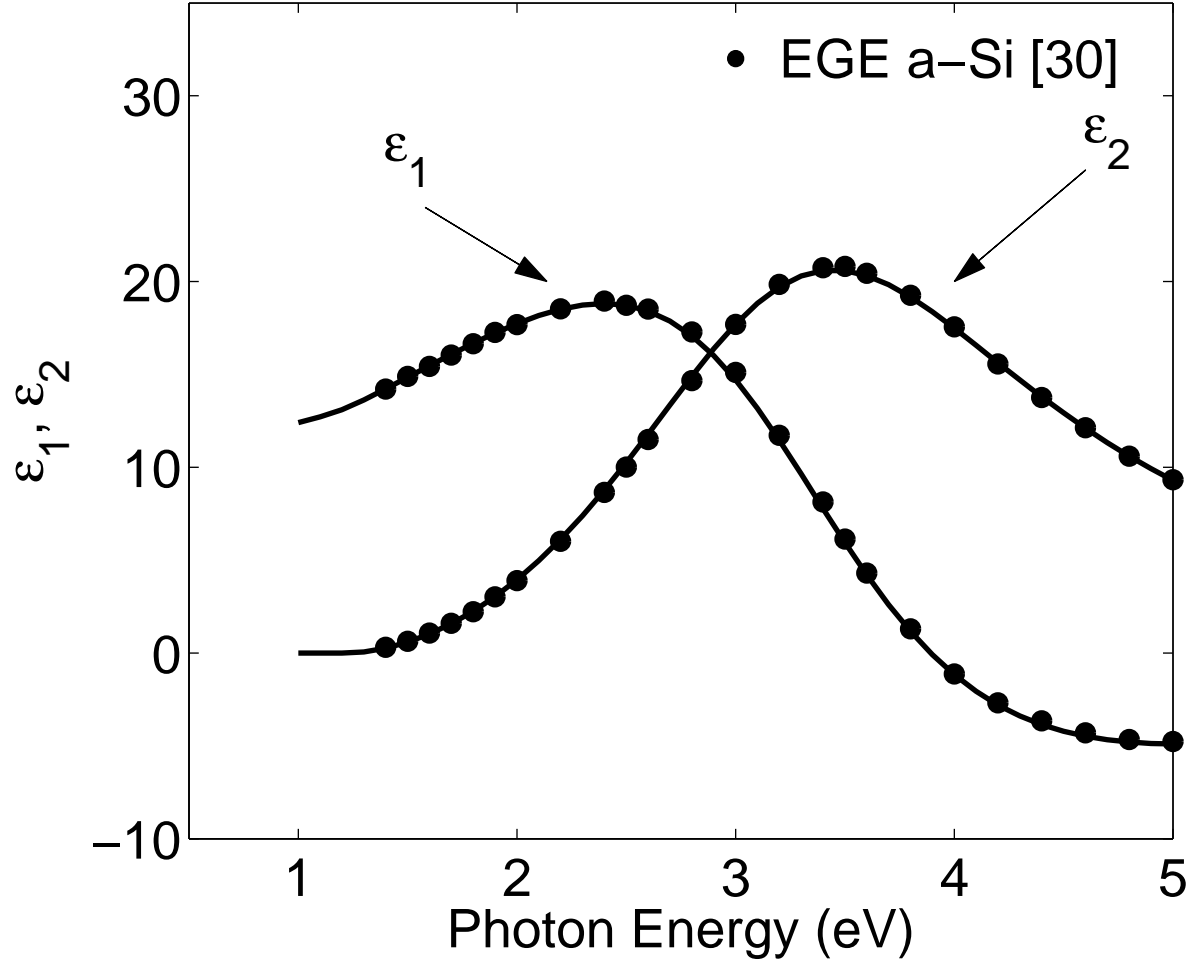
Figure 3.1: A "best-fit" of the Jellison and Modine model with the results of experiment corresponding to the EGE a-Si expermental data set [30]. These experimental results are from Piller [30]. The fits to experiment are shown with the solid lines. The experimental data, EGE a-Si [30], is depicted with the solid points.
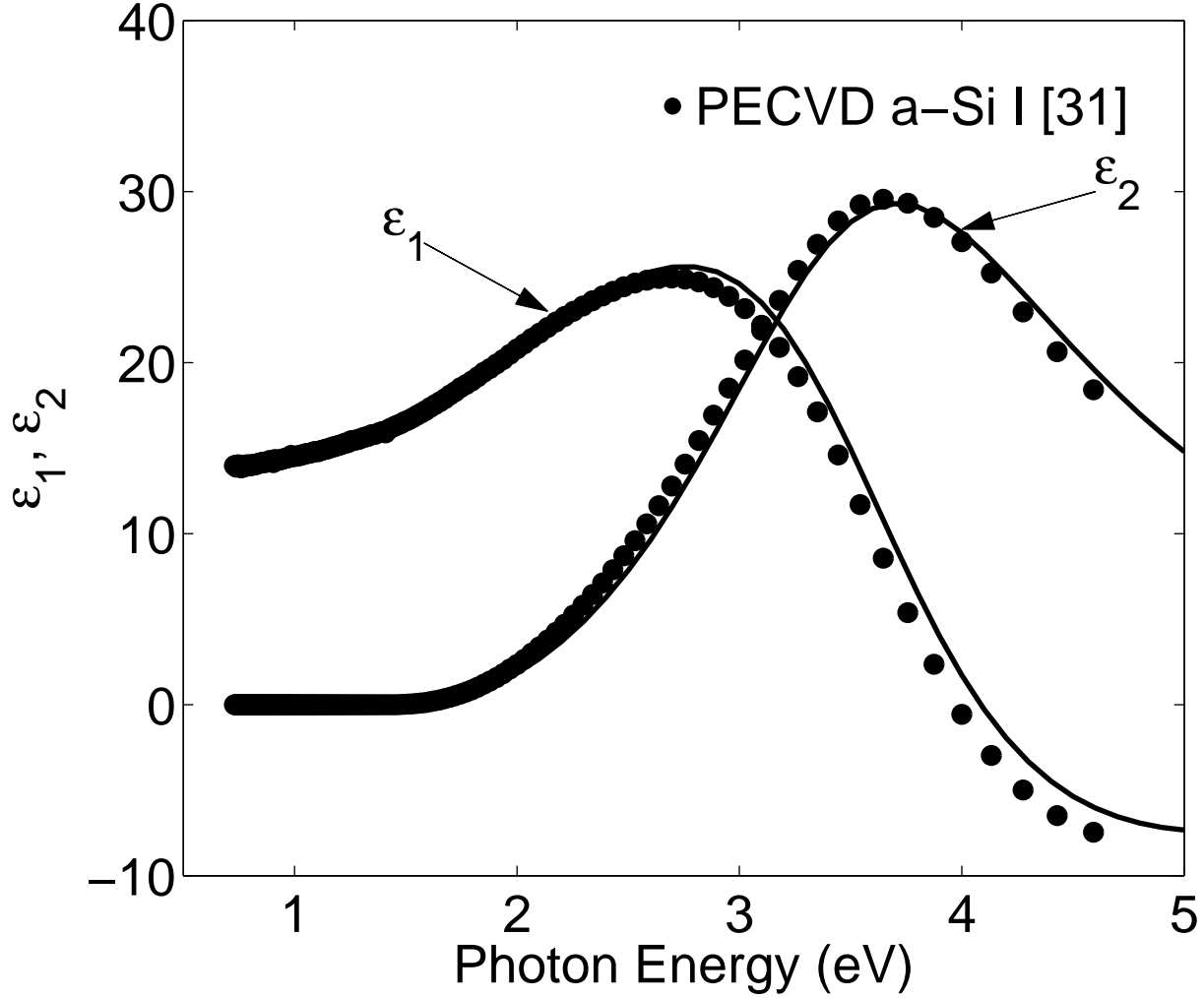
Figure 3.2: A "best-fit" of the Jellison and Modine model with the results of experiment corresponding to the PECVD a-Si I experimental data set [31]. These experimental results are from Synowicki [31]. The fits to experiment are shown with the solid lines. The experimental data, PECVD a-Si I [31], is depicted with the solid points.
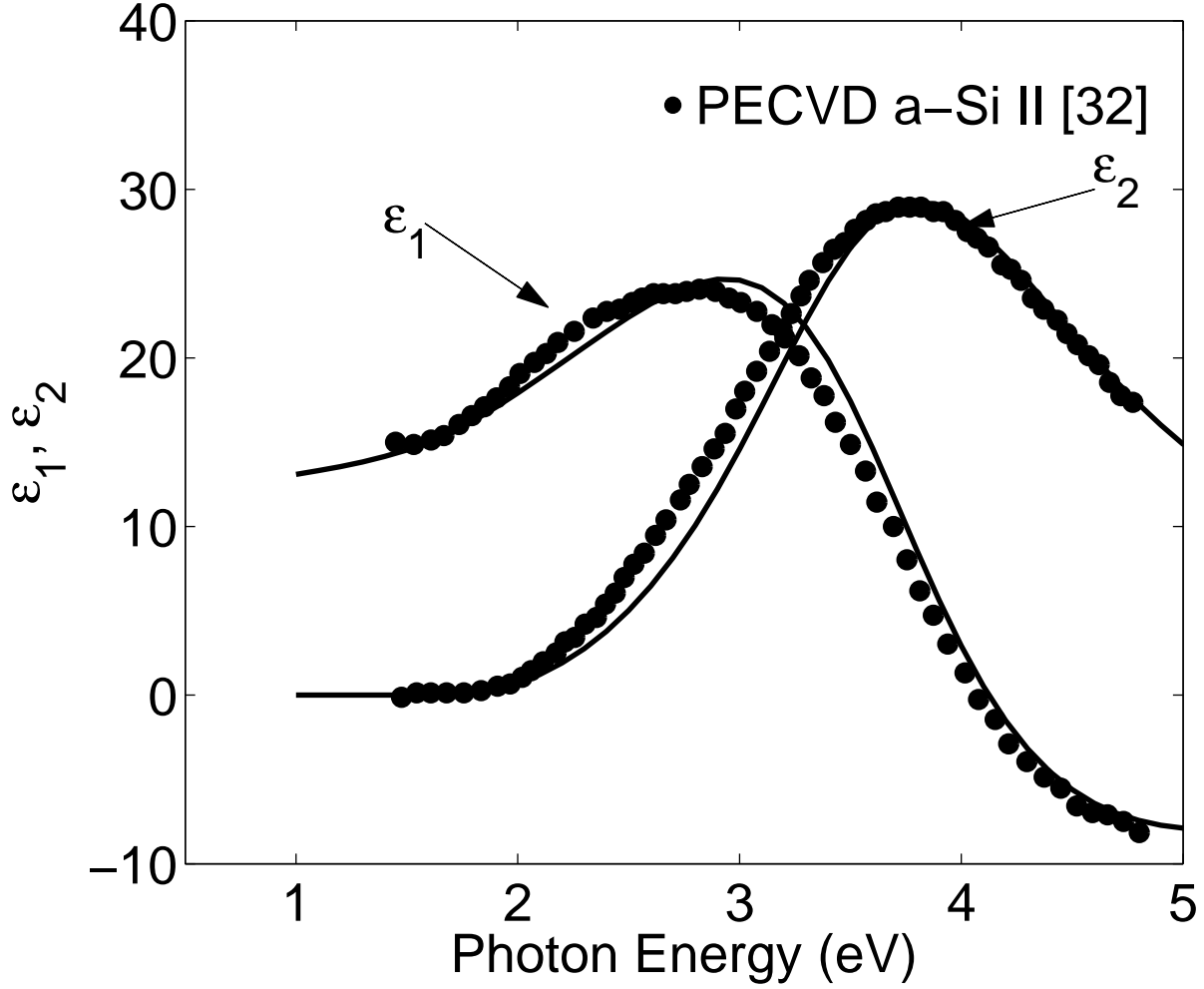
Figure 3.3: A "best-fit" of the Jellison and Modine model with the results of experiment corresponding to the PECVD a-Si II experimental data set [32]. These experimental results are from Ferluato *et al.* [32]. The fits to experiment are shown with the solid lines. The experimental data, PECVD a-Si II [32], is depicted with the solid points.

Chapter 4

A physically based Kramers-Kronig consistent model for the optical functions associated with amorphous semiconductors

4.1 Evaluating the JDOS function from the distributions of electronic states

One weakness associated with the models of Forouhi and Bloomer [20], McGahan *et al.* [21], and Jellison and Modine [15], is that they do not pro-

vide for a direct connection with the underlying distributions of electronic states. Even the model of Jellison and Modine [15], while being considerably improved over that of Forouhi and Bloomer [20] and McGahan *et al.* [21], fails to provide for a direct relationship between the underlying valence band and conduction band DOS functions, $N_v(E)$ and $N_c(E)$, respectively, with the spectral dependence of the optical functions, $\epsilon_1(E)$ and $\epsilon_2(E)$; Jellison and Modine [15] take a physically based model for the spectral dependence of the imaginary part of the dielectric function, $\epsilon_2(E)$, and employ a Kramers-Kronig transformation in order to obtain the spectral dependence of the real part of the dielectric function, $\epsilon_1(E)$. A direct relationship between the functional dependencies of these optical functions, $\epsilon_1(E)$ and $\epsilon_2(E)$, with the form of the distributions of electronic states, would allow for the gleaning of insights into the underlying electronic properties from experimental measurements of the spectral dependence of these optical functions.

In this chapter, an empirical model for the valence band and conduction band DOS functions, $N_v(E)$ and $N_c(E)$, is proposed, this model capturing the fundamental essence of an amorphous semiconductor, i.e., exponential distributions of tail states and square-root distributions of band states. Then, the corresponding joint density of states (JDOS) function is evaluated through

the use of Eq. (2.10). Through the application of a model for the aggregate optical transition matrix element, the corresponding spectral dependence of the imaginary part of the dielectric function, $\epsilon_2(E)$, is determined. A Kramers-Kronig transformation is then employed in order to determine the corresponding spectral dependence of the real part of the dielectric function, $\epsilon_1(E)$. A comparison with the results of experiment is then shown.

This chapter is organized in the following manner. In Section 4.2, an empirical model for the DOS functions is presented. Then, in Section 4.3, the corresponding JDOS function, $J(E)$, is determined. In Section 4.4, a model for the spectral dependence of the dipole optical matrix element is presented. Finally, in Section 4.5, a fit with the results of experiment, for the spectral dependence of real and imaginary parts of the dielectric function, $\epsilon_1(E)$ and $\epsilon_2(E)$, respectively, is shown. Finally, the implications of a non-unity $\epsilon_{1\infty}$ are described in Section 4.6.

4.2 Empirical model for the DOS functions

There is general consensus that the DOS functions associated with an amorphous semiconductor, i.e., $N_v(E)$ and $N_c(E)$, exhibit square-root func-

tional dependencies in the band regions and exponential functional dependencies in the tail regions. Following O'Leary [29], one can thus set

$$
N_v\left(E\right) = N_{vo}
\begin{cases}
\sqrt{E_v - E_{v_{\mathrm{T}}}} \ \exp\left(\dfrac{E_{v_{\mathrm{T}}} - E_v}{\gamma_v}\right) \ \exp\left(\dfrac{E_v - E}{\gamma_v}\right), & E > E_{v_{\mathrm{T}}} \\[4em]
\sqrt{E_v - E}, & E \leq E_{v_{\mathrm{T}}}
\end{cases}
,
$$

$$(4.1)$$

and

$$
N_c\left(E\right) = N_{co}
\begin{cases}
\sqrt{E - E_c}, & E \geq E_{c_{\mathrm{T}}} \\[4em]
\sqrt{E_{c_{\mathrm{T}}} - E_c} \ \exp\left(\dfrac{E_c - E_{c_{\mathrm{T}}}}{\gamma_c}\right) \ \exp\left(\dfrac{E - E_c}{\gamma_c}\right), & E < E_{c_{\mathrm{T}}}
\end{cases}
,
$$

$$(4.2)$$

where N_{vo} and N_{co} denote the valence band and conduction band DOS prefactors, respectively, E_v and E_c represent the valence band and conduction band band edges, γ_v and γ_c are the breadths of the valence band and conduction band tails, $E_{v_{\mathrm{T}}}$ and $E_{c_{\mathrm{T}}}$ being the critical energies at which the exponential and square-root distributions interface. It is clear, from Eqs. (4.1) and (4.2), that both $N_v\left(E\right)$ and $N_c\left(E\right)$ are continuous functions of energy.

In order to further simplify these DOS functions, it will be further assumed that the derivatives of these DOS functions, $N_v\left(E\right)$ and $N_c\left(E\right)$, are also continuous functions of energy, i.e., these functions are smooth func-

tions. For this to be the case, it may be shown that $E_{v_\mathrm{T}} = E_v - \gamma_v/2$ and

that $E_{c_\mathrm{T}} = E_c + \gamma_c/2$ [28]. With these simplifications, Eq. (4.1) reduces to

$$N_v\left(E\right) = N_{vo} \begin{cases} \sqrt{\dfrac{\gamma_v}{2}} \, \exp\left(-\dfrac{1}{2}\right) \, \exp\left(\dfrac{E_v - E}{\gamma_v}\right), & E > E_{v_\mathrm{T}} \\ \\ \\ \sqrt{E_v - E}, & E \leq E_{v_\mathrm{T}} \end{cases} , \qquad (4.3)$$

and Eq. (4.2) reduces to

$$N_c\left(E\right) = N_{co} \begin{cases} \sqrt{E - E_c}, & E \geq E_{c_\mathrm{T}} \\ \\ \\ \sqrt{\dfrac{\gamma_c}{2}} \, \exp\left(-\dfrac{1}{2}\right) \, \exp\left(\dfrac{E - E_c}{\gamma_c}\right), & E < E_{c_\mathrm{T}} \end{cases} , \qquad (4.4)$$

It is noted that in the disorderless limit, i.e., when $\gamma_v \to 0$ and $\gamma_c \to 0$, these

DOS functions reduce to

$$N_v\left(E\right) \to N_{vo} \begin{cases} 0, & E > E_v \\ \\ \\ \sqrt{E_v - E}, & E \leq E_v \end{cases} , \qquad (4.5)$$

and

$$N_c\left(E\right) \to N_{co} \begin{cases} \sqrt{E - E_c}, & E \geq E_c \\ \\ \\ 0, & E < E_c \end{cases} , \qquad (4.6)$$

respectively, these being the Tauc DOS functions, i.e., Eqs. (2.23) and (2.24),

respectively.

The valence band DOS function, $N_v(E)$, is depicted on a linear scale in Figure 4.1, N_{vo} and E_v being nominally set to 2×10^{22} cm^{-3} eV$^{-3/2}$ and 0.0 eV, respectively, for the purposes of this analysis, i.e., the valence band band edge forms the reference energy for this plot. A variety of selections of γ_v are made, these spanning over the range of values representative of amorphous semiconductors. It is clearly seen that for energies below the valence band band edge, E_v, with the tail breadth set to zero, the valence DOS function terminates abruptly, i.e., there are no electronic states within the gap. For finite γ_v, however, a distribution of tail states encroaches into the gap region, the amount of encroachment increasing with γ_v. In Figure 4.2, this plot is depicted on a logarithmic scale, the same parameter selections as that employed in Figure 4.1 also being used. The conduction band DOS function, $N_c(E)$, is depicted on linear and logarithmic scales in Figures 4.3 and 4.4, respectively, N_{co} and E_c being nominally set to 2×10^{22} cm^{-3} eV$^{-3/2}$ and 0.0 eV, respectively, for the purposes of this analysis. As with the valence band case, greater γ_c corresponds to greater encroachment into the energy gap.

Figure 4.1: A linear plot of the valence band DOS function as a function of energy, E, for various selections of γ_v. The DOS modeling parameters, N_{vo} and E_v, are nominally set to 2×10^{22} cm^{-3} eV$^{-3/2}$ and 0.0 eV, respectively, for the purposes of this plot. This figure is after O'Leary [17].

Figure 4.2: A logarithmic plot of the valence band DOS function as a function of energy, E, for various selections of γ_v. The DOS modeling parameters, N_{vo} and E_v, are nominally set to 2×10^{22} cm^{-3} eV$^{-3/2}$ and 0.0 eV, respectively, for the purposes of this plot. This figure is after O'Leary [17].
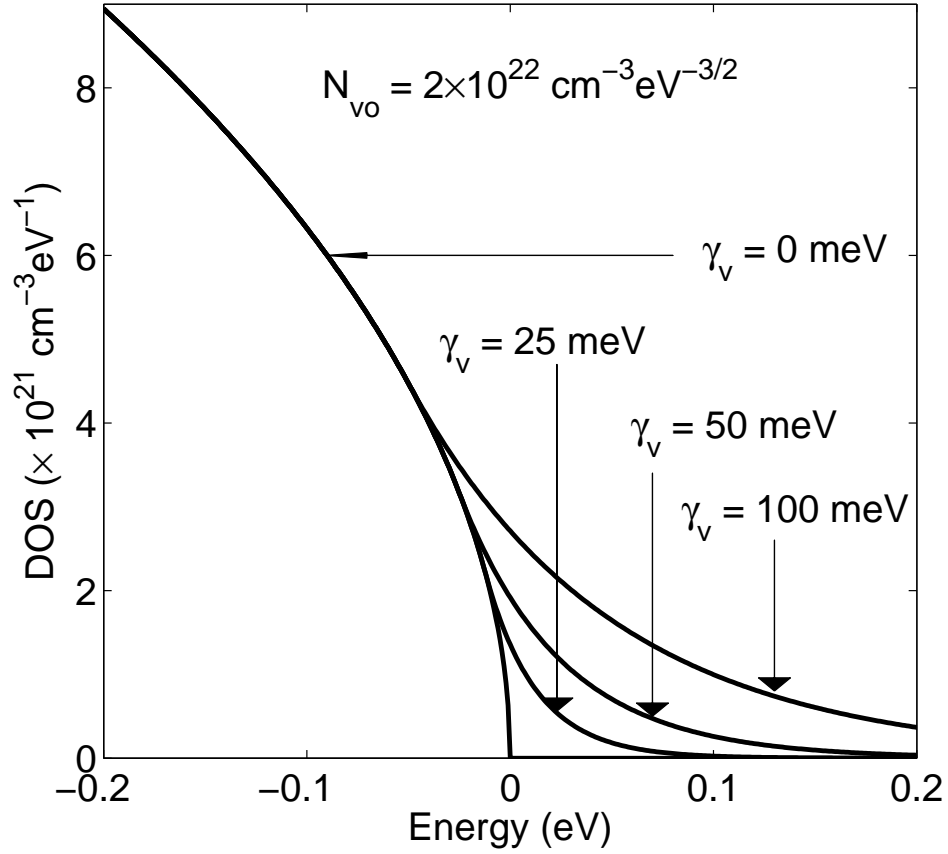
Figure 4.3: A linear plot of the conduction band DOS function as a function of energy, E, for various selections of γ_c. The DOS modeling parameters, N_{co} and E_c, are nominally set to 2×10^{22} cm^{-3} eV$^{-3/2}$ and 0.0 eV, respectively, for the purposes of this plot. This figure is after O'Leary [17].
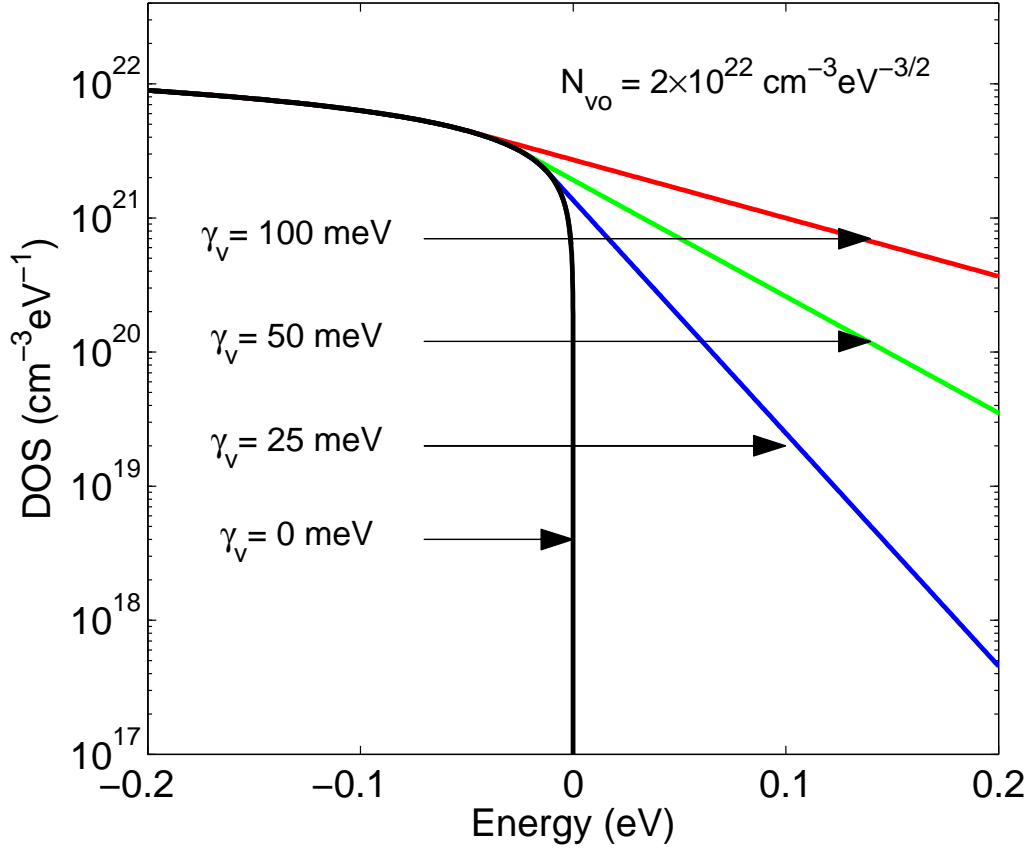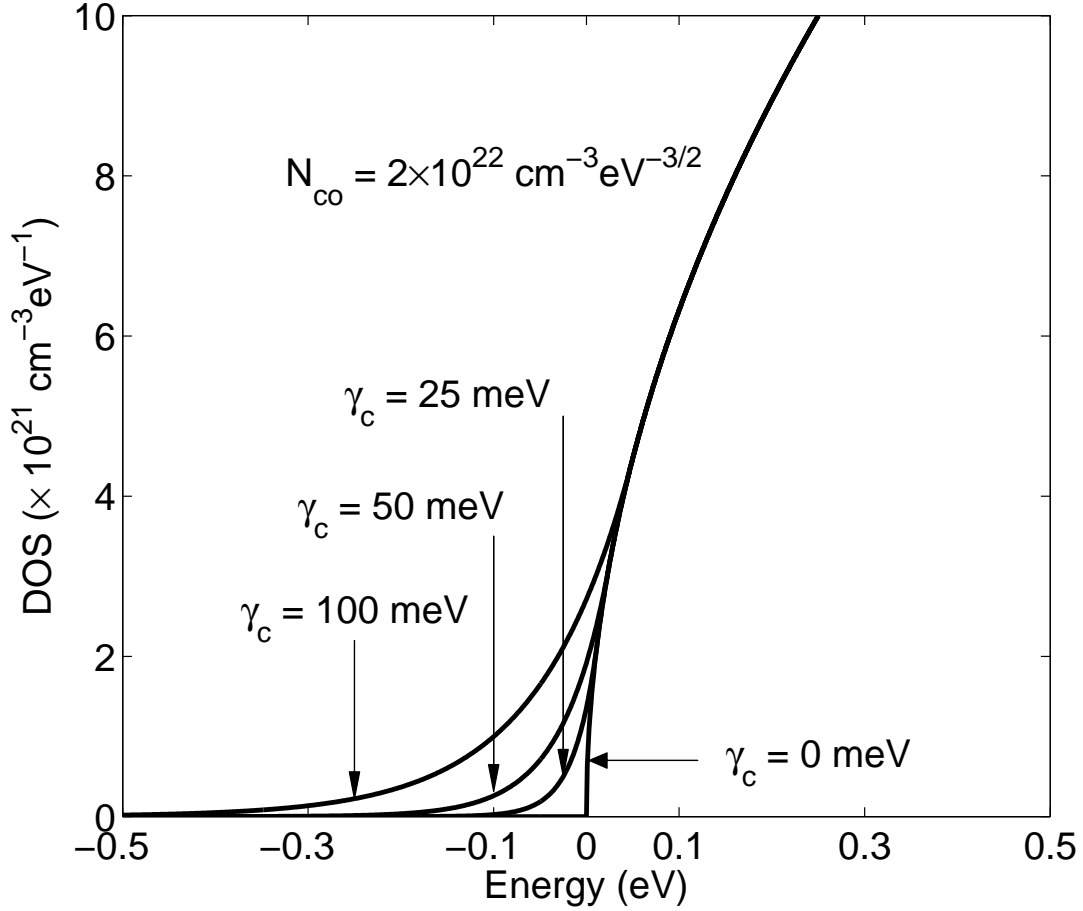
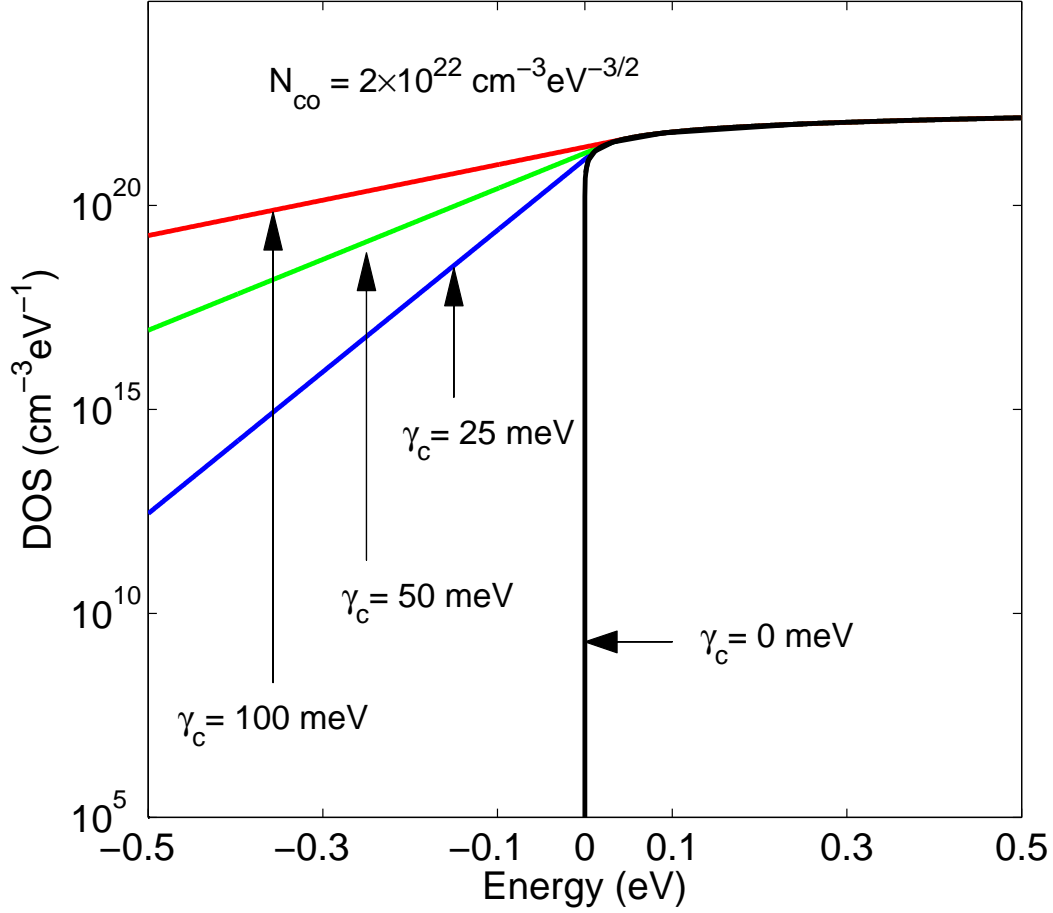Figure 4.4: A logarithmic plot of the conduction band DOS function as a function of energy, E, for various selections of γ_c. The DOS modeling parameters, N_{co} and E_c, are nominally set to 2×10^{22} cm^{-3} eV$^{-3/2}$ and 0.0 eV, respectively, for the purposes of this plot. This figure is after O'Leary [17].

4.3   JDOS evaluation and analysis

The JDOS function, $J(E)$, corresponding to the empirical model for the DOS functions, i.e., with $N_v(E)$ and $N_c(E)$ as set in Eqs. (4.3) and (4.4), respectively, is now evaluated using Eq. (2.10). This JDOS function may be used in order to determine the number of possible optical transitions between the valence band and the conduction band electronic states. In Figure 4.5, the JDOS function is depicted on a linear scale for a variety of selections of γ_v and γ_c, the DOS modeling parameters being nominally set to $N_{vo} = N_{co}$ = 2 $\times 10^{22}$ cm^{-3} eV$^{-3/2}$, $E_v = 0.0$ eV, and $E_c = 1.7$ eV; for all cases, γ_v is set equal to γ_c. This plot is shown on a logarithmic scale in Figure 4.6.

Eq. (2.25) suggests that the functional dependence of $\sqrt{J(E)}$ on the photon energy, E, for energies well above the band gap, allows one to determine the corresponding energy gap, E_g. In Figure 4.7, a linear plot of the functional dependence of $\sqrt{J(E)}$ on the photon energy, E, is depicted. It is clearly seen that for $\gamma_v = \gamma_c = 0$, that the $\sqrt{J(E)}$ function terminates abruptly at the band gap edge. For finite γ_v and γ_c, however, a tail in the JDOS function encroaches into the gap region, this tail representing the amount of disorder that is present.

Figure 4.5: A linear plot of the JDOS function as a function of the photon energy, E, for various selections of γ_v and γ_c. The DOS modeling parameters are nominally set to $N_{vo} = N_{co} = 2 \times 10^{22}$ cm^{-3} eV$^{-3/2}$, $E_v = 0.0$ eV, and $E_c = 1.7$ eV for the purposes of this plot. This figure is after O'Leary [17].
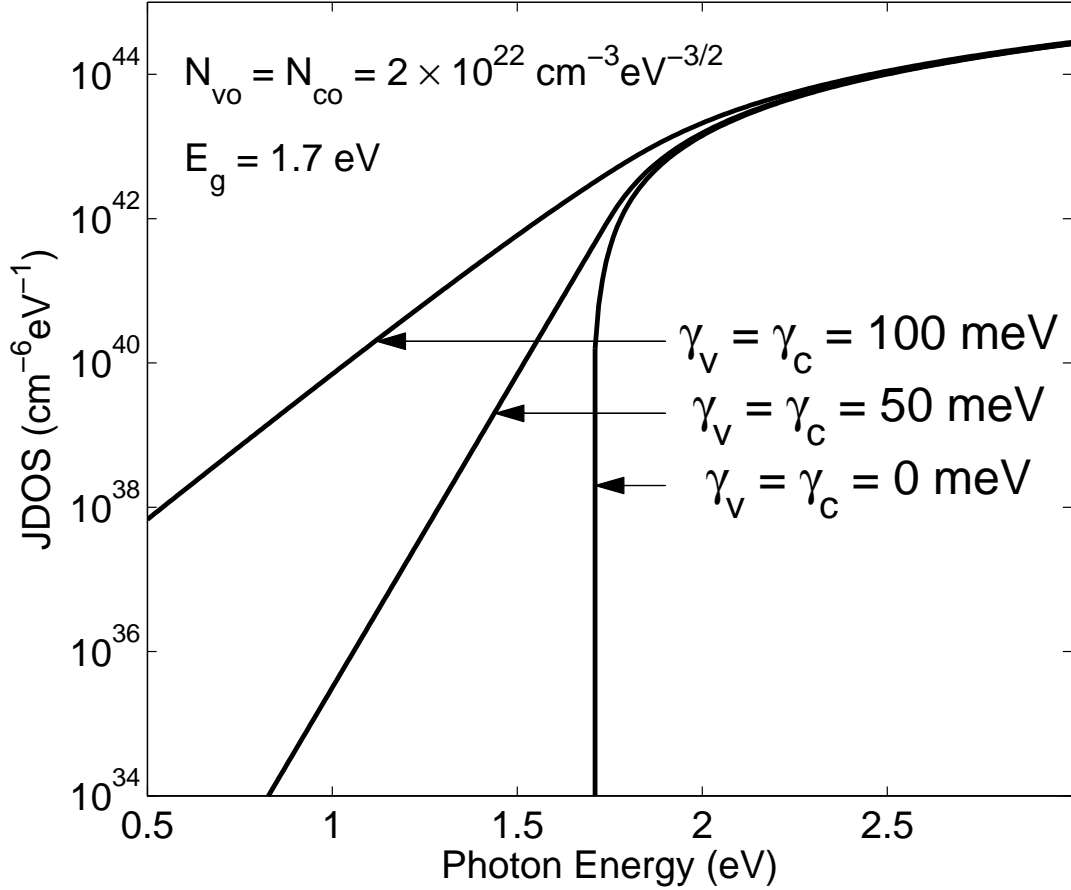
Figure 4.6: A logarithmic plot of the JDOS function as a function of the photon energy, E, for various selections of γ_v and γ_c. The DOS modeling parameters are nominally set to $N_{vo} = N_{co} = 2 \times 10^{22}$ cm^{-3} eV$^{-3/2}$, $E_v = 0.0$ eV, and $E_c = 1.7$ eV for the purposes of this plot. This figure is after O'Leary [17].

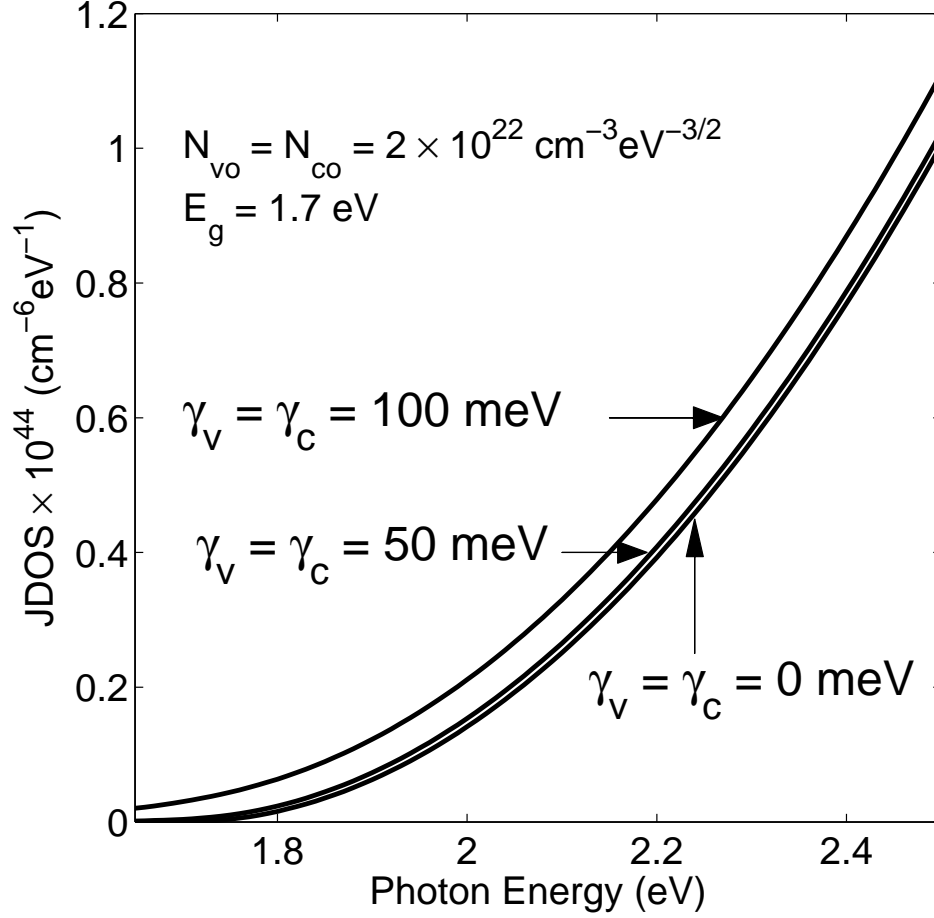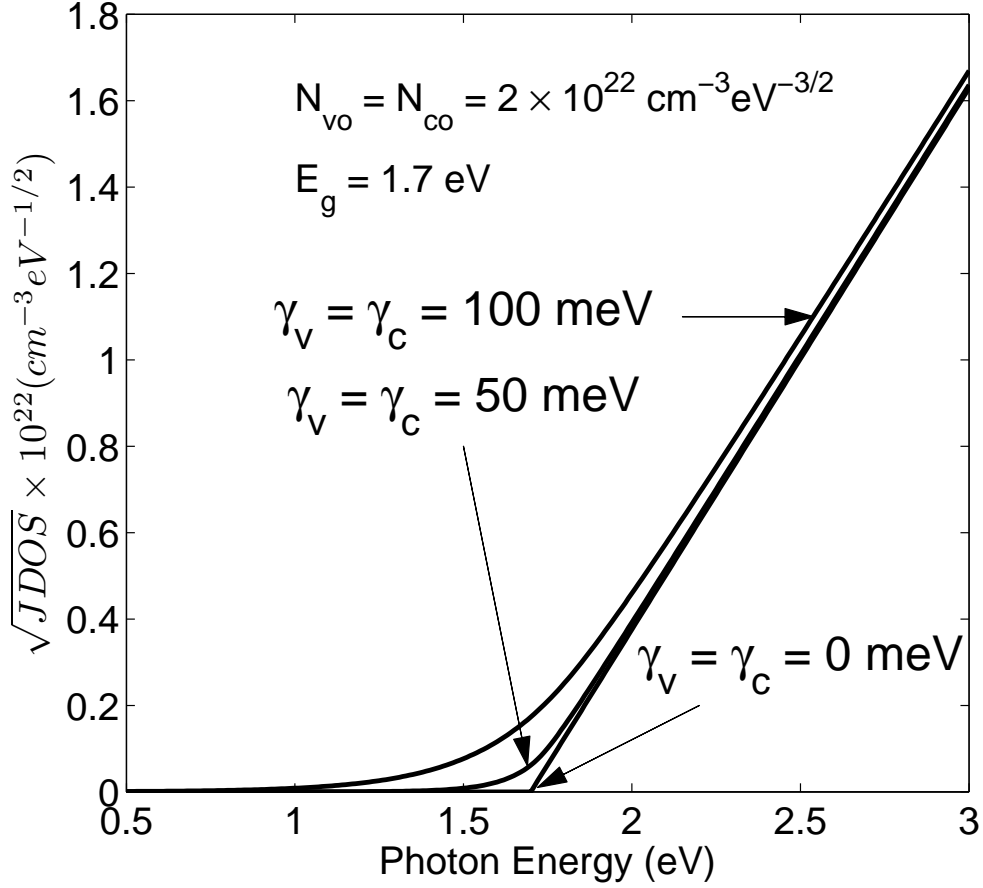Figure 4.7: A linear plot of the functional dependence of the square-root of the JDOS function on the photon energy, E, for various selections of γ_v and γ_c. The DOS modeling parameters are nominally set to $N_{vo} = N_{co} = 2 \times 10^{22}$ cm^{-3} eV$^{-3/2}$, $E_v = 0.0$ eV, and $E_c = 1.7$ eV for this plot. This figure is after O'Leary [17].

4.4   Modeling the optical functions associated with a-Si

In order to determine the spectral dependence of the a-Si optical functions, $\epsilon_1(E)$ and $\epsilon_2(E)$, the spectral dependence of the JDOS function associated with this material must be known. With a model for the JDOS function, in conjunction with a model for the spectral dependence of the aggregate dipole matrix element, $\mathcal{R}^2(E)$, the spectral dependence of the imaginary part of the dielectric function, $\epsilon_2(E)$, may be determined through the use of Eq. (2.17). Then, through the use of a Kramers-Kronig transformation, i.e., Eq. (2.45), the spectral dependence of the real part of the dielectric function, $\epsilon_1(E)$, may be determined.

For the purposes of this analysis, the spectral dependence of $J(E)$ and $\mathcal{R}^2(E)$ associated with a-Si will be independently modeled. Each of these models will then be contrasted with the corresponding results of experiment, these a-Si experimental results being from Jackson *et al.* [16]. From the spectral dependence of $J(E)$ and $\mathcal{R}^2(E)$, the spectral dependence of $\epsilon_2(E)$ will be determined, and compared with that of experiment. Following this analysis, fits with the results of experiment corresponding to other samples of a-Si will

be performed, it being expected that some variations in the DOS modeling parameters will occur from sample-to-sample, these variations representing the changes in the physics of each sample.

Thevaril and O'Leary [33] plotted the experimentally determined a-Si valence band tail breadth parameter, γ_v, as a function of the conduction band tail breadth parameter, γ_c, for the experimental data of Sherman *et al.* [23], Rerbal *et al.* [34], Teidje *et al.* [35], and Winer and Ley [36]. Fit values, obtained by O'Leary [17], were also considered. This experimental data, and the fit data, is depicted in Figure 4.8. It is noted that, in all cases, the valence band tail breadth parameter, γ_v, exceeds that associated with the conduction band, γ_c. Thevaril and O'Leary [28] demonstrated that when γ_v exceeds γ_c, the optical absorption coefficient is primarily determined by γ_v. Thus, many of the optical properties may be determined neglecting the conduction band tail states, i.e., assuming that γ_c is equal to zero. For the purposes of this analysis, γ_c will be set to zero for all cases.

In Figure 4.9, a plot of the experimental a-Si JDOS results of Jackson *et al.* [16] is depicted. This result is directly contrasted with that determined using the numerical evaluation procedure for the JDOS function for the DOS modeling parameters set to $N_{vo} = N_{co} = 2.48 \times 10^{22}$ cm^{-3} eV$^{-3/2}$,
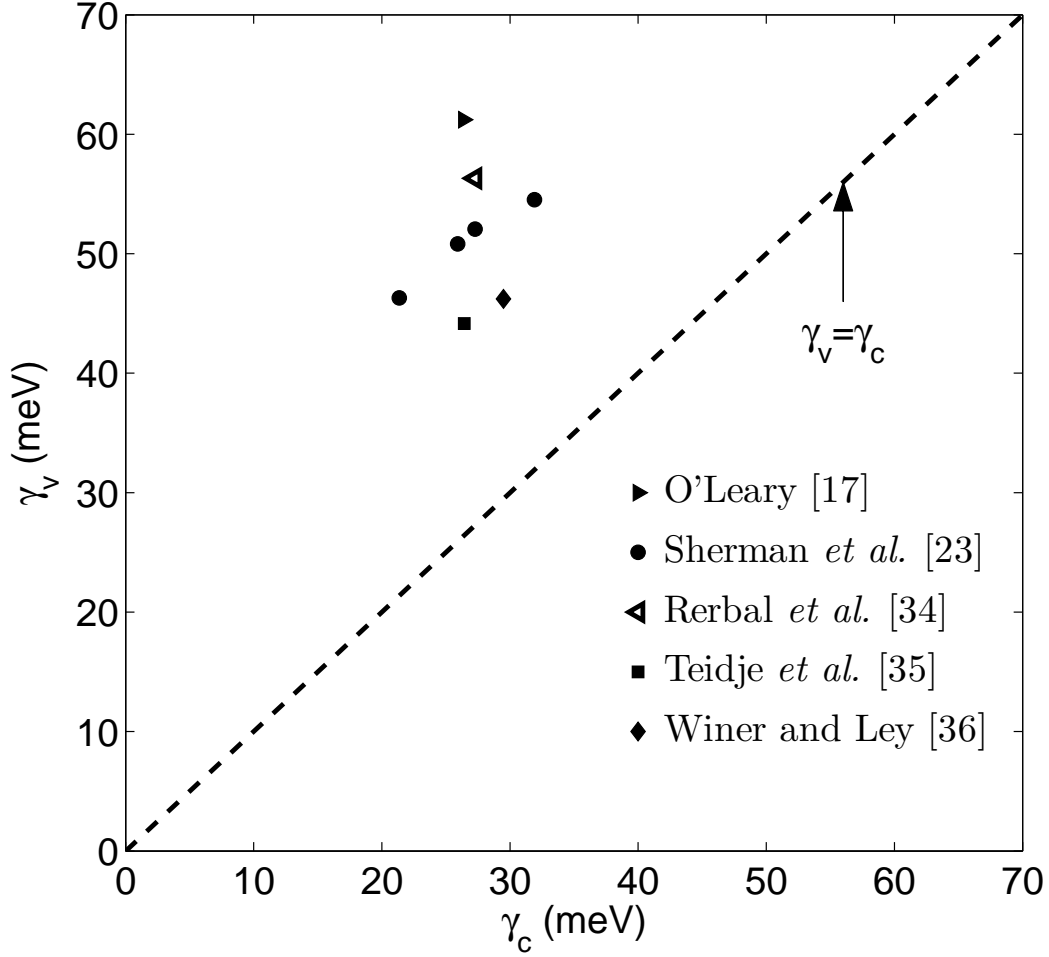
Figure 4.8: A plot of the dependence of γ_v on γ_c. Experimental results from Sherman *et al.* [23], Rerbal *et al.* [34], Teidje *et al.* [35], and Winer and Ley [36] are depicted. A modeling result, obtained through a fit with experimental data, from O'Leary [17], is also depicted on this plot. This figure is after Thevaril and O'Leary [33].
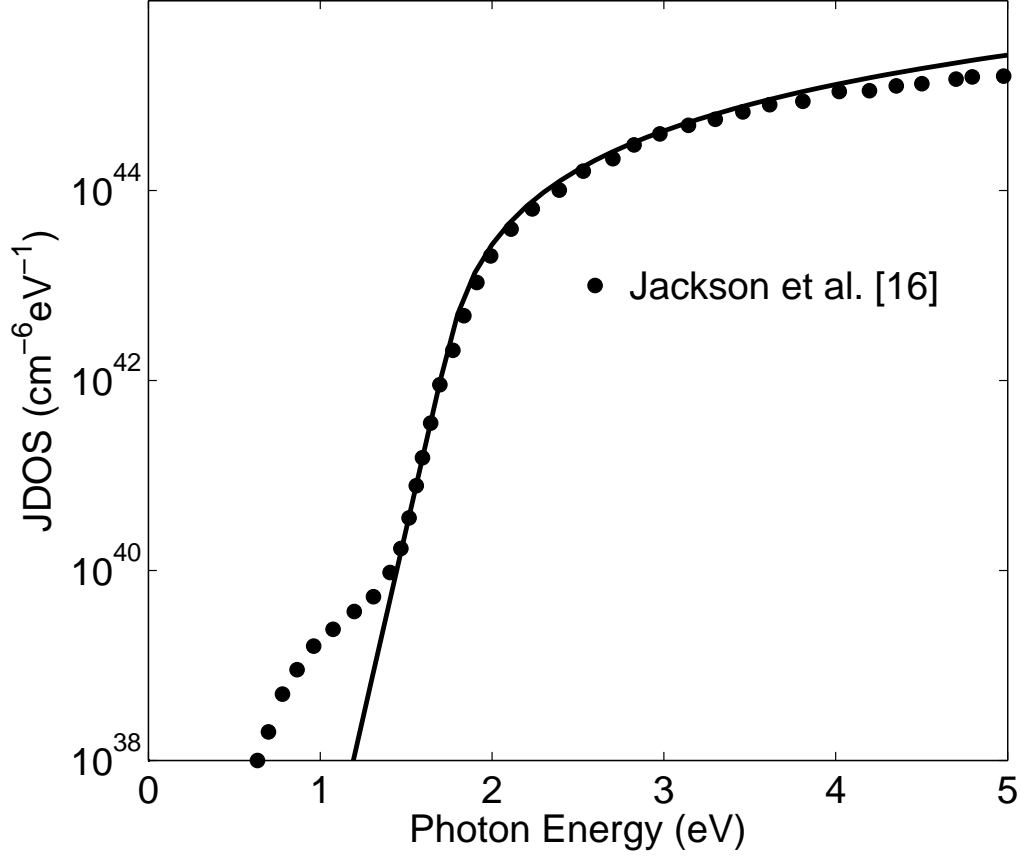
Figure 4.9: The spectral dependence of the JDOS function. The a-Si JDOS results of Jackson *et al.* [16] are depicted with the solid points. The JDOS fit result, obtained by setting $N_{vo} = N_{co} = 2.48 \times 10^{22}$ cm^{-3} eV$^{-3/2}$, $E_v = 0.0$ eV, $E_c = 1.68$ eV, and $\gamma_v = 40$ meV, is depicted with the solid line.

$E_v = 0.0$ eV, $E_c = 1.68$ eV, and $\gamma_v = 40$ meV. It is noted that the fit is reasonably satisfactory, except for low JDOS values, where defect absorption influences the results and high photon energies, where the non-parabolicity of the bands plays a role influencing the form of the JDOS function. This a-Si JDOS function will be used in the subsequent analysis.

For the case of a-Si, Jackson *et al.* [16] experimentally determined the spectral dependence of the aggregate dipole matrix element squared average, $\mathcal{R}^2(E)$. They found that for photon energies below 3.4 eV, this matrix element remains essentially constant, while for photon energies in excess of 3.4 eV, it falls off with the algebraic dependence E^{-5}. Based on these observations, Thevaril and O'Leary [28] modeled $\mathcal{R}^2(E)$ as

$$\mathcal{R}^2(E) = \mathcal{R}_o^2 \begin{cases} \left(\dfrac{E_d}{E}\right)^5, & E \geq E_d \\ \\ 1, & E < E_d \end{cases}, \qquad (4.7)$$

where E_d is the characteristic energy to which $\mathcal{R}^2(E)$ is constant, i.e., $\mathcal{R}^2(E) = \mathcal{R}_o^2$, where, for the case of the a-Si experimental data of Jackson *et al.* [16], $\mathcal{R}_o^2 = 10\text{Å}^2$. This spectral dependence for $\mathcal{R}^2(E)$, proposed by Thevaril and O'Leary [28], is contrasted with the experimental $\mathcal{R}^2(E)$ results of Jackson *et al.* [16] in Figure 4.10. The corresponding spectral dependence of $\epsilon_2(E)$,
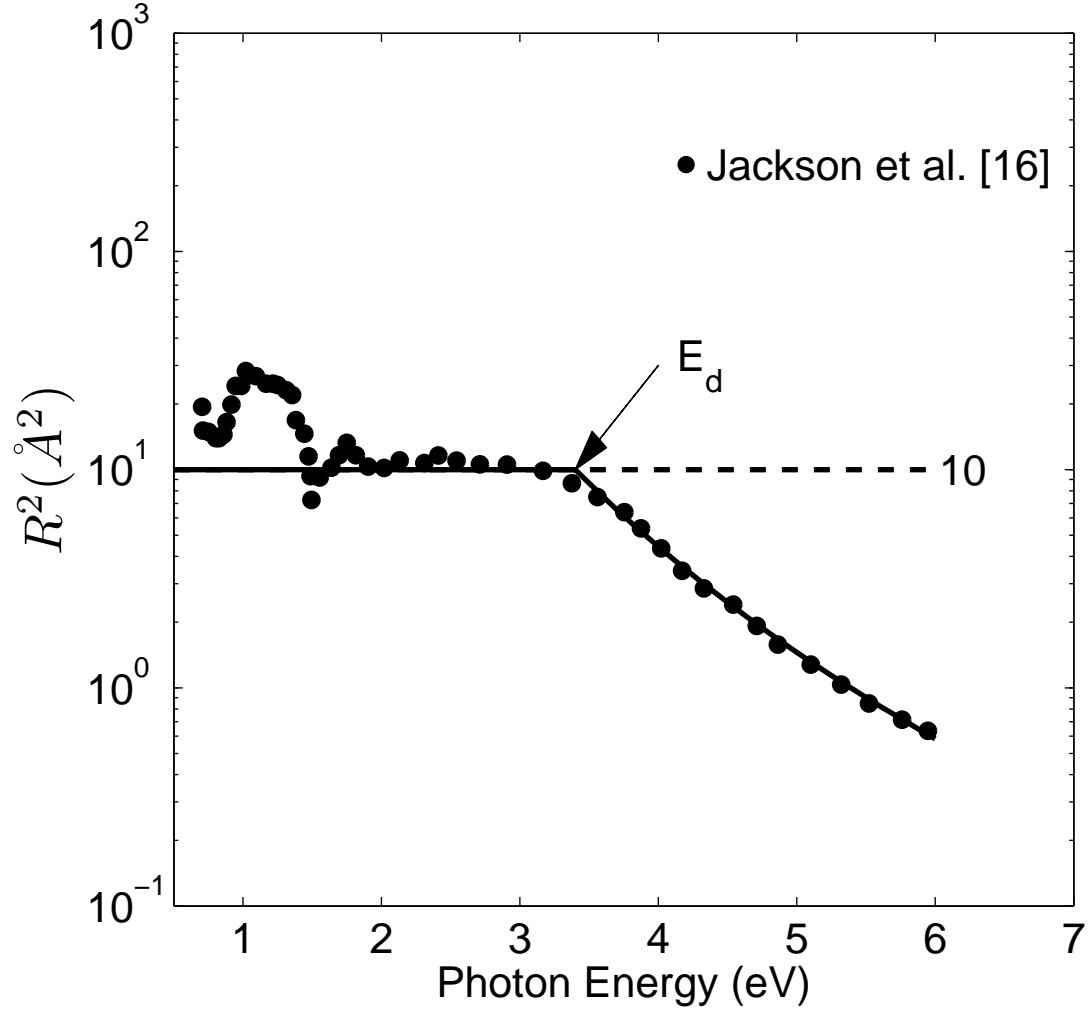
123

Figure 4.10: $\mathcal{R}^2(E)$ as a function of the photon energy, E, determined using Eq. (4.7), depicted with the solid lines. For the purposes of this fit, $\mathcal{R}_o^2$ is set to 10 Å^2 and E_d is set to 3.4 eV. The experimental results of Jackson *et al.* [16] are depicted with the solid points.

determined using Eq. (2.17), is depicted on a logarithmic scale in Figure 4.11 and on a linear scale in Figure 4.12.

The DOS modeling parameters are set to $N_{vo} = N_{co} = 2.48 \times 10^{22}$ cm^{-3} eV$^{-3/2}$, $E_v = 0.0$ eV, $E_c = 1.68$ eV, and $\gamma_v = 40$ meV for the purposes of this plot. It is also compared with the experimental $\epsilon_2(E)$ results of Jackson *et al.* [16].

While the comparison with the results of experiment is reasonably satisfactory for the case of the logarithmic plot, i.e., Figures 4.11, for the linear plot, i.e., Figure 4.12, it is seen that the spectral dependence of $\epsilon_2(E)$ does not follow the a-Si experimental results for photon energies in excess of 3.4 eV. From Figure 4.12, it is also seen that the spectral dependence of $\epsilon_2(E)$ exhibits a sharp peak at E_d, which does not accord with experimental observation. The formalism for the dipole matrix element squared average, $\mathcal{R}^2(E)$, expressed in Eq. (4.7), is responsible for this unphysical sharp peak in the spectral dependence of the imaginary part of the dielectric function, $\epsilon_2(E)$. In order to avoid this problem created with an abrupt transition model for the spectral dependence of $\mathcal{R}^2(E)$, $\mathcal{R}^2(E)$ is instead remodeled as

$$\mathcal{R}^2(E) = \frac{\mathcal{R}_o^2}{\left[1 + \left(\frac{E}{E_d}\right)^{2x}\right]^{\frac{1}{2}}}, \tag{4.8}$$

125
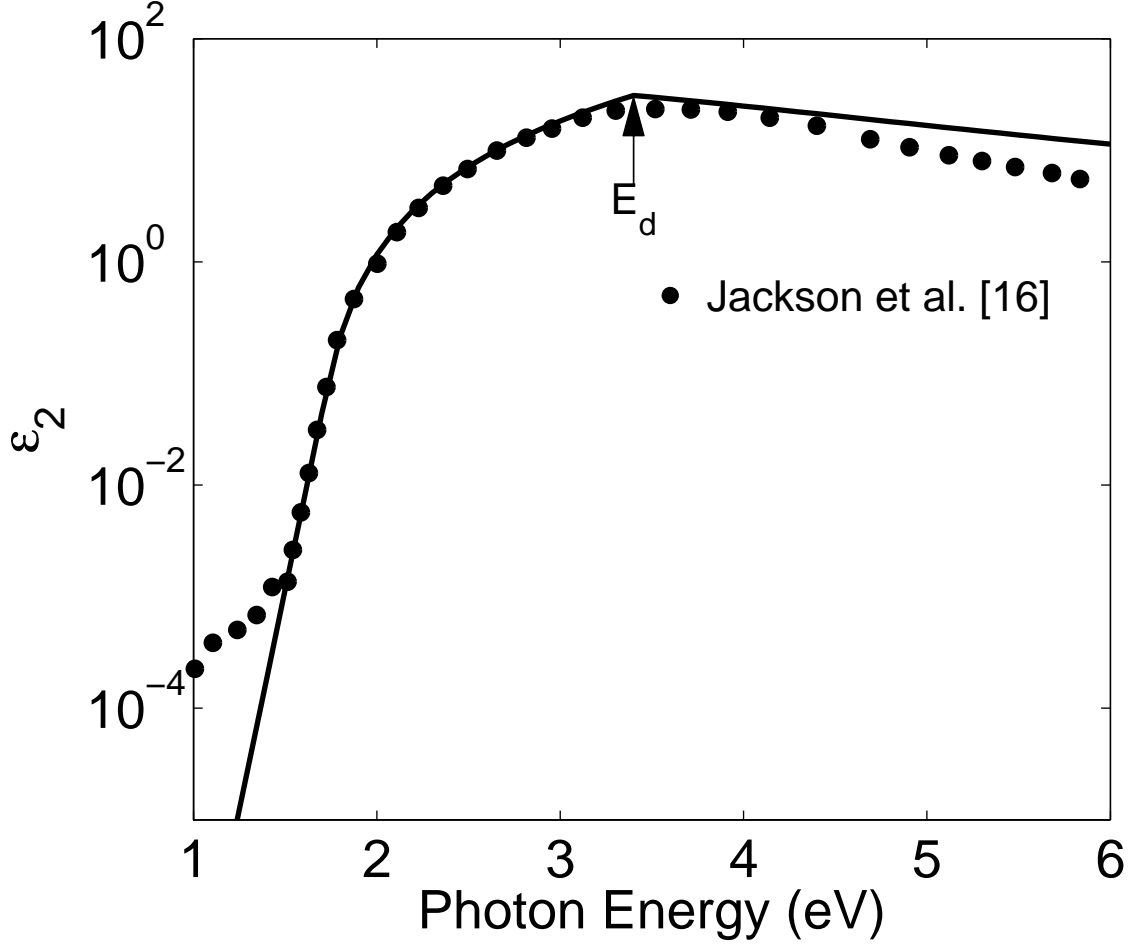
Figure 4.11: The spectral dependence for the imaginary part of the dielectric function, $\epsilon_2(E)$, determined using Eq. (2.17), where $\mathcal{R}^2(E)$ is determined using Eq. (4.7), on a logarithmic scale. The DOS modeling parameters are set to $N_{vo} = N_{co} = 2.48 \times 10^{22}$ cm^{-3} eV$^{-3/2}$, $E_v = 0.0$ eV, $E_c = 1.68$ eV, and $\gamma_v = 40$ meV for the purposes of this plot. The experimental results of Jackson et al. [16] are depicted with the solid points

126
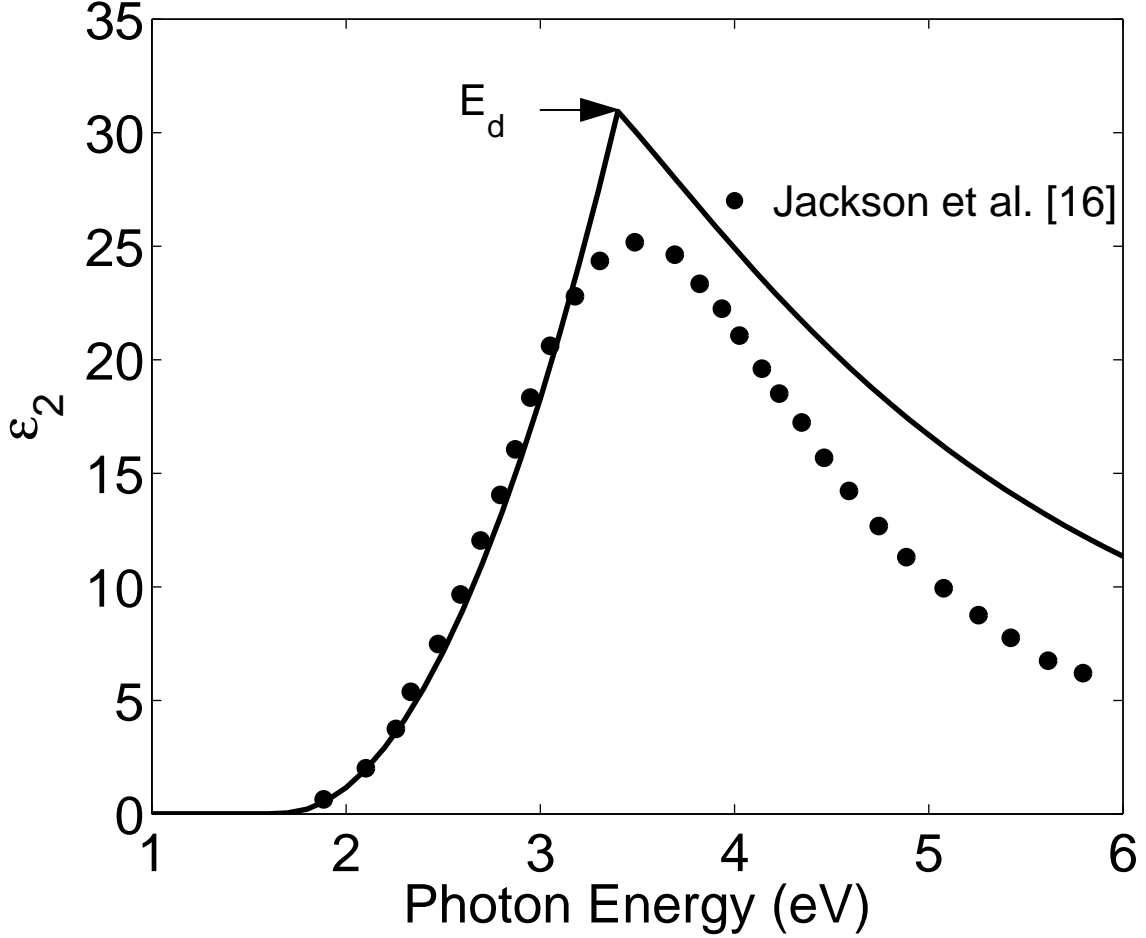
Figure 4.12: The spectral dependence of the imaginary part of the dielectric function, $\epsilon_2(E)$, determined using Eq. (2.17), where $\mathcal{R}^2(E)$ is determined using Eq. (4.7), on a linear scale. The DOS modeling parameters are set to $N_{vo} = N_{co} = 2.48 \times 10^{22}$ cm^{-3} eV$^{-3/2}$, $E_v = 0.0$ eV, $E_c = 1.68$ eV, and $\gamma_v = 40$ meV for the purposes of this plot. The experimental results of Jackson *et al.* [16] are depicted with the solid points

where x represents the asymptotic polynomial rate of attenuation, i.e., for the case of the experimental observations of Jackson *et al.* [16], it is found that $x = 5$. It is noted that for photon energies $E << E_d$, $\mathcal{R}^2(E) = \mathcal{R}_o^2$. For photon energies greater than E_d, however, $\mathcal{R}^2(E)$ asymptotically approaches $\mathcal{R}_o^2(\frac{E_d}{E})^x$. The spectral dependence of this remodeled $\mathcal{R}^2(E)$ is contrasted with the experimental $\mathcal{R}^2(E)$ results of Jackson *et al.* [16] and the spectral dependence of $\mathcal{R}^2(E)$, proposed by Thevaril and O'Leary [28], i.e., Eq. (4.7), in Figure 4.13.

The spectral dependence of ϵ_2 associated with the a-Si, evaluated using Eq. (2.17), where $\mathcal{R}^2(E)$ is determined using Eq. (4.8), is depicted on a logarithmic scale in Figure 4.14 and on a linear scale in Figure 4.15. The DOS modeling parameters are set to $N_{vo} = N_{co} = 2.48 \times 10^{22}$ cm^{-3} eV$^{-3/2}$, $E_v = 0.0$ eV, $E_c = 1.68$ eV, and $\gamma_v = 40$ meV for the purposes of this analysis. The asymptotic polynomial rate of attenuation, x, is set to 6.6 for the purposes of this plot. The experimental $\epsilon_2(E)$ results of Jackson *et al.* [16] are depicted with the solid points. It is noted that the fit is reasonably satisfactory for both cases. The evaluation of the real part of dielectric function, $\epsilon_1(E)$, may be directly determined from a Kramers-Kronig transformation, i.e., Eq. (2.45). Numerical integration is employed for the
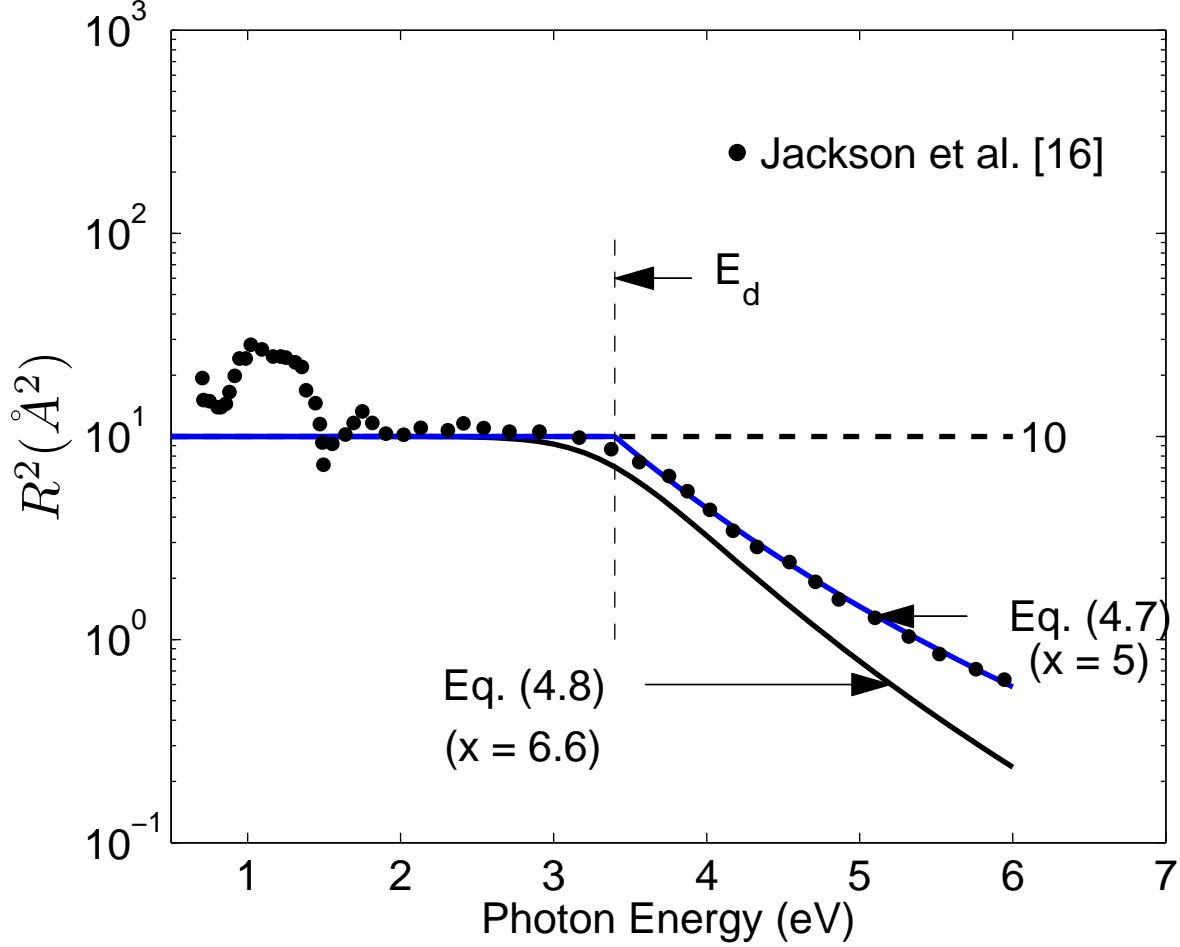
Figure 4.13: $\mathcal{R}^2(E)$ as a function of the photon energy, E, determined using Eqs. (4.7) and (4.8), are depicted with the solid lines. For the purposes of this fit, $\mathcal{R}_o^2$ is set to 10 Å^2 and E_d is set to 3.4 eV. The asymptotic polynomial rate of attenuation, x, is set to 6.6 for the purposes of the Eq. (4.8) plot. The experimental results of Jackson *et al.* [16] are depicted with the solid points.
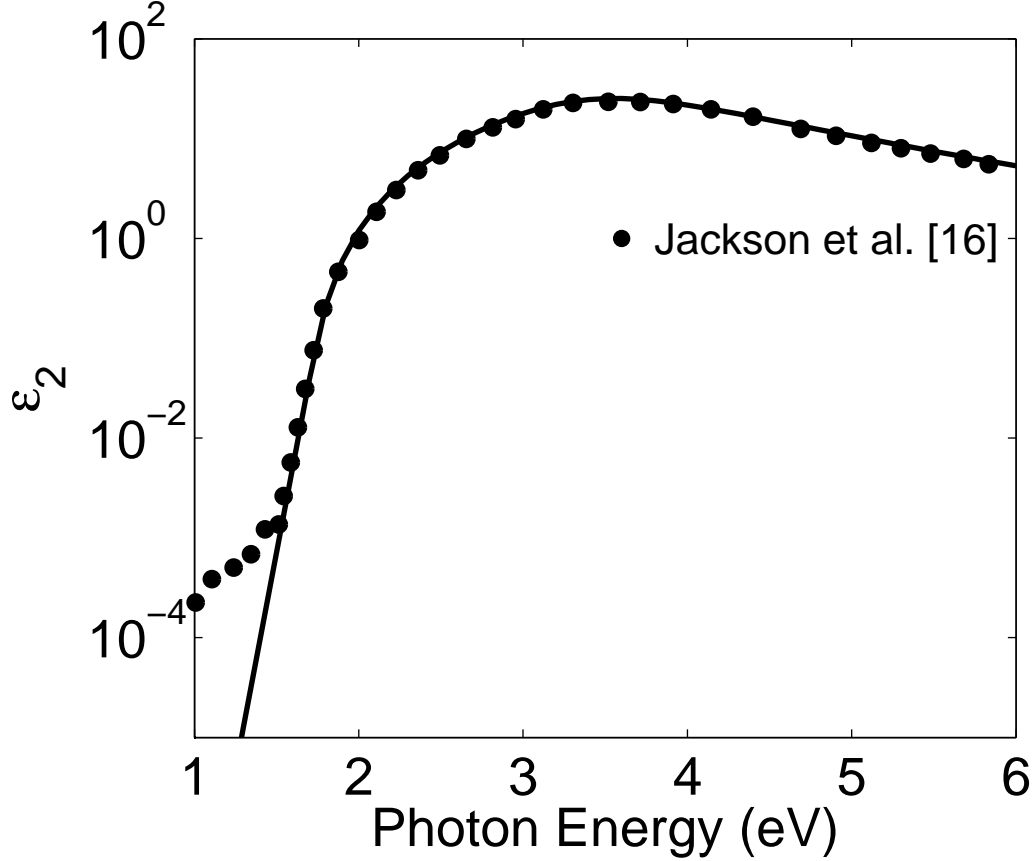
Figure 4.14: The spectral dependence of the imaginary part of the dielectric function, $\epsilon_2(E)$, determined using Eq. (2.17), where $\mathcal{R}^2(E)$ is determined using Eq. (4.8), on a logarithmic scale. The DOS modeling parameters are set to $N_{vo} = N_{co} = 2.48 \times 10^{22}$ cm^{-3} eV$^{-3/2}$, $E_v = 0.0$ eV, $E_c = 1.68$ eV, and $\gamma_v = 40$ meV for the purposes of this plot. The asymptotic polynomial rate of attenuation, x, is set to 6.6 for the purposes of this plot. The experimental results of Jackson *et al.* [16] are depicted with the solid points

Figure 4.15: The spectral dependence of the imaginary part of the dielectric function, $\epsilon_2(E)$, determined using Eq. (2.17), where $\mathcal{R}^2(E)$ is determined using Eq. (4.8), on a linear scale. The DOS modeling parameters are set to $N_{vo} = N_{co} = 2.48 \times 10^{22}$ cm^{-3} eV$^{-3/2}$, $E_v = 0.0$ eV, $E_c = 1.68$ eV, and $\gamma_v = 40$ meV for the purposes of this plot. The asymptotic polynomial rate of attenuation, x, is set to 6.6 for the purposes of this plot. The experimental results of Jackson *et al.* [16] are depicted with the solid points
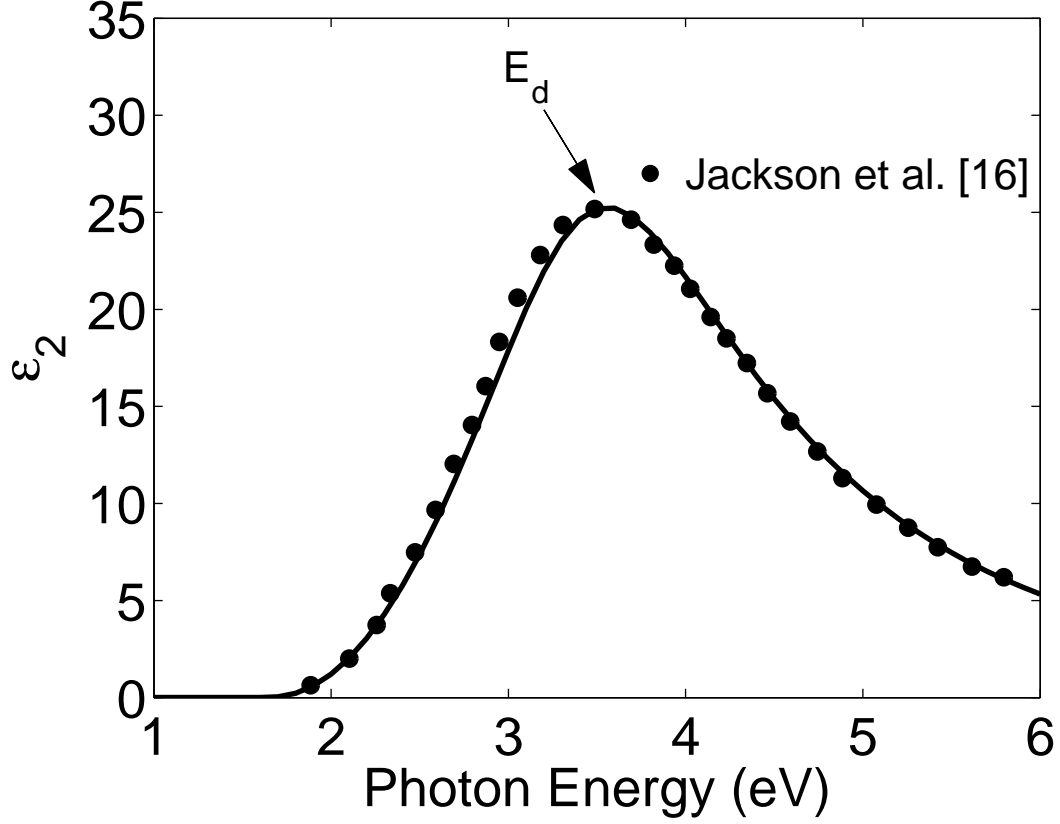
purposes of this analysis.

4.5   Results

Three sets of experimental results are used in order to validate the afore-mentioned model for the spectral dependence of dielectric functions; these are the same experimental data sets as that considered earlier. In Figures 4.16, 4.17, and 4.18, the model results are compared with the experimental EGE a-Si data set [30], the PECVD a-Si I data set [31], and the PECVD a-Si II data set [32], respectively. The "best-fit" is obtained through visual inspection. For every case, this model perfectly fits with these three different sets of experimental data. The fitting parameters values are tabulated in Table 4.1. As this model is directly related to the DOS modeling parameters, it is possible to extract the underlying fundamental properties related to the underlying distributions of electronic states from knowledge of the spectral dependence of these optical functions. This information could help to predict the behavior of the optical response over a broad range of energies and can guide the fabrication of optical devices.

Table 4.1: The "best-fit" a-Si DOS modeling parameter selections employed for the purposes of this analysis. These modeling parameters relate to Eqs. (2.17), (2.45), and (4.8)

parameter (units)	EGE a-Si [30]	PECVD a-Si I [31]	PECVD a-Si II [32]
N_{vo} $(\text{cm}^{-3}\text{eV}^{-3/2})$	1.88×10^{22}	2.33×10^{22}	2.42×10^{22}
N_{co} $(\text{cm}^{-3}\text{eV}^{-3/2})$	1.88×10^{22}	2.33×10^{22}	2.42×10^{22}
E_v (eV)	0.0	0.0	0.0
E_c (eV)	1.21	1.51	1.68
E_g (eV)	1.21	1.51	1.68
E_d (eV)	3.42	3.64	3.72
γ_v (meV)	83	40	50
$\epsilon_{1\infty}$	1.0	1.0	0.65
$\mathcal{R}o^2(\text{Å}^2)$	10	10	10
x	5.87	6.6	6.6

Figure 4.16: A "best-fit" of the model results with the results of experiment corresponding to EGE a-Si [30]. These experimental results are from Piller [30]. The fits to experiment are shown with the solid lines. The experimental data, EGE a-Si [30], is depicted with the solid points.

Figure 4.17: A "best-fit" of the model results with the results of experiment corresponding to PECVD a-Si I [31]. These experimental results are from Synowicki [31]. The fits to experiment are shown with the solid lines. The experimental data, PECVD a-Si I [31], is depicted with the solid points.
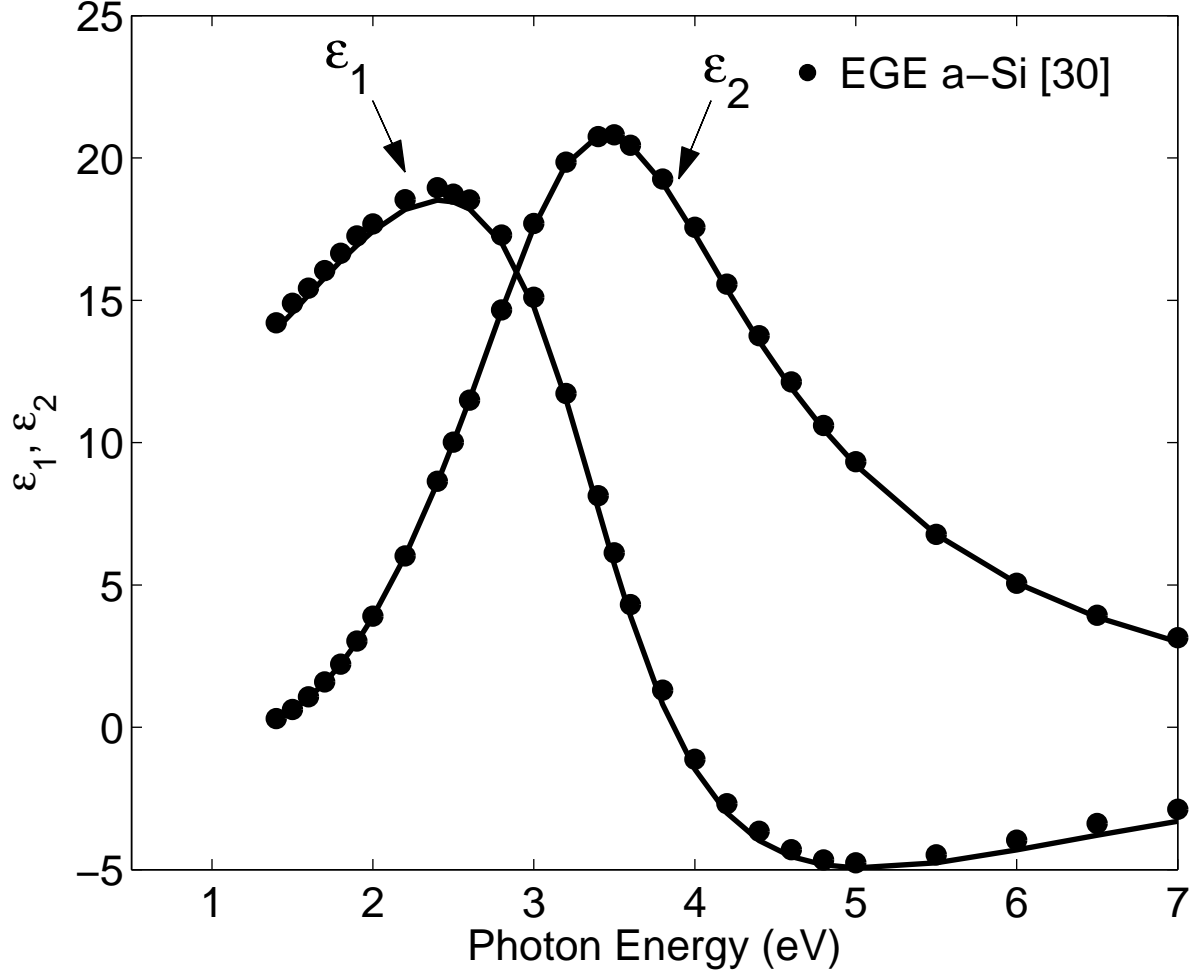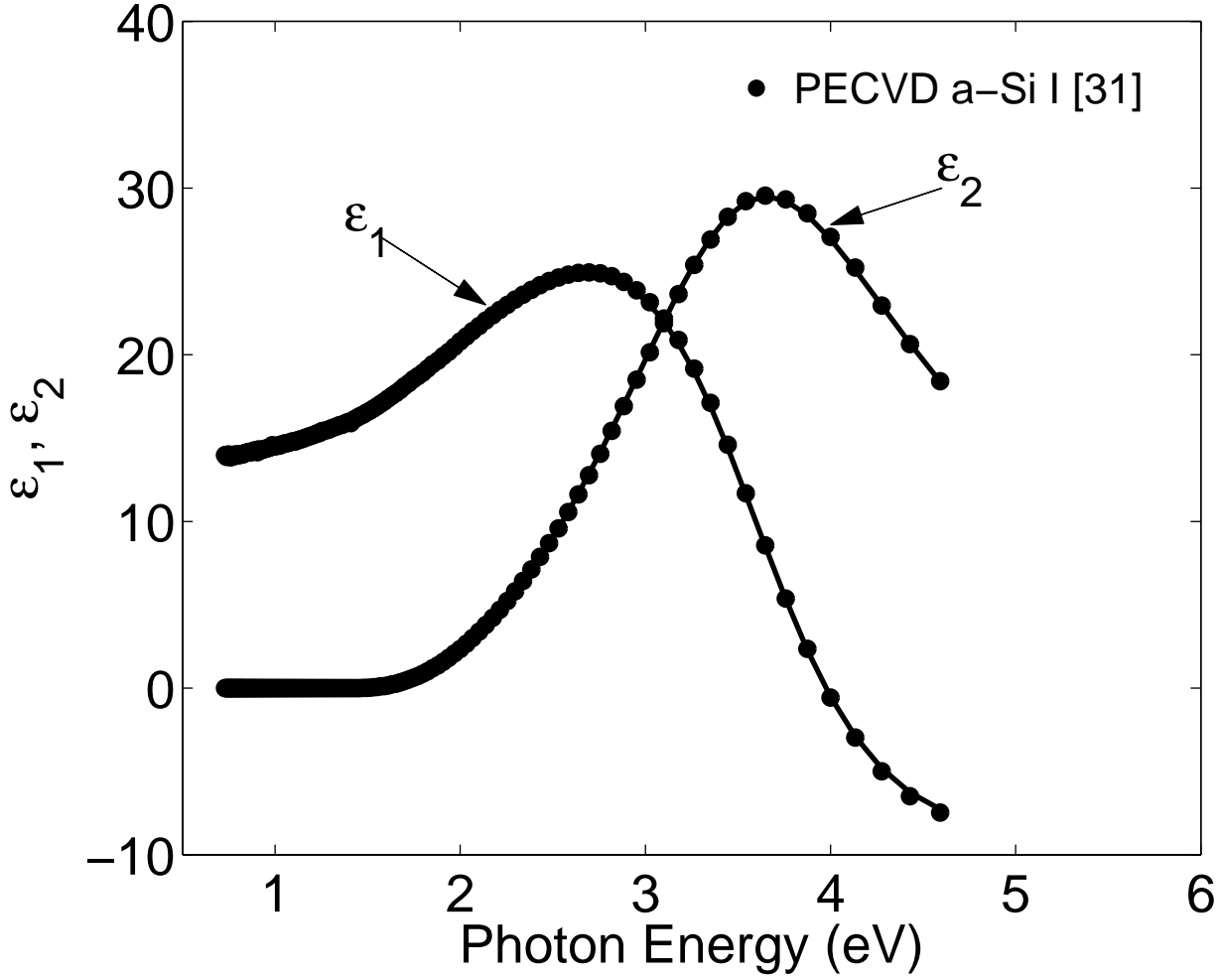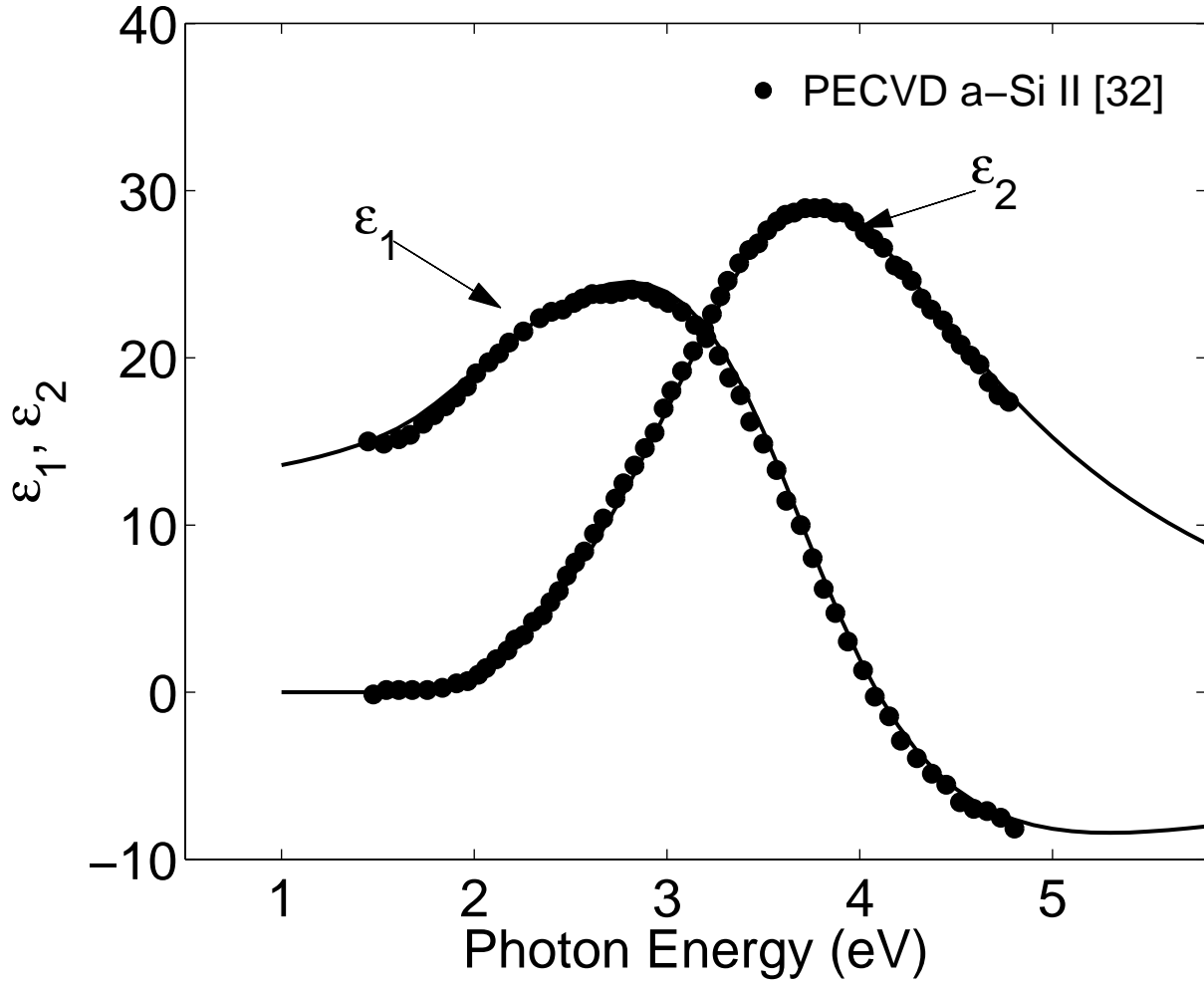
Figure 4.18: A "best-fit" of the model results with the results of experiment corresponding to PECVD a-Si II [32]. These experimental results are from Ferluato *et al.* [32]. The fits to experiment are shown with the solid lines. The experimental data, PECVD a-Si II [32], is depicted with the solid points.

4.6 Implications of a non-unity $\epsilon_{1\infty}$

Ideally, $\epsilon_{1\infty}$ should be equal to unity when all the electronic transitions are considered in the model for the spectral dependence of the imaginary part of the dielectric function, $\epsilon_2(E)$ [32]. Ferlauto *et al.* [32] experienced that $\epsilon_{1\infty}$ departs from unity depending upon the band gap differences amongst the a-Si samples. They also commented that $\epsilon_{1\infty}$ is less than unity for pure a-Si samples. From Tables 3.1 and 4.1, it is seen that for the EGE a-Si [30] and the PECVD a-Si I [31] samples, $\epsilon_{1\infty}$ is unity, whereas for the PECVD a-Si II [32] sample, it is less than unity, which is itself a pure a-Si material.

Chapter 5

Conclusions

Models for the spectral dependence of the real and imaginary components of the dielectric function, $\epsilon_1(E)$ and $\epsilon_2(E)$, respectively, appropriate for the case of amorphous semiconductors, are considered. In the first phase of this analysis, from an empirical expression for imaginary part of the dielectric function, this expression corresponding with that of the model of Jellison and Modine [15], a closed-form expression for the real part of the dielectric function is determined using a Kramer-Kronig transformation. The resultant expression for the real and imaginary components of the dielectric function corresponds with the model of Jellison and Modine [15]. The comparison with experiment is found to be satisfactory. Then, in the latter stage of the analysis, through the application of a Kramers-Kronig transformation on an empirical model for the imaginary part of the dielectric function, this model stemming from a model for the distributions of electronic states, the spectral

138

dependence of the real part of the dielectric function. Fits with the results of experiment are also found to be satisfactory.

There are a number of matters related to these models for the real and imaginary components of the dielectric function, $\epsilon_1(E)$ and $\epsilon_2(E)$, that could be pursued in the future. A critical comparison between the fits obtained using the model of Jellison and Modine [15] and that obtained using the new model would be instructive. The gleaning of insights into the underlying distributions of electronic states from experimental measurements of these optical functions, $\epsilon_1(E)$ and $\epsilon_2(E)$, would also be worthy of further investigation. Finally, the use of these models for the purposes of device design and device optimization would be of interest. These topics will have to be addressed in the future.

References

[1] G. E. Moore, "Cramming more components onto integrated circuits," *Electronics*, pp. 114-117, 1965.

[2] M. Riordan and H. Lillian, "The Moses of silicon valley," *Physics Today*, vol. 50, pp. 42-47, 1997.

[3] I. M. Ross, "The foundation of the silicon age," *Physics Today*, vol. 50, pp. 34-39, 1997.

[4] A. J. Snell, K. D. Mackenzie, W. E. Spear, P. G. Le Comber, and A. J. Hughes, "Application of amorphous silicon field effect transistors in addressable liquid crystal display panels," *Applied Physics Letters*, vol. 24, pp. 357-362, 1981.

[5] P. G. Le Comber, W. E. Spear, and A. Ghaith, "Amorphous-silicon field-effect device and possible application," *Electronics Letters*, vol. 15, pp. 179-181, 1979.

References

---

[6] M. G. Clark, "Current status and future prospects of poly-Si devices," *IEEE Proceedings-Circuits, Devices and Systems*, vol. 141, pp. 3-8, 1994.

[7] S. O. Kasap and J. A. Rowlands, "X-ray photoconductors and stabilized a-Se for direct conversion digital at-panel X-ray image-detectors," *Journal of Materials Science: Materials in Electronics*, vol. 11, pp. 179-198, 2000.

[8] H. Fujioka, M. Oshima, C. Hu, M. Sumiya, N. Matsuki, K. Miyazaki, and H. Koinuma, "Characteristics of field effect a-Si:H solar cell," *Journal of Non-Crystalline Solids*, vol. 227-230, pt. 2, pp. 1287-1290, 1998.

[9] H. Pawlikiewicz and S. Guha, "Performance comparison of triple and tandem multi-junction a-Si:H solar cells: A numerical study," *IEEE Transactions on Electron Devices*, vol. 37, pp. 1758-1762, 1990.

[10] "Displays as key driver for large area electronics in intelligent environments: A vision for Europe 2007+", *A proposal for the advancement of the IST thematic priority*, Information Society Technologies, May 2005.

References

[11] R. A. Street, Editor, *Technology and Applications of Amorphous Silicon*. New York, New York: Springer-Verlag, 2000.

[12] T. H. Nguyen, "A theory of occupation statistics for disordered semiconductors with applications," Master's Thesis, University of Regina, Regina, Saskatchewan, May 2000.

[13] J. J. Thevaril, "The optical response of hydrogenated amorphous silicon," Ph. D. Thesis, University of Windsor, Windsor, Ontario, Canada, 2011.

[14] F. Orapunt, "The optical response of hydrogenated amorphous silicon," Ph. D. Thesis, University of Regina, Regina, Saskatchewan, 2012.

[15] G. E. Jellison, Jr. and F. A. Modine, "Parameterization of the optical functions of amorphous materials in the interband region," *Applied Physics Letters*, vol. 69, pp. 371-373, 1996.

[16] W. B. Jackson, S. M. Kelso, C. C. Tsai, J. W. Allen, and S.-J. Oh, "Energy dependence of the optical matrix element in hydrogenated amorphous and crystalline silicon," *Physical Review B*, vol. 31, pp. 5187-5198, 1985.

References

---

[17] S. K. O'Leary, "An empircal density of states and joint density of states analysis of hydrogenated amorphous silicon: a review," *Journal of Material Science: Materials in Electronics*, vol. 15, pp. 401-410, 2004.

[18] J. Tauc, R. Grigorovici, and A. Vancu, "Optical properties and electronic structure of amorphous germanium, *Physica Status Solidi*, vol. 15, pp. 627-637, 1966.

[19] G. D. Cody, B. G. Brooks, and B. Abeles, "Optical absorption above the optical gap of amorphous silicon hydride," *Solar Energy Materials*, vol. 8, pp. 231-240, 1982.

[20] A. R. Forouhi and I. Bloomer, "Optical dispersion relations for amorphous semiconductors and amorphous dielectrics," *Physical Review B*, vol. 34, pp. 7018-7026, 1986.

[21] W. A. McGahan, T. Makovicka, J. Hale, and J. A. Woollam, "Modified Forouhi and Bloomer dispersion model for the optical constants of amorphous hydrogenated carbon thin films," *Thin Solid Films* , vol. 253, pp. 57-61, 1994.

[22] W. A. McGahan and J. A. Woollam, "Optical characterization and

modeling of amorphous hydrogenated carbon films," *Materials Research Society Symposium Proceedings*, vol. 349, pp. 453, 1994.

[23] S. Sherman, S. Wagner, and R. A. Gottscho, "Correlation between the valence and conduction band tail energies in hydrogenated amorphous silicon," *Applied Physics Letters*, vol. 69, pp. 3242-3244, 1996.

[24] S. A. Alterovitz, N. Savvides, F. W. Smith, and J. A. Woollam, *Handbook of Optical Constants of Solids II*, edited by E. D. Palik (Academic Press, New York), 1991, pp. 837-840.

[25] J. Tauc, *Optical Properties of Solids*, edited by S. Nudelman and S. S. Mitra (Plenum, New York), 1969, pp. 123.

[26] F. Wooton, *Optical Properties of Solids*, (Academic press, New York), 1972, pp. 42-49.

[27] S. K. O'Leary and S. M. Malik, "A simplified joint density of states analysis of hydrogenated amorphous silicon," *Journal of Applied Physics*, vol. 92, pp. 4276-4282, 2002.

[28] J. J. Thevaril and S. K. O'Leary, "A dimensionless joint density of states formalism for the quantitative characterization of the opti-

cal response of hydrogenated amorphous silicon," *Journal of Applied Physics*, vol. 107, pp. 083105-1-6, 2010.

[29] S. K. O'Leary, "An analytical density of states and joint density of states analysis of amorphous semiconductors," *Journal of Applied Physics*, vol. 96, pp. 3680-3686, 2004.

[30] H. Piller, in *Handbook of Optical Constants of Solids I*, edited by E. D. Palik (Academic, New York, 1985), pp. 571-586.

[31] R. Synowicki, J.A. Woollam Co., Inc.Ellipsometry Services Laboratory.

[32] A. S. Ferlauto, G. M. Ferreira, J. M. Pearce,C. R. Wronski, R. W. Collins, X. Deng, and G. Ganguly, "Analytical model for the optical functions of amorphous semiconductors from the near-infrared to ultraviolet: Applications in thin film photovoltaics," *Journal of Applied Physics*, vol. 92, pp. 2424-2436, 2002.

[33] J. J. Thevaril and S. K. O'Leary, "The role that conduction band tail states play in determining the optical response of hydrogenated amorphous silicon," *Solid State Communications*, vol. 151, pp. 730-733, 2011.

[34] K. Rerbal, J.-N. Chazalviel, F. Ozanam, and I. Solomon, "Measurement of band tail widths in hydrogenated amorphous silicon," *Journal of Non-Crystalline Solids*, vol. 299-302, pp. 585-588, 2002.

[35] T. Tiedje, J.M. Cebulka, D.L. Morel, B. Abeles, "Evidence for exponential band tails in amorphous silicon hydride," *Physical Review Letters*, vol. 46, pp. 1425-1428, 1981.

[36] K. Winer and L. Ley, "Surface states and the exponential valence-band tail in a-Si:H," *Physical Review B*, vol. 36, pp. 6072-6078, 1987.